SAPIENZA
UNIVERSITÀ DI ROMA

Superfluidity of light in a nonlinear atomic medium

Facoltà di Scienze Matematiche, Fisiche e Naturali

Corso di Laurea Magistrale in Fisica

Candidato

Agostino Aprà
Matricola 1482271

Relatori

Paolo Mataloni
Alberto Bramati
Quentin Glorieux

Anno Accademico 2016/2017

Tesi discussa il 16 April 2017
di fronte a una commissione esaminatrice composta da:

Prof. Nome Cognome (presidente)

Prof. Nome Cognome

Dr. Nome Cognome

Superfluidity of light in a nonlinear atomic medium
Tesi di Laurea Magistrale. Sapienza – Università di Roma

Questa tesi è stata composta con LaTeX e la classe Sapthesis.

Versione: 23 giugno 2017

Email dell'autore: apraagostino@gmail.com

Dedicato a

Sommario

Over the past decade, theoretical and experimental studies of photon fluids have opened new routes to realizing quantum many-body systems.

This thesis reports the study of a photon fluid i.e. a system where a collective behaviour of the photons is introduced through the light-matter interaction.

As in atomic many-body systems, the photon fluid can be described by a Gross-Pitaevskii equation, where the electric field plays the role of the order parameter, a macroscopic wave function with a clear resemblance to dilute-gas Bose-Einstein condensates (BEC) and superfluid helium.

A photon fluid is created by propagating a laser beam through a defocusing nonlinear medium. Such platform is described by a nonlinear Schrödinger equation (NLSE) that, with a space-time mapping, is analogue to the GPE.

In this analogy the photon fluid is considered in the transverse plane and the propagating direction play the role of a temporal coordinate. Therefore studying the spatial evolution of the beam profile it is possible to simulate the temporal evolution of a 2-D gas of weakly interacting bosons.

Much research with photon fluids has centered on exploring characteristics of superfluidity, such as the nucleation of quantized vortices and the circulation in the flow past an obstacle.

In this thesis two experiments will be described from a theoretical and experimental perspective. All the experiments are performed at room-temperature and, differently from polaritonic platforms, our system is not confined into a single plane.

The aim of the first experiment (Chapter 5) we perform is to measure the Bogoliubov dispersion relation from the phase shift induced by atomic the nonlinearity.

The aim of the second experiment (Chapter7) is to verify the suppression of the scattering from an optically induced defect that, in analogy with the GPE, act as an external potential.

From both the experiment turns out that the nonlinear response of our medium is intrinsically nonlocal, therefore we designed another experiment to understand better this effect.

Ringraziamenti

Ringraziamenti

Indice

Capitolo 1

Introduction

In the last century tremendous progress has been done in understanding the mechanisms that are responsible of superfluidity.

In 1908 K.Onnes was the first to liquefy ^{4}He at the University of Leiden. Several years later, in 1937, P.Kapitsa [1], and independently John F. Allen and D.Misener [2], observed superfluidity in liquid ^{4}He.

In 1938 F.London [3] noticed that the so-called λ point, i.e. the temperature such as normal fluid He-I makes the transition to superfluid He-II ($T_\lambda = 2.17K$ for a pressure of 1 atm), was close to the critical temperature T_C for the Bose-Einstein condensate (BEC) transition. This suggests that the two phenomena are related, anyway not all the superfuids are BEC and viceversa.

What is certain is that superfluidity can be observed only in bosonic system, but this requirement is not enough. Superfluidity in fact arises from a collective behaviour of the particles, that cannot be explained only in terms of the Bose statistics. What is required is an interaction between the particles of the bosonic system under exam.

The main idea of our project is to simulate a superfluid using photons as bosons and to introduce an effective interaction between them through light-matter coupling. Is well known that photons in a box can be interpreted as a perfect gas of non-interacting bosons and they cannot show any superfluid behaviour. Indeed, the photon-photon interaction in vacuum can occur only via virtual excitation of electron-positron pairs [37] but the cross-section is so small that we can't expect it to play any role in realistic experiments. However through light-matter interaction photons can acquire an effective mass and an effective interaction and therefore they can be considered as a "quasi-perfect" Bose gas. A weakly interacting many-photon system in fact follows the dynamic of a weakly interacting Bose gas, that was described by N.Bogoliubov in 1947 [4].

In his theory he demonstrates that the Hamiltonian of a weakly interacting bosonic many-body system can be diagonalized through the so-called Bogoliubov transformation and this leads to reconsider the system in terms of non-interacting quasi-particles. The function that links the energy of these quasi-particles to their momentum is the so called Bogliubov dispersion relation. The particular form of this energy-momentum relation is due to a collective behaviour of the system for small momentum. For large momentum instead the collective excitations are suppressed

and the energy-momentum relation converges to the behaviour expected for a single particle.

The key point to understand the microscopical origin of superfluid phenomenas is in fact to consider the collective elementary excitations instead of considering individual atoms or molecules, as suggested by L.Landau when he was trying to understand the superfluid behaviour of Helium II [6][1].

The Bogoliubov theory for weakly interacting Bose gas will be described in detail in Chapter 2.

Such many-body system of weakly interacting photons can be defined as a Quantum fluid of light (QFL). In this kind of system the quantum mechanical effects manifest themselves on a macroscopic scale, in fact the dynamics of the whole fluid is governed by a single wave function.

The concept of quantum fluids of light applies to a broad range of different physical systems such as bulk nonlinear crystals, atomic clouds embedded in optical fibers and cavities, photonic crystal cavities and superconducting quantum circuits based on Josephson junctions[9]. Also superfluid shock waves and condensation of classical waves have been observed in defocusing bulk nonlinear medium using photo refractive crystals [43].

The LKB research team is focusing his attention on exciton-polaritons in semiconductor microcavities and photons in a propagating geometry.

Polaritons can be generated using a setup where photons entering in a Fabry-Perot microcavity strongly couple with the excitonic transition through quantum well located in the middle of the cavity, where the electric field is maximized, as shown in Fig. 1.1 a).

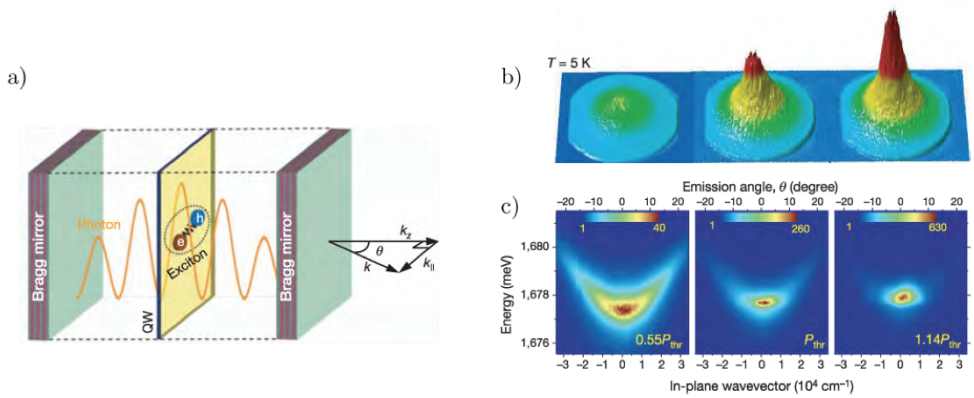

Figura 1.1. The photon mode is strongly coupled to the excitons in the quantum well (QW) giving rise to an effective photon photon interaction. The photon fluid is considered in the transverse plane: a mode with frequency ω and in-plane vector k_{II} is excited by a laser beam with an incident angle θ. b) and c) Farfield spectrum showing the Bose-Einstein condensation of an exciton-polariton condensate while the intensity is increased from left to right. The colour scale is normalized with the intensity. Taken from [15].

[1] Also if the He II must be considered as a strongly interacting Bose gas.

Photons and excitons has both an integer spin and therefore the resulting quasi-particles will maintain bosonic properties, with the advantage of a bigger interaction range compared to a fluid of photons. The temporal evolution of the wavefunction in a gas of polaritons follows a similar dynamic of a diluted BEC. In fact several experimental demonstrations of superfluidity and other quantum hydrodynamics effects have been performed using semi-conductor planar micro-cavities and a rich variety of hydrodynamic-like effects have been observed using polaritons, from the superfluid flow around a defect at low speeds, to the appearance of a Mach-Cherenkov cone in a supersonic flow [12] and to the hydrodynamic formation of topological excitations such as quantized vortices and dark solitons at the surface of large impenetrable obstacles[21][22].

The optical nonlinearity in such a system comes from the strong interactions between the excitons. The small mass and the large interaction range of exciton-polaritons allow condensation at higher temperatures compared to atoms. In particular using organic microcavities, instead of semiconductor, is possible to observe superfluidity also at room temperature [13]. Fig. 1.1 b), c) shows Bose-Einstein condensation of exciton-polaritons, observed in [15] .

If we considered a non-interacting photon fluid as the blackbody radiation (radiation in thermal equilibrium with the cavity walls) is well known that it does not show any BEC transition. In such systems photons have a vanishing chemical potential, so their number is not conserved when the temperature of the photon gas is varied. Therefore at low temperatures, photons disappear in the cavity walls instead of occupying the cavity ground state. Anyways recently a BEC of photons has been observed in a cavity filled with fluorescent dye that allow the thermalization of photons [14].

The detection scheme of experiments with exciton-polaritons is relatively simple because the measurement can be performed on the photons exiting from the cavity. However measuring photons coming out from the cavity means to deal with open systems, which dynamic is intrinsically driven-dissipative. Moreover experiments with polaritons are limited to the study of the effects in the plane of the quantum well.

In the systems under exams in this thesis, that consist basically in one or more nearly-detuned laser beams propagating through a Rb vapour, we want to establish a new approach to study the properties of a QFL with a conservative system and in a propagating geometry. This approach has been recently formalized by I.Carusotto [5] that, based on the proposal of R.Chiao in 1999 [28], has suggested two experiments to demonstrate superfluidity with photon fluids in a propagating geometry.

In such a geometry the complex amplitude of the optical field is a slowly varying function of time and space and its propagation, in absence of losses, is ruled by a nonlinear Schrödinger equation (NLSE) that is mathematically identical to the Gross-Pitaevskii equation (GPE) of a dilute BEC.

Therefore, under the paraxial approximation, the amplitude of the electric field $A(\vec{r}_\perp, z)$ of the monochromatic light play the role of the order parameter $\hat{\Psi}$ of a superfluid or equivalently the macroscopic wave-function of a diluted BEC.

The following equations describe respectively the time-evolution of a gas of weakly interacting bosons and the spatial propagation of the electric field in a nonlinear

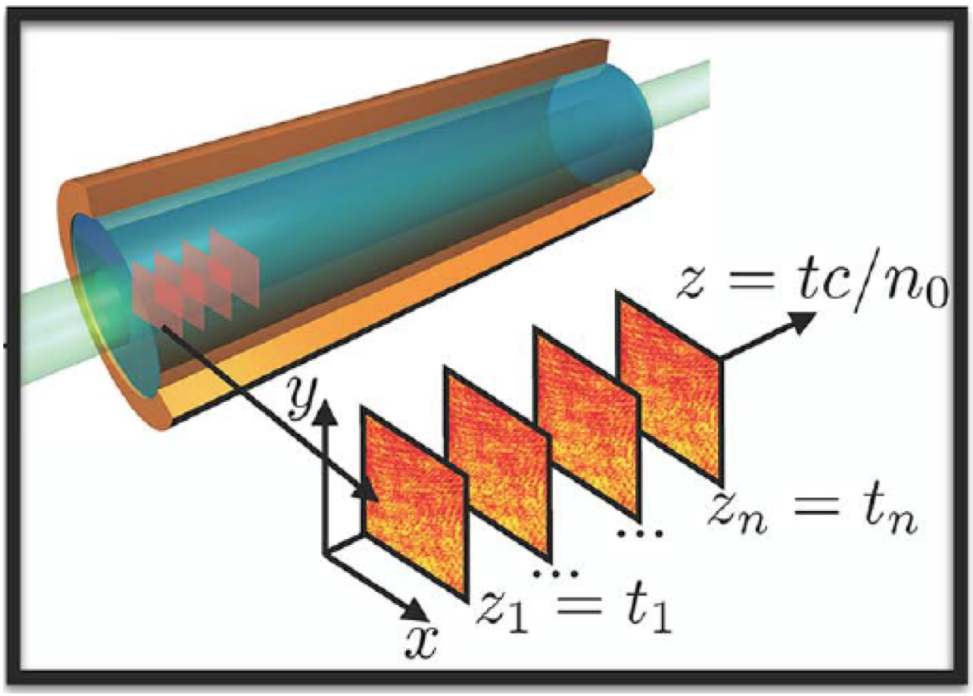

Figura 1.2. Scheme of the propagation of the 2-d photon fluid along the z axis. Each snapshot along the spatial coordinate corresponds to a time frame of the evolution of a 2-d Bose gas. Taken from [11].

medium without losses:

$$\begin{aligned} i\hbar\frac{d\hat{\Psi}}{dt} &= \left(-\frac{\hbar^2\nabla^2}{2m} + V + g|\hat{\Psi}|^2\right)\hat{\Psi} \quad , \\ i\frac{|\partial A(\vec{r}_\perp,z)|}{\partial z} &= (-\frac{1}{2k_0}\nabla_\perp^2 + V + g|A(\vec{r}_\perp,z)|^2)A(\vec{r}_\perp,z) \quad . \end{aligned} \tag{1.1}$$

Where V is an external potential and g is a coupling constant that determines the strength of the interactions. In particular to have a proper mapping between the two systems this coupling constant must have a positive sign, and for an optical system this condition corresponds to the case of a negative nonlinearity.

Despite the two equations are formally similar two main aspects must be highlighted:

- The GPE describes the evolution of the wave-function of a Bose gas in time, while the nonlinear Schrödinger equation (NLSE) for the electric field determines an evolution in space.

- The laplacian of the NLSE is considered in the transverse plane, therefore we can simulate the evolution of the wave function $\hat{\Psi}$ of a two dimensional Bose gas.

This space-time mapping is schematized in Fig.1.2 and it will be discussed in detail in Chapter 3, where I will describe also the theory behind the experiments.

Compared to other platforms for quantum simulation, as for instance cold atoms, our platform has the experimental advantage of being able to work at room temperature. Moreover heating the Rb vapour we can enhance the nonlinear response of the medium. At the same time the absorption spectrum of the Rb gas is increased due to Doppler broadening, and this can be a problem because we want to work under the theoretical assumption of a lossless system. The nonlinearity in fact depends on the intensity of the beam, the temperature of the medium and by the detuning from the center of the atomic transition. Therefore we have to find a detuning such as we have a good trade-off between a high nonlinearity and negligible absorption.

In chapter 4 it will be discussed theoretically how to find the nonlinear response for a two-level system, how we extrapolate the temperature of the cell from the absorption profile and how we choose the working frequency for the experiments.

In chapter 5 it will be discussed in detail the experiment that we performed to measure the Bogoliubov dispersion relation. Recently the Bogoliubov dispersion relation has been measured also in a non-local medium (methanol mixed with graphene flakes), where the nonlinearity has a thermal origin [11]. Anyway, despite the physical system is different from ours, there are several analogies with our experiment and is worth to discuss it more in detail, especially for what concerns the origin of non locality.

In fact during the measurement of the dispersion relation turns out that also our medium exhibit a strong non-locality and in Chapter 6 it will be discussed how we tried to quantify it. The origin of non-local phenomena can basically be reconducted to the fact that the excited particles are free to move in the diluted gas and therefore the size of the modulation of the refractive index results bigger than the size of the spot who excites the medium.

One of the main features that demonstrate a superfluid behaviour is the suppression of the drag force when the fluid pass thorough an obstacle. We will try to investigate this effect using an optically induced defect, that modify the refractive index of the medium and can be interpreted as an external potential in the NLSE. Through the analogy between the GPE and the NLSE we want also to reconsider the interpretation of well-known nonlinear and quantum optics phenomena in an hydrodynamical framework. Is in this context the results obtained in Chapter 7 can find an interpretation.

Capitolo 2

Theory

2.1 Superfluidity

Superfluidity is the characteristic property of a fluid with zero viscosity which therefore flows without losses of kinetic energy.

The discovery of superconductivity by Kamerlingh Onnes (Nobel Prize 1913) and of superfluid helium-II by Pyotr Kapitsa (Nobel Prize 1978) established the existence of superfluid phases of matter. The two phenomenas are strictly linked and the common feature of these states of matter is condensation which is most simply understood in a gas of non-interacting bosons where, below the BEC critical temperature, a macroscopic number of particles will populate the lowest quantum mechanical energy eigenstate.

The case of the superconductor is somewhat more complicated. What condenses here are bosonic Cooper pairs of electrons, as explained by the BCS theory of superconductivity (Nobel Prize 1972 to John Bardeen, Leon Cooper and John Schrieffer). This interpretation leads to a correct description of superfluid behaviour in a fermionic system as ^{3}He. These condensates can also be described by an order parameter which can be thought of as a macroscopic wave function for the bosons or for the Cooper pairs.

In 1950, before of the advent of the BCS theory, Ginzburg and Landau proposed a model for the order parameter that describes the phase transitions between the normal and superconducting phases. Some years later the corresponding theory for the normal to superfluid transition in a gas of bosons, was given by Gross and Pitaevskii.

The classical example of a phase transition is a system going from a disordered phase to an ordered phase as the temperature is lowered below a critical value. More recently, the phase transition concept has been extended to quantum systems at zero temperature. In a quantum system the behaviour of the particles in the ground state changes suddenly when one of the parameters in its Hamiltonian, such as impurity concentration or pressure, is modified until a threshold value.

In a phase ordered state, or a condensate, the phase is constant, or slowly varying, in the whole system. This property is often referred to as phase rigidity.

In a superfluid state the order parameter can be written as $\psi = \sqrt{\rho}e^{i\phi}$. The important thermal fluctuations are only in the phase and are hence described by a

single angle ϕ, just as in a 2-d magnetic spin model.

Since the planar magnet and a superfluid both have order parameters described by a single angle, they belong to the same universality class and can be described by the same effective theory.

In the last decades the interest in the studying of superfluid effects is growing, as proved by the assignation of the last Nobel Prize (2016) to J.Kosterlitz, D.Thouless and D.Haldane "for theoretical discoveries of topological phase transitions and topological phases of matter" [27].

Basically their theory can be explained with simple thermodynamic argument and the mechanism that bind the vortices is responsable for the phase transition. These vortices were originally defined as quasi-particles called rotons.

Kosterlitz and Thouless understood that, below a certain temperature T_{KT}, the unpaired vortex and antivortex, with vorticity $v = \pm 1$, bind into vortex antivortex pairs. The vorticity can be defined as the circuitation of the phase gradient of the order parameter, or most simply as the number of time the phase change of 2π.

$$v = \oint_C \vec{\nabla}\phi(\vec{r})d\vec{r} \qquad . \tag{2.1}$$

Vortex generation becomes thermodynamically favorable above the critical temperature T_{KT}.

Cold atomic gases have turned out to be a good platform to quantum simulate this phase transition, as has been studied by I.Bloch in collaboration with LKB researchers [55].

An important tool in these experiments is the optical lattices that are formed as an interference pattern by intersecting laser beams. An example of this is the observation of the KT-transition in a layered Bose-Einstein condensate of ^{87}Rb atoms. At low temperatures one observes coherence effects characteristic of the phase with power law correlations, and at higher temperatures one sees free vortices [56].

Anyway the investigation of the microscopic effect that leads to the superfluid phase transition goes beyond the scope of this thesis. We focus our attention mainly on macroscopic effects, in fact in our project the wavefunction is considered in a mean field approximation and the local fluctuations of the phase are not taken in account. Are these local phase fluctuations that are responsable of the mechanism that leads to the unbinding of a single vortex into vortex-antivortex pairs.

Moreover it is known that elementary excitations in an inhomogeneous flow behave analogous to scalar fields in curved spacetime [57]. This may be more evident rewriting the GPE in the so-called Madelung rappresentation that will be presented in section 3.3. In this context the linearity of the low-momentum dispersion relation allows to build an analogy with the space-time metrics. In that sense, a constant speed of sound corresponds to the constant light speed in vacuum that guarantees local Lorentz invariance [41].

2.2 Landau criterion

In 1941 Lev Landau established a superfluidity criteria under the hypothesis that the system in question could be able to exchange energy with the environment only

through the creation or annihilation of elementary excitations (quasi-particles) with energy ϵ and momentum $\mathbf{p}$ related by a dispersion relation $\epsilon = \epsilon(\mathbf{p})$ specific for each system.

Landau's theory of superfluids is based on the Galilean transformation of energy and momentum. Let E and $\mathbf{P}$ be the energy and momentum of the fluid in a reference frame K. If we try to express the energy and momentum of the same fluid but in a moving frame K', which has a relative velocity $\mathbf{V}$ with respect to a reference frame K, we have the following relations:

$$\mathbf{P'} = \mathbf{P} - M\mathbf{V} \quad , \tag{2.2}$$

$$E' = \frac{|\mathbf{P'}^2|}{2M} = \frac{|\mathbf{P} - M\mathbf{V}|^2}{2M} = E - \mathbf{PV} - \frac{M|\mathbf{V}|^2}{2} \quad , \tag{2.3}$$

where M is the total mass of the fluid.

We consider here a fluid at zero temperature where all the particles are in the ground state and flowing along a capillary at $\mathbf{v} = const.$

In a viscous fluid we expect that the motion will produce dissipation of kinetic energy through friction with the capillary wall.

Assuming that the interaction between the obstacle and the flow is such that it can only create elementary excitations in the fluid and not change the overall flow. These elementary excitations are the Bogoliubov quasi-particles for the case of a weakly interacting Bose gas.

Let's consider the case where a single excitation with momentum $\mathbf{p}$ appears in the fluid and then the total energy in the reference frame K is $E_0 + \epsilon(\mathbf{p})$.

In the co-moving frame K', moving with $\mathbf{V} = -\mathbf{v}$, we have:

$$\mathbf{P'} = \mathbf{p} + M\mathbf{v} \quad , \tag{2.4}$$

$$E' = E_0 + \epsilon(\mathbf{p}) + \mathbf{pv} + \frac{M|\mathbf{V}|^2}{2} \quad . \tag{2.5}$$

The equation2.5 indicates that the changements in energy and momentum, due to one elementary excitation, are respectively $\epsilon(\mathbf{p}) + \mathbf{pv}$ and $\mathbf{p}$.

Spontaneous creation of elementary excitations (energy dissipation) can happen only if the process is energetically favorable, that means that the energy of an elementary excitation in the co-moving frame K' have to be negative :

$$\epsilon(\mathbf{p}) + \mathbf{pv} < 0 \quad . \tag{2.6}$$

That means:

$$\begin{cases} |\mathbf{v}| > \frac{\epsilon(\mathbf{p})}{|\mathbf{p}|} \\ \mathbf{pv} < 0 \end{cases} \quad . \tag{2.7}$$

The second condition states that, to satisfy the superfluidity condition, the elementary excitations must have a momentum $\mathbf{p}$ opposite to the fluid velocity $\mathbf{v}$.

And then it is possible to define a minimum critical velocity v_c, such as the spontaneous formation of quasi-particles will be energetically unfavorable for $v < v_c$:

$$v_c = min_p \frac{eps(\mathbf{p})}{|\mathbf{p}|} \quad . \tag{2.8}$$

The critical velocity is dependent by the excitation spectrum as shown in Fig. 2.1. For a weakly interacting Bose Gas, it coincides with the sound velocity c_s.

Instead for a strongly interacting gas, that can therefore be considered in the liquid regime, as ^{4}He the dispersion relation is such that it have a minimum for $v_c < c_s$.

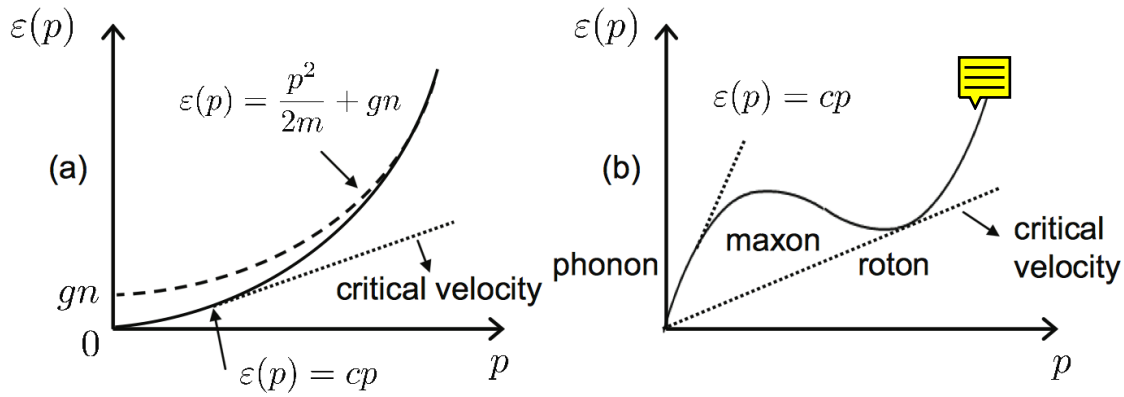

Figura 2.1. On the left is shown the excitation spectrum of a weakly interacting Bose gas, for which the critical velocity is equal to the sound velocity, $v_c = c_s$. On the right the excitation spectrum of a strongly interacting Bose liquid as ^{4}He, for which the critical velocity is smaller than the sound velocity, $v_c < c_s$. Taken from [8].

A perfect gas does not show any fluid behaviour. In fact in such a system the particles are non interacting and then there is no collective behaviour. The dispersion is the single particle relation that lead to a $v_c = 0$:

$$\epsilon(\mathbf{p}) = \frac{\mathbf{p}^2}{2m} \longrightarrow v_c = 0 \quad . \tag{2.9}$$

The particle-particle interaction in fact is a crucial requirement for the appearance of superfluidity. That is like to say that a necessary condition for the appearance of superfluidity is that our object can be considered as a fluid i.e $v_c \neq 0$.

2.3 Bogoliubov theory for a weakly interacting Bose gas

In presence of a BEC, the ideal Bose gas has a constant pressure against variation of volume, so that the system exhibits an infinite compressibility. This feature originates from the absence of particle-particle interaction. Therefore, as consequence of the interactions between particles the properties of the gas are modified significantly, even for very dilute samples.

The first who studied a dilute Bose gas of weakly interacting particles was N.Bogoliubov that in an article of 1947 [4], using a perturbative approach, provides the theoretical framework to describe such many-body system.

The hypothesis of a dilute gas is reliable if r_0, that is the range of the inter-particle forces, is much smaller then the average distance between 2 particles:

$$r_0 \ll \left(\frac{N}{V}\right)^{\frac{1}{3}} \quad . \tag{2.10}$$

This condition allows to consider only two-body interactions, while the configurations with with three or more simultaneously interacting particles can be neglected. Furthermore we can consider only the asymptotic behaviour of the wave function of their relative motion. This means that the propriety of the system can be expressed as a function of the scattering length a.

In addition, we require that the temperature of the gas have to be smaller than the critical temperature for the Bose-Einstein condensation. So the momentum has to satisfy

$$p \ll \frac{\hbar}{r_0} \quad . \tag{2.11}$$

In this situation the scattering amplitude can be regarded as independent from the s-wave scattering length a, that is defined as the following low energy limit:

$$\lim_{k\to 0} k \cot \delta(k) = -\frac{1}{a} \quad , \tag{2.12}$$

where k is the wave number and $\delta(k)$ is the s-wave phase shift.

In a dilute gas the medium distance between the particles is way bigger than the scattering length. Defining the atomic density $\rho = N/V$ as the ratio between the total number of atoms N and the volume V, the diluteness condition is:

$$|a| \ll \rho^{-\frac{1}{3}} \quad . \tag{2.13}$$

The Hamiltonian can be expressed as a kinetic term plus a two-body potential[1]:

$$\hat{\mathcal{H}} = \int \frac{\hbar^2}{2m} \bar{\nabla}\hat{\Psi}^\dagger(\bar{r})\bar{\nabla}\hat{\Psi}(\bar{r})d\bar{r} + \frac{1}{2}\int \hat{\Psi}^\dagger(\bar{r})\hat{\Psi}^\dagger(\bar{r}')V(\bar{r}-\bar{r}')\hat{\Psi}(\bar{r})\hat{\Psi}(\bar{r}')d\bar{r}d\bar{r}' \quad . \tag{2.14}$$

Where $V(\bar{r}-\bar{r}')$ is a two-body scattering potential. For a uniform gas occupying a volume L^3 the field operator $\hat{\Psi}(\bar{r})$ can be expanded as a sum of plane waves:

$$\hat{\Psi}(\bar{r}) = \frac{1}{\sqrt{L^3}}\sum_{\bar{p}} \hat{a}_{\bar{p}} e^{i\bar{p}\bar{r}/\hbar} \quad . \tag{2.15}$$

By substituting 2.15 in 2.14, and integrating over the volume L^3:

$$\hat{\mathcal{H}} = \sum_{\bar{p}} \frac{\bar{p}^2}{2m}\hat{a}^\dagger_{\bar{p}}\hat{a}_{\bar{p}} + \frac{1}{2L^3}\sum_{\bar{p}_1,\bar{p}_2,\bar{q}} V_q \hat{a}^\dagger_{\bar{p}_1+\bar{q}}\hat{a}^\dagger_{\bar{p}_1-\bar{q}}\hat{a}_{\bar{p}_1}\hat{a}_{\bar{p}_2} \quad . \tag{2.16}$$

[1]For a graphic reason in this chapter the vectorial notation is indicated with $\bar{}$ instead of $\vec{}$

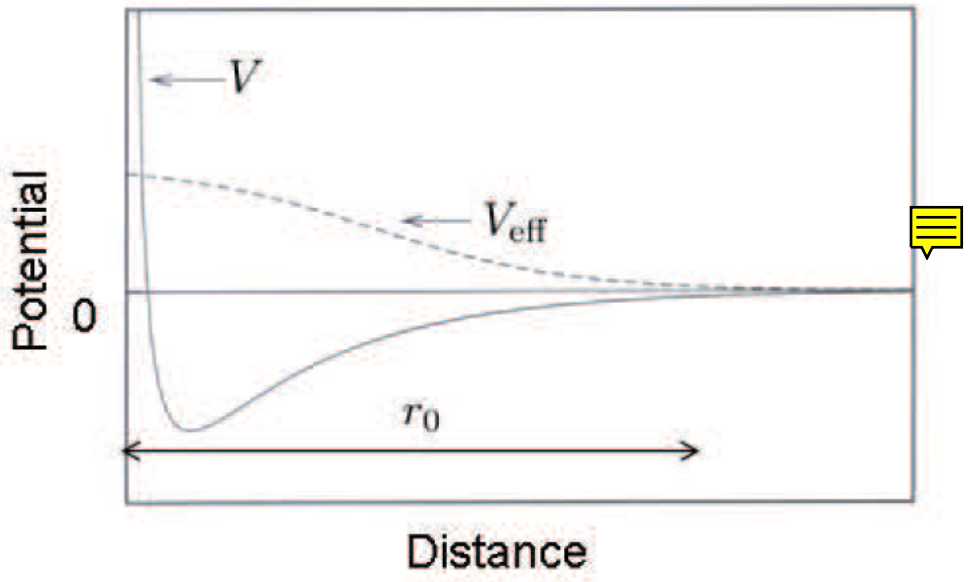

Figura 2.2. The two-body scattering potential $V(r)$ and the effective, smooth potential $V_{eff}(r)$. Taken from [8].

Where the mean-field potential:

$$V_q = \int V(\bar{r}) e^{-i\bar{q}\bar{r}/\hbar} d\bar{r} \quad . \tag{2.17}$$

is the Fourier transform of the two-body scattering potential $V(r)$. In real systems V (r) always contains a short-range term, as shown in Fig. 2.2 which makes it difficult to solve the Schrödinger equation at the microscopic level. Since the scattering length is constant under the approximation of diluted gases it is possible to substitute the real potential V with an effective potential such it is possible to apply a perturbation theory.

The zero-order approximation introduced by Bogoliubov is valid under the initial hypothesis 2.10 of a diluted gas, such as the ground state is macroscopically occupied:

$$\hat{a}_0 = \sqrt{N_0} \simeq \sqrt{N} \quad . \tag{2.18}$$

So it is possible to approximate the number of particle occupying the ground state N_0 with the total number of particles N. Therefore also the density of particles in the ground state is $\rho_0 \simeq \rho$.

With this condition it is possible to neglect the quantum fluctuations, that means to neglect all the terms of the sum with $p \neq 0$.

The macroscopic properties of the system as well depends on low momentum values for the Fourier transform of $V_{q \ll \hbar/r_0}$.

So we can replace this term with an effective potential:

$$V_{q=0} = \int V_{eff}(\bar{r}) d\bar{r} \quad . \tag{2.19}$$

Here V_0 can be expressed in terms of the s-wave scattering length a using the Born approximation and it represents the mean field energy:

$$V_0 = \frac{4\pi\hbar^2 a}{m} = g \qquad . \tag{2.20}$$

Now the ground state's energy takes the form:

$$E_0 = \frac{V_0 N_0^2}{2L^3} \simeq \frac{gN^2}{2L^3} \qquad . \tag{2.21}$$

We can define also the chemical potential μ as the interaction energy in the mean field approximation:

$$\mu = \frac{\partial E_0}{\partial N} = g\rho_0 \qquad . \tag{2.22}$$

Differently to the BEC of an ideal Bose gas, the pressure of a BEC of weakly-interacting Bose gas does not vanish at T=0:

$$P = -\frac{\partial E_0}{\partial L^3} = g\rho_0^2/2 \qquad . \tag{2.23}$$

In an optical context the pressure of the fluid can be interpreted as the radiation pressure. This is important especially when one try to suppress the drag force around a defect [19].

Below the healing length ξ, that can be defined as the distance such as the fluid self-heal itself, the fluid behaves as an incompressible fluid ($C \to \infty$, $P \to 0$). Another equivalent definition for ξ is the length scale over which a perturbation of the complex field Ψ recover its ground state value[17].

This parameter is not an absolute length scale and depends mainly on the strength of the interaction and the density of the fluid. The condensate density grows from 0 to ρ_0 over this length scale and we can quantify it as the distance such as the kinetic energy of a particle $E_{kin} = \frac{\hbar^2}{2m\xi^2}$ with a momentum ($p = \hbar/\xi$) such as it is comparable with the mean field interaction energy $E_{int} = \mu = g\rho_0$ [18].

Therefore we find the following equivalent expression for ξ :

$$\xi = \frac{1}{\sqrt{8\pi\rho_0 a}} = \frac{\hbar}{\sqrt{2mg\rho_0}} = \frac{\hbar}{mc_s\sqrt{2}} \qquad . \tag{2.24}$$

In the mean-field approximation, i.e. above the healing length, instead the compressibility is a finite value:

$$C = \frac{1}{\frac{\partial P}{\partial \rho_0}} = \frac{1}{g\rho_0} \qquad . \tag{2.25}$$

Using the hydrodynamic relation between the sound velocity c_s and the compressibility C is possible to obtain an expression of the sound velocity:

$$mc_s^2 = \frac{\partial P}{\partial \rho_0} \longrightarrow c_s = \sqrt{\frac{g\rho_0}{m}} \qquad . \tag{2.26}$$

2.4 Bogoliubov first order approximation

Decomposing the Hamiltonian of Eq. 2.16 in terms of the ground state annihilation operator $\hat{a}_0$ and the excited states operators $\hat{a}_{\bar{p}}$:

$$\hat{\mathcal{H}} = \frac{V_0}{2L^3}\hat{a}_0^\dagger\hat{a}_0^\dagger\hat{a}_0\hat{a}_0 + \sum_{\bar{p}} \frac{\bar{p}^2}{2m}\hat{a}_{\bar{p}}^\dagger\hat{a}_{\bar{p}} + \frac{V_0}{2L^3}\sum_{\bar{p}\neq 0}(4\hat{a}_0^\dagger\hat{a}_{\bar{p}}^\dagger\hat{a}_0\hat{a}_{\bar{p}} + \hat{a}_{\bar{p}}^\dagger\hat{a}_{-\bar{p}}^\dagger\hat{a}_0\hat{a}_0 + \hat{a}_0^\dagger\hat{a}_0^\dagger\hat{a}_{\bar{p}}\hat{a}_{-\bar{p}}) \quad . \tag{2.27}$$

Where, imposing the momentum conservation, there are only quadratic terms in $\hat{a}_{\bar{p}}$. In particular, a factor 4 in the first term of the second sum corresponds to the following cases:

1. $\bar{p_1} = 0, \qquad \bar{p_2} = \bar{p}, \qquad \bar{q} = 0$
2. $\bar{p_1} = 0, \qquad \bar{p_2} = \bar{p}, \qquad \bar{q} = \bar{p}$
3. $\bar{p_1} = \bar{p}, \qquad \bar{p_2} = 0, \qquad \bar{q} = 0$
4. $\bar{p_1} = \bar{p}, \qquad \bar{p_2} = 0, \qquad \bar{q} = -\bar{p}$

The cases 1,3 do not involve the transfer of momentum between two particles ($\bar{q} = 0$) and are called "direct terms". In thlengthe cases 2,4 instead there is a transfer of momentum between the particles, so are called "exchange terms".

Now further simplification are necessary:

- In the third term of 2.27, considering all the particles in the ground state, $\hat{a}_0^\dagger\hat{a}_0 = N$. Where N is the total number of particles.
- To simplify the first term, it is possible to use the complete normalization relation $\hat{a}_0^\dagger\hat{a}_0 + \sum_{\bar{p}\neq 0}\hat{a}_{\bar{p}}^\dagger\hat{a}_{\bar{p}} = N$

The normalization relation can be rewritten as :

$$\hat{a}_0^\dagger\hat{a}_0^\dagger\hat{a}_0\hat{a}_0 \simeq N^2 - 2N\sum_{\bar{p}\neq 0}\hat{a}_{\bar{p}}^\dagger\hat{a}_{\bar{p}}^\dagger \quad . \tag{2.28}$$

Substituting the 2 relations above and 2.20 in eq 2.27:

$$\hat{\mathcal{H}} = \frac{1}{2}g\rho N + \sum_{\bar{p}}\hat{a}_{\bar{p}}^\dagger\hat{a}_{\bar{p}} + \frac{1}{2}g\rho\sum_{\bar{p}\neq 0}(2\hat{a}_{\bar{p}}^\dagger\hat{a}_{\bar{p}} + \hat{a}_{\bar{p}}^\dagger\hat{a}_{-\bar{p}}^\dagger + \hat{a}_{\bar{p}}\hat{a}_{-\bar{p}}) \quad . \tag{2.29}$$

It is possible also to express the potential V_0 using a first order perturbation theory:

$$V_0 = g(1 + \frac{g}{V}\sum_{\bar{p}\neq 0}\frac{m}{\bar{p}^2}) \tag{2.30}$$

This adds a diagonal term in the Hamiltonian :

$$\hat{\mathcal{H}} = \frac{1}{2}g\rho N + \sum_{\bar{p}}\hat{a}_{\bar{p}}^\dagger\hat{a}_{\bar{p}} + \frac{1}{2}g\rho\sum_{\bar{p}\neq 0}(2\hat{a}_{\bar{p}}^\dagger\hat{a}_{\bar{p}} + \hat{a}_{\bar{p}}^\dagger\hat{a}_{-\bar{p}}^\dagger + \hat{a}_{\bar{p}}\hat{a}_{-\bar{p}} + \frac{mg\rho}{\bar{p}^2}) \quad . \tag{2.31}$$

The equation 2.31 can be diagonalized using the linear transformation known as the Bogoliubov transformation:

$$\hat{a}_{\bar{p}} = u_{\bar{p}}\hat{b}_{\bar{p}} + v^*_{-\bar{p}}\hat{b}^\dagger_{-\bar{p}}, \qquad \hat{a}^\dagger_{\bar{p}} = u^*_{\bar{p}}\hat{b}^\dagger_{\bar{p}} + v_{-\bar{p}}\hat{b}_{-\bar{p}} \qquad . \tag{2.32}$$

The operators $\hat{b}^\dagger_{\bar{p}}, \hat{b}_{\bar{p}}$ will obey the same bosonic commutation rules of the original operators $\hat{a}^\dagger_{\bar{p}}, \hat{a}_{\bar{p}}$:

$$[\hat{a}_{\bar{p}}, \hat{a}^\dagger_{\bar{p}'}] = [\hat{b}_{\bar{p}}, \hat{b}^\dagger_{\bar{p}'}] = \delta_{\bar{p},\bar{p}'} \qquad . \tag{2.33}$$

This commutation relation imposes a constraint on the parameters $u_{\bar{p}}, v_{-\bar{p}}$ such as:

$$|u|^2_{\bar{p}} - |v|^2_{-\bar{p}} = 1 \qquad , \tag{2.34}$$

or:

$$u_{\bar{p}} = cosh(\alpha_{\bar{p}}), \qquad v_{-\bar{p}} = sinh(\alpha_{\bar{p}}) \qquad . \tag{2.35}$$

The value of $\alpha_{\bar{p}}$ have to be choosen in order to cancel the off-diagonal terms in 2.31 that are generated after the Bogoliubov transformation.

So the condition that $\alpha_{\bar{p}}$ has to satisfy is:

$$\frac{g\rho}{2}(|u|^2_{\bar{p}} + |v|^2_{-\bar{p}}) + (\frac{\bar{p}^2}{2m} + g\rho)u_{\bar{p}} - v_{-\bar{p}} = 0 \qquad . \tag{2.36}$$

Using the duplication relations for hyperbolic functions $cosh(2\alpha_{\bar{p}}) = cosh^2(\alpha_{\bar{p}}) + sinh^2(\alpha_{\bar{p}})$ and $\sinh(2\alpha_{\bar{p}}) = 2sinh(\alpha_{\bar{p}})cosh(\alpha_{\bar{p}})$ the condition is :

$$cotgh(2\alpha_{\bar{p}}) = \frac{-(\frac{\bar{p}^2}{2m} + g\rho)}{g\rho} \qquad . \tag{2.37}$$

So finally the two coefficients are:

$$u_{\bar{p}}, v_{-\bar{p}} = \pm\sqrt{\frac{\bar{p}^2/2m + g\rho}{2\epsilon(\bar{p})} \pm \frac{1}{2}} \qquad . \tag{2.38}$$

where $\epsilon(\bar{p})$ is the dispersion law of the Bogoliubov excitation spectrum:

$$\epsilon(\bar{p}) = \sqrt{\frac{g\rho}{m}\bar{p}^2 + \left(\frac{\bar{p}^2}{2m}\right)^2} \qquad . \tag{2.39}$$

Substituting the obtained values of $u_{\bar{p}}, v_{-\bar{p}}$ of Eq. 2.38 in 2.29, the diagonalized form of the Hamiltonian is:

$$\hat{\mathcal{H}} = E_0 + \sum_{\bar{p}\neq 0} \epsilon(\bar{p})\hat{b}^\dagger_{\bar{p}}\hat{b}_{\bar{p}} \qquad . \tag{2.40}$$

Where E_0 is the ground state energy (calculated with a first order perturbation theory) :

$$E_0 = \frac{1}{2}g\rho N + \frac{1}{2}\sum_{\bar{p}\neq 0}\left[\epsilon(\bar{p}) - g\rho - \frac{\bar{p}^2}{2m} + \frac{m(g\rho)^2}{\bar{p}^2}\right] \qquad . \tag{2.41}$$

The physical meaning of the Bogoliubov transformation is to reconduct the original system made by interacting particles (described by the standard creation

and annihilation operators) to a system of non-interacting quasi-particles (collective excitations). In particular a real particle $\hat{a}_{\bar{p}}$ can be described as the superposition of the forward propagating many quasi-particles $u_{\bar{p}}\hat{b}_{\bar{p}}$ and the backward propagating many quasi-particles $v^*_{-\bar{p}}\hat{b}^\dagger_{-\bar{p}}$

The ground state for an interacting Bose gas at T=0 now is defined as the vacuum state for the Bogoliubov annihilation operator:

$$\hat{b}_{\bar{p}}\,|0\rangle = 0 \qquad \forall \bar{p} \neq 0 \qquad . \tag{2.42}$$

2.5 Gross-Pitaevskii equation

Applying the Schrödinger equation $i\hbar\frac{d\hat{\Psi}}{dt} = \hat{\mathcal{H}}\hat{\Psi}$ where the Hamiltonian, in the mean field approximation and in presence of an external potential, is $\hat{\mathcal{H}} = \frac{\hat{p}^2}{2m} + V_{ext} + g|\hat{\Psi}|^2$ we find the time independent Gross Pitaevskii equation (GPE):

$$i\hbar\frac{d\hat{\Psi}}{dt} = \left(-\frac{\hbar^2\nabla^2}{2m} + V_{ext} + g|\hat{\Psi}|^2\right)\hat{\Psi} \qquad . \tag{2.43}$$

Where the classic wave function[2] of the condensate is $\Psi(r) = \sqrt{\rho}\phi(r)$ and ϕ is the single particle wave function, that is normalized by $|\phi|^2 = 1$. Therefore the particle density is $\rho(r) = |\Psi(r)|^2$. This replacement of $\hat{\Psi}$ with a classic Ψ would be wrong for a realistic potential but it is accurate if one uses an effective mean field potential (eq.2.20) where the Born approximation is applicable.

In the GPE the total potential consists of an external potential V_{ext} and a nonlinear term $g\rho$ which describes the mean field potential of the other atoms.

In general the chemical potential μ is the eigenvalue who solves the GPE:

$$\mu\Psi = \left(-\frac{\hbar^2\nabla^2}{2m} + V_{ext} + g\rho\right)\Psi \qquad . \tag{2.44}$$

Considering the ground state ($p = -i\hbar\nabla = 0$) of an homogeneous and interacting gas, without an external potential, the GPE reduces to $g|\Psi|^2 = \mu$, coherently with the value found in Eq. 2.22, and therefore the unperturbed wave function Ψ_0 will evolve as following :

$$i\hbar\frac{\partial\Psi_0}{\partial t} = \mu\Psi_0 \longrightarrow \Psi_0 e^{-\frac{i}{\hbar}\mu t} \qquad . \tag{2.45}$$

2.5.1 Bogoliubov excitation spectrum

In order to calculate the excitation spectrum it is possible to replace the field operator 2.15 with a classical field, not only for the ground state as done in the preceding section, but also for excited states with momentum $k \neq 0$. With this treatment of the GPE Bogoliubov founds the dispersion relation for elementary excitations of a BEC.

The classical field, including an explicit time dependence for the elementary excitations is:

$$\Psi(\bar{r},t) = \Psi_0(\bar{r})e^{-\frac{i}{\hbar}\mu t} + \Psi_{\bar{k}}e^{\frac{i}{\hbar}[\bar{k}\bar{r}-(\mu+\omega)t]} + \Psi_{-\bar{k}}e^{-\frac{i}{\hbar}[\bar{k}\bar{r}-(\mu-\omega)t]} \qquad . \tag{2.46}$$

[2]The operatorial notation $\hat{}$ is eliminated from now on.

Where $\Psi_{\bar{k}}$ and $\Psi_{-\bar{k}}$ are the amplitudes of the excitations respectively for forward and backward propagating plane waves. Furthermore $\Psi_{\bar{k}}$ and $\Psi_{-\bar{k}}$ are introduced to satisfy the energy conservation during the simultaneous creation or annihilation of two particles in the excited states with momentum respectively $\bar{k}$ or $-\bar{k}$, as shown in Fig. 2.3.

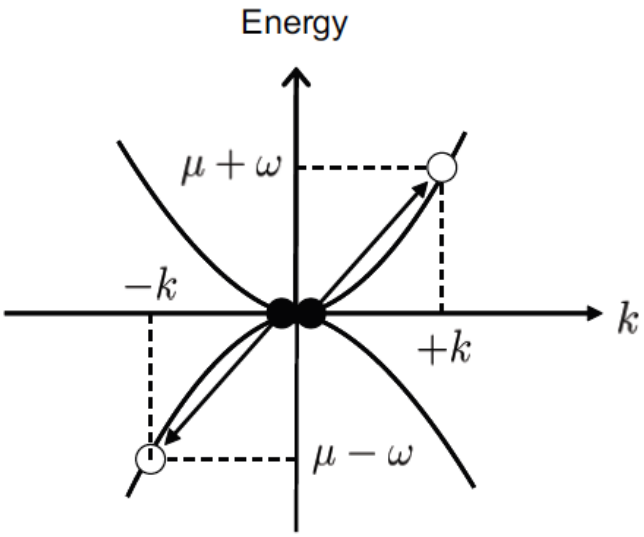

Figura 2.3. Conservation of the energy for the simultaneous creation of two quasi-particles with opposite momentum. Taken from **??**.

With this approach we are looking for weak deviations around a homogeneous and stationary state of density ρ_0 and energy μ. We will obtain the linear evolution equations for $\Psi_{\bar{k}}$ and its complex conjugate $\Psi_{-\bar{k}}$. Such equations are known as the Bogoliubov-De Gennes equations.

The BdG matrix in momentum space has diagonal terms shifted to μ and the off-diagonal ones are nonzero and proportional to μ.

Substituting the trial function 2.46 in the GPE 2.44, without an external potential, the GPE becomes:

$$i\hbar\frac{\partial\Psi}{\partial t} = e^{-i\frac{\mu}{\hbar}t}[\mu\psi_0 + (\mu+\omega)\Psi_{\bar{k}})e^{-\frac{i}{\hbar}\omega t} + (\mu-\omega)\Psi_{-\bar{k}})e^{\frac{i}{\hbar}\omega t}] = (\frac{\hbar^2k^2}{2m}+\mu)\Psi(\bar{r},t) \quad . \tag{2.47}$$

At this point equating terms in $e^{-\frac{i}{\hbar}[(\mu+\omega)t]}$ and $e^{-\frac{i}{\hbar}[(\mu-\omega)t]}$ in the equation above we obtain a system of two coupled equations :

$$\begin{cases} (\mu+\omega)\Psi_{\bar{k}} &= (\frac{\hbar^2k^2}{2m}+2\mu)\Psi_{\bar{k}} + \mu\Psi_{-\bar{k}} \\ (\mu-\omega)\Psi_{-\bar{k}} &= (\frac{\hbar^2k^2}{2m}+2\mu)\Psi_{-\bar{k}} + \mu\Psi_{\bar{k}} \end{cases} \quad . \tag{2.48}$$

That can be rewritten in matricial form:

$$[\mathbf{M}]\begin{bmatrix}\Psi_{\bar{k}}\\ \Psi_{-\bar{k}}\end{bmatrix} = \begin{bmatrix}\frac{\hbar^2k^2}{2m}+\mu & -\mu \\ -\mu & \frac{\hbar^2k^2}{2m}+\mu\end{bmatrix}\begin{bmatrix}\Psi_{\bar{k}}\\ \Psi_{-\bar{k}}\end{bmatrix} = \omega\begin{bmatrix}\Psi_{\bar{k}} \\ -\Psi_{-\bar{k}}\end{bmatrix} \quad . \tag{2.49}$$

So it is possible to obtain the eigen-energies $\omega_\pm$ finding the eigenvalues of :

$$\begin{bmatrix} \frac{\hbar^2 k^2}{2m} + \mu - \omega & -\mu \\ -\mu & \frac{\hbar^2 k^2}{2m} + \mu + \omega \end{bmatrix} \begin{bmatrix} \Psi_{\bar{k}} \\ \Psi_{-\bar{k}} \end{bmatrix} = 0 \quad . \tag{2.50}$$

It follows that the eigen-energies of the excitations are given by:

$$\omega(k)_\pm = \pm\sqrt{\frac{\hbar^2 k^2}{2m}\left(\frac{\hbar^2 k^2}{2m} + 2g|\Psi_0|^2\right)} \quad . \tag{2.51}$$

To obtain the solutions for positive frequencies ω_+, it is necessary to combine one of the preceding equations 2.48 with the normalization condition:

$$\begin{cases} \Psi^{(+)}_{\bar{k}} = -\frac{\mu}{\frac{\hbar k^2}{2m} + \mu - \omega_+}\Psi^{(+)}_{-\bar{k}} = -\frac{\mu \Psi^{(+)}_{-\bar{k}}}{\Delta} \\ |\Psi^{(+)}_{\bar{k}}|^2 + |\Psi^{(+)}_{-\bar{k}}|^2 = 1 \end{cases} , \tag{2.52}$$

The solution are two plane waves $\Psi^{(+)}_{\bar{k}}$ and $\Psi^{(+)}_{-\bar{k}}$:

$$\begin{cases} \Psi^{(+)}_{\bar{k}} = \frac{\mu}{\sqrt{\mu^2+\Delta^2}} \\ \Psi^{(+)}_{-\bar{k}} = -\frac{\Delta}{\sqrt{\mu^2+\Delta^2}} \end{cases} . \tag{2.53}$$

With the same procedure for the negative frequencies ω_- we obtain:

$$\begin{cases} \Psi^{(-)}_{\bar{k}} = \frac{\mu}{\sqrt{\mu^2+\Delta^2}} \\ \Psi^{(-)}_{-\bar{k}} = \frac{\Delta}{\sqrt{\mu^2+\Delta^2}} \end{cases} . \tag{2.54}$$

The eigen-functions are a linear combination of forward and backward propagating waves :

$$\Psi^{(+)}(\bar{r},t) = \Psi^{(+)}_{\bar{k}} e^{i[+\bar{k}\bar{r}-(\mu+\omega_+)t]} + \Psi^{(+)}_{-\bar{k}} e^{i[-\bar{k}\bar{r}-(\mu+\omega_+)t]} \quad . \tag{2.55}$$

At small wave-numbers $\Delta \simeq \mu$ and the two solutions can be expressed in a trigonometric form:

$$\begin{cases} \Psi^{(+)}(\bar{r},t) = i\sqrt{2}\sin(\bar{k}\bar{r})e^{-i(\mu+\omega_+)t} \\ \Psi^{(-)}(\bar{r},t) = \sqrt{2}\cos(\bar{k}\bar{r})e^{-i(\mu+\omega_-)t} \end{cases} . \tag{2.56}$$

The complex solution $\Psi^{(+)}(\bar{r},t)$ represent the spatial phase modulation of a weakly interacting BEC.

As well the real solution $\Psi^{(-)}(\bar{r},t)$ is the spatial amplitude modulation of the condensate.

For large wave-numbers the shift from the excitation spectrum $\Delta \simeq 0$ and both the eigen-states become plane waves.

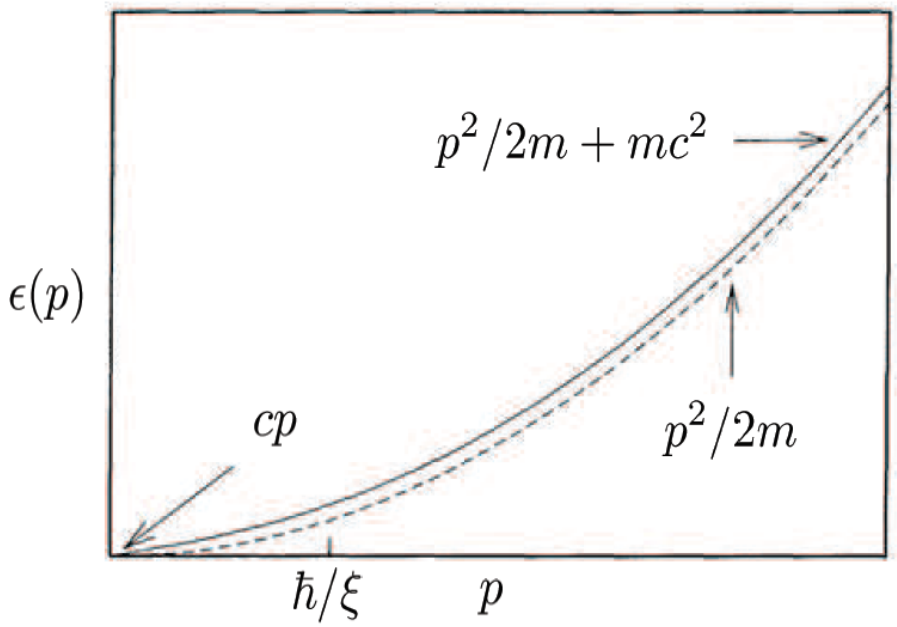

Figura 2.4. Bogoliubov dispersion of elementary excitations. The transition between the phonon mode ($\epsilon(p) = cp$) and the free particle mode ($\epsilon(p) = p^2/2m + mc^2$) takes place at $p \simeq \hbar/\epsilon$.

2.5.2 Sound velocity and healing length in the Bogoliubov framework

Taking a look at the upper branch of the Bogoliubov dispersion law[3] (plotted in fig 2.4):

$$\epsilon(p) = \sqrt{\frac{g\rho}{m}p^2 + \left(\frac{p^2}{2m}\right)^2} \quad , \tag{2.57}$$

is clear that for low momentum $p \ll mc_s = \sqrt{mg\rho}$ the Bogoliubov dispersion law is well approximated by a phonon-like linear dispersion:

$$\epsilon(p) = c_s p \tag{2.58}$$

where $c_s = \sqrt{g\rho/m}$ is the sound velocity. This result is in agreement with the formula 2.26, extrapolated only by hydrodynamical consideration.

According to the Bogoliubov theory, the low momentum excitations of an interacting Bose gas are the sound waves.

These excitations can also be regarded as the Nambu-Goldstone modes associated with breaking of gauge symmetry caused by Bose-Einstein condensation[24].

In this low momentum regime, a real particle is represented by the coherent superposition of forward and backward propagating many quasi-particles: $\hat{a}_p = u_p\hat{b}_p + v^*_{-p}\hat{b}^\dagger_{-p}$, where $|u_p| \simeq |v_{-p}| \simeq \sqrt{mc_s/2p} \gg 1$.

[3] That is the only one that can have an optical equivalent.

Looking at the high momentum limit $p \gg mc_s$ the dispersion law is reduced to the free-particle form:

$$\epsilon(p) = \frac{p^2}{2m} + g\rho \qquad . \tag{2.59}$$

The interaction energy $g\rho = mc_s^2$ can be reconducted to the third perturbative term in Eq. 2.29 that take in account the contribution coming from the excited states. In this high momentum regime a forward propagating real particle is almost identical to a forward propagating quasi-particles: $\hat{a}_p \simeq \hat{b}_p$, $(u_p \simeq 1, v_{-p} \simeq 0)$.

The transition from the phonon to the free-particle regime takes place when the kinetic energy is equal to the interaction energy:

$$\frac{p^2}{2m} = g\rho \qquad . \tag{2.60}$$

The healing length can be defined again as the cross-point lenght between the two regimes. Writing $p = \frac{\hbar}{\xi}$ in fact we find:

$$\xi = \frac{\hbar}{\sqrt{2}mc_s} \qquad . \tag{2.61}$$

This is the length scale such that density and phase fluctuations in the condensate are removed by the interaction between the particles.

In the following chapter all the quantities expressed in this section will be translated in the optical context.

Capitolo 3

NLSE vs GPE: a space-time mapping

In this chapter it will be derived the NLSE for a lossless system in the paraxial approximation. After that it will be discussed the analogy between our optical system and a weakly interacting Bose Gas. Finally it will be discussed the theoretical proposals for the experiments that we realized.

3.1 Propagation of light through a Kerr nonlinear medium

This section focuses on the derivation of the general propagation equation for laser light in a passive optical medium. The general equations that describe the propagation of light through a nonlinear medium can be derived starting from the Maxwell's equations. In all this thesis we deal with non magnetic materials so from now on $\mu_r = 1$.

Considering a medium with no free charges ($\rho(\vec{r},t) = 0$, $\vec{J}(\vec{r},t) = 0$) and substituting $\vec{D} = \epsilon_0\vec{E} + \vec{P}$ the Maxwell's equations are:

$$\begin{cases} \vec{\nabla}\cdot\vec{D} = 0 & , \\ \vec{\nabla}\cdot\vec{B} = 0 & , \\ \vec{\nabla}\times\vec{E} = \frac{\partial\vec{B}}{\partial t} & , \\ \vec{\nabla}\times\vec{B} = \mu_0\frac{\partial\vec{D}}{\partial t} = \frac{1}{c^2}\frac{\partial\vec{E}}{\partial t} + \frac{\partial\vec{P}}{\partial t} & . \end{cases} \tag{3.1}$$

Taking the curl of both the sides of the third equation above and using the identity $\vec{\nabla}\times\vec{\nabla}\times\vec{E} = \vec{\nabla}\cdot(\vec{\nabla}\cdot\vec{E}) - \vec{\nabla}^2\vec{E}$ we obtain the well known wave equation :

$$-\vec{\nabla}^2\vec{E} = -\frac{\partial}{\partial t}(\vec{\nabla}\times\vec{B}) \longrightarrow \vec{\nabla}^2\vec{E} - \frac{1}{c^2}\frac{\partial^2\vec{E}}{\partial t^2} = \mu_0\frac{\partial^2\vec{P}}{\partial t^2} \quad . \tag{3.2}$$

We need two assumptions on the polarization of the medium:

- The polarization response of the material is instantaneous[1].

[1]This assumption is not valid for a non local medium, where the polarization response spreads in space in a small time dependent on the characteristic of the medium.

- The nonlinearity is weak enough that the polarization can be treated perturbatively i.e $\vec{P}_{NL} \ll \vec{P}_L$.

The second assumption can be rewritten as:

$$\vec{P} = \epsilon_0(\chi^{(1)}\vec{E} + \chi^{(2)}\vec{E}^2 + \chi^{(3)}\vec{E}^3 + ...) = \vec{P}_L + \vec{P}_{NL} \quad . \tag{3.3}$$

In our experiment we deal with a centro-symmetric material where the second order susceptibility $\chi^{(2)} = 0$. Since the polarization can be treated perturbatively the wave equation can be solved initially with $\vec{P}_{NL} = 0$ and the nonlinear polarization dependence will be added later[30][31].

Because Eq. 3.2 is linear with the electric field, it is useful to write it in the frequency domain ($\frac{\partial}{\partial t} \to i\omega$), without the nonlinear polarization.

The electric field in the frequency domain is obtained by a Fourier transform

$$\tilde{E}(\vec{r},\omega) = \int_{-\infty}^{+\infty} dt A(\vec{r},t)e^{i(k_0 z-\omega t)}e^{i\omega t} = A(\vec{r},\omega)e^{ik_0 z} \quad . \tag{3.4}$$

Where $k_0 = \frac{\omega_0}{c}\sqrt{\epsilon(\omega_0)}$.

The frequency dependent linear polarization is [2]

$$\tilde{P}_{linear}(\omega) = \epsilon_0(\omega)\tilde{\chi}^{(1)}(\omega)\tilde{E}(\omega) \quad . \tag{3.5}$$

So we can write the well-known Helmholtz equation:

$$[\vec{\nabla}^2 + \frac{\omega^2}{c^2}(1 + \tilde{\chi}^{(1)}(\omega)]\tilde{E}(\vec{r},\omega) = 0 \quad . \tag{3.6}$$

Where the electrical permittivity $\epsilon(\omega)$ can be expressed in function of the first order susceptibility $\tilde{\chi}^{(1)}$. Moreover, from the real and imaginary part of $\epsilon(\omega)$ (related by the Kramers-Kronig relations), we can extrapolate respectively the linear refractive index n and the absorption coefficient α.

$$\begin{cases} 1 + \tilde{\chi}^{(1)}(\omega) = \epsilon(\omega) & , \\ \epsilon(\omega) = (n + i\frac{\alpha c}{2\omega})^2 & , \\ n(\omega) = 1 + \frac{1}{2}Re[\tilde{\chi}^{(1)}(\omega)] & , \\ \alpha(\omega) = \frac{\omega}{nc}Im[\tilde{\chi}^{(1)}(\omega)] & . \end{cases} \tag{3.7}$$

A further necessary simplification is to consider the imaginary part of the first order susceptibility (the absorption coefficient $\alpha(\omega)$), that is responsable of the losses, small compared to the real part, so that we can replace $\epsilon(\omega)$with n^2. If necessary the losses can be introduced later in a perturbative manner.

The Helmholtz equation for a linear polarization and neglecting the losses becomes:

$$[\vec{\nabla}^2 + \frac{\omega^2}{c^2}n^2(\omega)]\tilde{E}(\vec{r},\omega) = 0 \quad . \tag{3.8}$$

Adding a spatial dependence in the general form (frequency-dependent) of the electric susceptibility we can write it as :

$$\chi(\vec{r}_\perp,\omega) = \chi(\omega) + \delta\chi(\vec{r}_\perp) \quad , \tag{3.9}$$

[2]The notation ˜ indicates a Fourier transform: $\tilde{\chi}^{(1)}(\omega) = \int_{-\infty}^{+\infty}\chi^{(1)}(t-t')e^{i\omega t'}dt'$.

where the homogeneous contribution $\chi(\omega) = \tilde{\chi}^{(1)}(\omega) + \frac{3}{4}\tilde{\chi}^{(3)}(\omega)|\tilde{E}(\vec{r},\omega)|^2$ takes into account the chromatic dispersion of the medium, while the linear modulation $\delta\chi(\vec{r}_\perp)$ can comes from the existence of spatial inhomogeneities and/or from an optical confinement [29].

In the experiments described in Chapters 6 and 7 a spatial modulation of the susceptibility can be introduced with a spatially dependent intensity profile of the beam that excites the medium and induce a non uniform nonlinear response.

Now we want to introduce the nonlinear polarization term in 3.6, that can be written as $\vec{P}_{NL} = \frac{3}{4}\epsilon_0\chi^{(3)}\vec{E}^2\vec{E}$.

We consider a monochromatic beam and therefore $\omega = \omega_0$ and for simplicity of notation also $\tilde{\chi}(\omega_0) = \chi$.

First to insert the nonlinear polarization in the wave equation we have to assume that the nonlinear polarization is a slowly varying function in time.

In fact in the time domain

$$\vec{P}_{NL}(z,t) = \vec{p}_{NL}(z,t)e^{i(\omega_0 t - k_0 z)} \quad , \tag{3.10}$$

where $\vec{p}_{NL} = \epsilon_0\frac{3}{4}\chi^{(3)}|\vec{A}|^2\vec{A}$.

Expanding the double time derivative and doing the solid (for a CW) SVEA in time, i.e $\frac{\partial^2\vec{P}_{NL}}{\partial t^2} \simeq \omega_0\frac{\partial\vec{p}_{NL}}{\partial t} \ll \omega_0^2\vec{p}_{NL}$, the nonlinear polarization can be simplified as following :

$$\frac{\partial^2\vec{P}_{NL}}{\partial t^2} = (\frac{\partial^2\vec{p}_{NL}}{\partial t^2} + 2i\omega_0\frac{\partial\vec{p}_{NL}}{\partial t} - \omega_0^2\vec{p}_{NL})e^{i(\omega_0 t - k_0 z)} \to -\omega_0^2\vec{p}_{NL}e^{i(\omega_0 t - k_0 z)} \quad . \tag{3.11}$$

Now the nonlinear polarization 3.11 can be added to the Helmholtz equation 3.6. Separating the gradient for the propagation direction z and the transverse plane $(x,y) = r_\perp$, this leads to:

$$[\vec{\nabla}_\perp^2 + \frac{\partial^2}{\partial z^2} + \frac{\omega_0^2}{c^2}(1 + \chi^{(1)} + \delta\chi(\vec{r}_\perp) + \frac{3}{4}\chi^{(3)}|\vec{E}|^2)]\vec{E}(\vec{r}_\perp, z) = 0 \quad . \tag{3.12}$$

That can be rewritten in terms of the permittivity ϵ:

$$[\vec{\nabla}_\perp^2 + \frac{\partial^2}{\partial z^2} + \frac{\omega_0^2}{c^2}(\epsilon + \delta\epsilon(\vec{r}_\perp) + \frac{3}{4}\chi^{(3)}|\vec{E}(\vec{r}_\perp, t)|^2)]\vec{E}(\vec{r}_\perp, z) = 0 \quad . \tag{3.13}$$

The spatial modulation of the linear dielectric constant $\delta\epsilon(\vec{r}_\perp, z) \simeq \delta\epsilon(\vec{r}_\perp)$ is assumed to be slowly varying along the propagation direction z.

Another assumption that must be done is that the local propagation direction of the energy can be identified with a direction normal to the wavefronts. This is the so-called paraxial wave approximation and it remains valid as long as divergence angles remain well below 1 rad. Decomposing the electric field in its real and complex part :

$$\vec{E}(\vec{r}_\perp, z) = \frac{1}{2}A(\vec{r}_\perp, z)e^{ik_0 z} + c.c. \tag{3.14}$$

where $A(\vec{r_\perp}, z)$ is the envelope of the electric field.

Injecting this into 3.13 we obtain:

$$\frac{\partial^2 A(\vec{r}_\perp,z)}{\partial z^2}e^{ik_0 z} + 2ik_0\frac{\partial A(\vec{r}_\perp,z)}{\partial z}e^{ik_0 z} - k_0^2 A(\vec{r}_\perp,z)e^{ik_0 z} = \\ -\nabla_\perp^2 A(\vec{r}_\perp,z)e^{ik_0 z} - \frac{\omega^2}{c^2}[\epsilon + \delta\epsilon(\vec{r}_\perp,z) + \frac{3}{4}\chi^{(3)}|A(\vec{r}_\perp,z)|^2]A(\vec{r}_\perp,z)|e^{ik_0 z} \quad . \tag{3.15}$$

Now it is possible to simplify the exponential terms and to assume that the envelope $A(\vec{r}_\perp,z)$ is a slowly varying function in space (SVEA approximation in space.) or in other terms that :

$$\frac{|\nabla_\perp^2 A|}{k_0^2} \simeq \frac{1}{k_0}\frac{|\partial A|}{\partial z} \ll 1 \quad . \tag{3.16}$$

Under this assumption the second derivative in z can be neglected.

Defining also a coupling constant $g = -\frac{3k_0\chi^{(3)}}{8\epsilon}$ and an external potential $V_0(\vec{r}_\perp,z) = -k_0\delta\epsilon(\vec{r}_\perp,z)/(2\epsilon)$, we can rewrite the nonlinear Schrödinger equation (NLSE) in the form:

$$i\frac{|\partial A(\vec{r}_\perp,z)|}{\partial z} = (-\frac{1}{2k_0}\nabla_\perp^2 + V_0 + g|A(\vec{r}_\perp,z)|^2)A(\vec{r}_\perp,z) \quad , \tag{3.17}$$

that is the one that will be considered in this report for its immediate analogy with the GPE 2.43.

3.1.1 General propagation equation

For completeness here is reported also the more general propagation equation for a quasi-monochromatic beam.

Going back to 3.8 we can define the medium-dependent wave vector

$$k(\omega) = \frac{\omega}{c}n(\omega) \quad , \tag{3.18}$$

and applying the same SVEA approximation after expressing the electric field in its real and complex part:

$$(\nabla_\perp^2 + 2ik_0\frac{\partial}{\partial z} - k_0^2 + k^2(\omega))A(\vec{r}_\perp,t) = 0 \quad , \tag{3.19}$$

and:

$$k^2(\omega) - k_0^2 = (k(\omega)-k_0)(k(\omega)+k_0) \simeq 2k_0(k(\omega)-k_0) \quad . \tag{3.20}$$

If we want to obtain also information about the group velocity and the second order dispersion we can make the usually well justified approximation (a continuous signal is $\simeq \delta(\omega-\omega_0)$ in the frequency domain) that $k(\omega)$ is a slowly varying function of ω and can be expanded in a power series:

$$k(\omega) = k_0 + \frac{\partial}{\partial\omega}k(\omega)|_{\omega=\omega_0)}(\omega-\omega_0) + \frac{1}{2!}\frac{\partial^2}{\partial\omega^2}k(\omega)|_{\omega=\omega_0}(\omega-\omega_0)^2 + ... \tag{3.21}$$

Here, $k_0 = n_0\omega_0/c$ is related to the phase velocity in the medium ($v_{ph} = \frac{\omega}{k_0}$, $k_1 = \frac{\partial k}{\partial \omega}|_{\omega=\omega_0} = \frac{1}{v_g}$ is the inverse of the group velocity. $k_2 = \frac{\partial^2 k}{\partial \omega^2}|_{\omega=\omega_0}$ is the group velocity dispersion.

The group velocity dispersion can be positive or negative and it is responsable of chirp .

Now it is possible to add again the nonlinear polarization term and the modulation of the dielectric constant, that manifests itself as an external potential V_0.

Finally the expansion of $k(\omega)$ can be rewritten in the time-domain. Adding also the losses we obtain a complete waves equation:

$$i\frac{|\partial A(\vec{r}_\perp, z)|}{\partial z} = (-\frac{1}{2k_0}\nabla_\perp^2 + V_0 + g|A(\vec{r}_\perp, z)|^2 - \frac{i}{v_g}\frac{\partial}{\partial t} + \frac{k_2}{2}\frac{\partial^2}{\partial t^2})A(\bar{r}_\perp, z) - \frac{i}{2}\alpha A \quad , \tag{3.22}$$

that describes the wave-matter interaction for a broadband continuous laser or a pulsed laser.

3.2 A space-time mapping

As seen in the preceding section when the classical optical field is a slowly varying function of space and time it satisfies a nonlinear wave equation that is formally analogue to the GPE for a weakly interacting Bose gas.

Here the amplitude of the electric field of the optical beam play the role of the order parameter for a BEC.

We recall the main equations (3.17,2.43) obtained in the preceding chapter, adding an external potential V to the GPE:

$$\begin{aligned} i\hbar\frac{d\hat{\Psi}}{dt} &= \left(-\frac{\hbar^2\nabla^2}{2m} + V + g|\hat{\Psi}|^2\right)\hat{\Psi} \\ i\frac{|\partial A(\bar{r}_\perp,z)|}{\partial z} &= (-\frac{1}{2k_0}\nabla_\perp^2 + V_0 + g|A(\bar{r}_\perp, z)|^2)A(\bar{r}_\perp, z) \quad . \end{aligned} \tag{3.23}$$

We remark that these two equations are equivalent mathematically, even though they represent two different physical situations.

To understand the equivalence between the two equations we identify the time t of GPE with the space z of NLSE, and the complete laplacian ∇^2 with the transverse laplacian $\nabla_\perp^2$. If these two equations are equivalent (upto some transformations), we expect also that the systems that they describe will exhibit a similar behaviour.

In fact, as said in the introduction, to achieve superfluid phenomenas it is required to deal with a system of weakly-interacting bosons.It is exactly the case of our platform where photons (i.e bosons) weakly interact through optical Kerr effect (OKE).

In particular the interaction constant $g = \frac{4\pi\hbar^2 a}{m}$ in the GPE is positive because of a repulsive mean-field interaction. The interaction constant of the NLSE instead is defined as $g = -\frac{3k_0\chi^{(3)}}{8\epsilon}$.

In order to achieve a superfluid-like behaviour we want the same kind of interaction of the GPE, then the required condition is $\chi^{(3)} < 0$. In this situation the OKE introduced a positive (repulsive) photon-photon interaction that manifest itself as a Kerr self-defocusing.

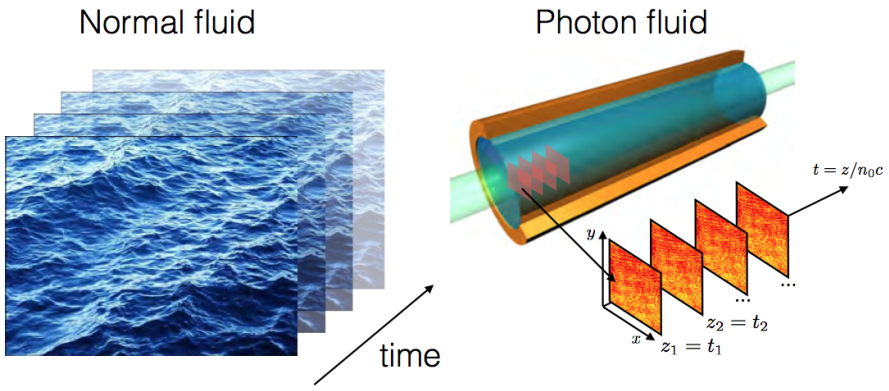

Figura 3.1

In particular, as will be shown in chapter 4, to achieve a self defocusing we work with a frequency smaller than the resonant frequency, i.e. the center of the ^{85}Rb D_2 transition, schematized in 4.1. If we are in the opposite situation, that is blue-detuning (or bigger energy) from the same transition, the system will exhibit a positive nonlinearity and then Kerr self-focusing.

In this framework every slice of the transverse plane of our Rb cell at a given value of the propagation length z can be regarded as corresponding to an instant of time in the GPE dynamic as shown in Fig. 3.1. Therefore every transverse plane is analogue to a snapshot of the time evolution of a 2-D quantum fluid.

The spatial profile of the refractive index $V_0(\bar{r}_\perp, z) = -k_0\delta\epsilon(\bar{r}_\perp, z)/(2\epsilon)$ provides the analog of an external potential for the paraxial photons.

The equivalence between the two equations can be formally established by the equivalence of the following parameters:

$$\begin{cases} \rho \longrightarrow |A|^2 \\ t \longrightarrow \frac{zn_0}{c} \\ \nabla \longrightarrow \nabla_\perp \\ v \longrightarrow \frac{c}{k}\nabla\phi \\ m \longrightarrow k_0 \\ c_s = \sqrt{\frac{g\rho}{m}} \longrightarrow c_s^* = \sqrt{\frac{g|A|^2}{k_0}} \\ \xi = \frac{\hbar}{\sqrt{2}mc_s} \longrightarrow \frac{2\pi}{\sqrt{2}k_0 c_s^*} \end{cases} \tag{3.24}$$

where v denotes the velocity of the fluid of light, $\nabla\phi$ is the phase of the electric field, and ξ is the healing length.

It is worth to notice that, as a consequence of the space–time mapping, the frequencies $\Omega_{Bog}(k_\perp)$ are measured in inverse lengths, in fact in this framework a frequency can be defined as the inverse of the equivalent of the time parameter that corresponds to the propagation length z. Moreover speeds like v_{ph}, c_s and $v_{gr} = \nabla_k\Omega_{Bog}(k_\perp)$ are measured in adimensional units, because they have the physical meaning of propagation angles with respect to the z-axis.

3.3 Hydrodynamical analogy

Once that the space-time mapping presented in the preceding section is clear it can be shown that by reformulating the NLSE it is possible to describe the transverse beam profile as photon a fluid.

In fact the NLSE can be rewritten in terms of hydrodynamical variables, that are similar to the Navier-Stokes equations of fluid dynamics.

The electric field can be re-expressed in terms of a density and a phase as:

$$E_0(r_\perp, z) = \sqrt{\rho(r_\perp, z)} e^{i\phi(r_\perp, z)} \quad . \tag{3.25}$$

where ρ is the photon fluid density with phase ϕ. The photon fluid density, as expected, can be linked with the intensity of the laser beam:

$$\rho = |A|^2 = \frac{2I}{cn_0\epsilon_0} \quad . \tag{3.26}$$

With the relation above we can link the square modulus of the electric field, measured in $\frac{V^2}{m^2}$, with the intensity that experimentally is measured in $\frac{W}{m^2}$.

It is important to remark that in the literature there is a bit of confusion about the definition of n_2, that sometimes comes from $\Delta n = n_2|A|^2$ and sometimes from $\Delta n = n_2 I$ with the quantity Δn that is ever dimensionless.

Depending on this convention the dimensions of n_2 can be $\frac{m^2}{V^2}$ in the first definition or $\frac{m^2}{W}$ in the second one.

Having defined the relation between the square modulus of the of the electric field and the beam intensity the NLSE can be re-expressed writing the interaction term $g|A|^2 = -\frac{k_0 n_2^*}{n_0} I = \frac{k_0 \Delta n}{n_0}$:

$$i\frac{|\partial A(\vec{r}_\perp, z)|}{\partial z} = (-\frac{1}{2k_0}\nabla_\perp^2 + V_0 - \frac{k_0 n_2^*}{n_0} I)A(\vec{r}_\perp, z) \quad , \tag{3.27}$$

where the nonlinear refractive index is

$$n_2^* = -\frac{3}{4}\frac{\chi^{(3)}}{\epsilon_0^2 c} \quad , \tag{3.28}$$

and in this case the dimension-less quantity $\Delta n = n_2^* I$.

In this hydrodinamic approach instead the dimension-less quantity is $\Delta n = n_2\rho = n_2|A|^2$ and therefore $g|A|^2 = k_0\frac{n_2}{n_0}|A|^2$ leads to:

$$n_2 = \frac{gn_0}{k_0} = -\frac{3\chi^{(3)}}{8\epsilon_0} n_0 \quad . \tag{3.29}$$

In both the cases $\chi^{(3)}$ is measured in Cm/V^3 and the factor that allow to do the conversion is $\epsilon_0 c n_0/2$, measured in $\frac{C^2}{Js}$:

$$n_2 = n_2^* \epsilon_0 c n_0/2 \quad . \tag{3.30}$$

And the NLSE can be written as:

$$i\frac{|\partial A(\vec{r}_\perp, z)|}{\partial z} = (-\frac{1}{2k_0}\nabla_\perp^2 + V_0 - \frac{k_0 n_2}{n_0}|A|^2)A(\vec{r}_\perp, z) \quad . \tag{3.31}$$

For this report I have choosen the convention $\Delta n = n_2|A|^2$.

By using the so-called Madelung transformation [40] , that consist in splitting the NLSE 3.27 into real and imaginary part one finds the following hydrodynamical-like equations:

$$\partial_t \rho + \nabla(\rho v) = 0 \qquad , \tag{3.32}$$

$$\partial_t \psi + \frac{v^2}{2} + \frac{c^2 n_2}{n_0^3}\rho - \frac{c^2\nabla^2(\sqrt{\rho})}{2k_0^2 n_0^2\sqrt{\rho}} = 0 \qquad . \tag{3.33}$$

Apart the optical coefficients, Eq. 3.32, 3.33 are identical to those describing the density and the phase dynamics of a 2-D BEC in presence of an attractive (for Kerr self-defocusing) atomic interactions [**?**].

The first one is a continuity equation for the density of the fluid that leads to the mass conservation. In case if it necessary also losses can be added in 3.32 and in such a case it express the non- conservation of the "current" ρ [54].

The second one is an Euler equation that describes a flow with $\vec{v} = \frac{c}{kn_0}\nabla\phi = \nabla\psi$ of an incompressible fluid with density ρ. In this equation the optical nonlinearity, corresponding to the atomic interaction, provides the bulk pressure:

$$P = \frac{c^2 n_2 \rho^2}{2n_0^3} \qquad . \tag{3.34}$$

Also here, as in eq. 2.26, deriving the pressure respect to the density it is possible to obtain an expression for the speed of sound in the optical framework $c_s = \frac{\partial P}{\partial \rho_0}$ [3] :

$$c_s^2 = \frac{c^2 n_2 |A|^2}{n_0^3} \qquad . \tag{3.35}$$

The last term in Eq. 3.33 is the so called quantum potential. In the framework of the de Broglie–Bohm[26] theory, the quantum potential is a term within the Schrödinger equation which acts to guide the movement of quantum particles. It does not have an analogy in real fluids. In quantum fluids it comes from the uncertainty principle, i.e. a local compression of the fluid leads to an increase of the localization of particles Δx and consequently to an increase in the particles momenta Δp.

Therefore the Bohm quantum potential opposes any contraction or stretching of the fluid over distances smaller than the healing length ξ.

3.4 Sound waves in the fluid of light

For our purpose we want to translate in an optical context the Bogoliubov theory for weak perturbations on top of a weakly interacting Bose condensate [8].

The small amplitude perturbations can be described (using the analogy between NLSE and GPE) within the framework of the Bogoliubov theory in terms of sound waves on top of the fluid of light.

[3] In the article of Carusotto [**?**] the speed of sound is instead considered dimension-less and it differ from this expression for a factor c/n_0, i.e. the speed of light in the medium.

So it is possible to affirm that is possible to simulate a phonon-like behaviour (in the context of GPE) using a small perturbation on top of an optical beam because the maths behind is analogue. In order to do that is necessary to calculate how small perturbations on top of a background fluid will propagate.

Experimentally such small perturbation can be generated superposing a low intensity beam (probe) with another one (pump) that is 50-100 times more intense using a Mach-Zender interferometer. The low intensity beam is called probe in the sense that it creates small perturbation on top of the pump beam but the collective motion of the photon-matter coupled quasi-particles is due to the high intensity (or high density in the hydrodynamic context) of the pump.

The approach consists in expressing the density ρ in the equations 3.32, 3.33 as a first order fluctuation ρ_1 around a background solution ρ_0 ($\rho_1 \ll \rho_0$, $\vec{v}_1 \ll \vec{v}_0$):

$$\begin{cases} \rho = \rho_0 + \rho_1 & , \\ \vec{v} = \vec{v}_0 + \vec{v}_1 & . \end{cases} \tag{3.36}$$

If we assume that $\rho_0 = const$ and therefore $\vec{v}_0 = 0$ the continuity equation 3.32 can be rewritten as:

$$\partial_t \rho_1 + \rho_0 \nabla_\perp (\vec{v}_1) = 0 \qquad . \tag{3.37}$$

Considering instead the derivative in the transverse plane of the Euler equation 3.33 we obtain :

$$\partial_t \vec{v}_1 + \vec{v}_1 \nabla \vec{v}_1 + \frac{c^2 n_2}{n_0^3} \nabla_\perp \rho_1 - \frac{c^2}{2k_0^2 n_0^2} \nabla_\perp \left(\frac{\nabla_\perp^2 \sqrt{\rho}}{\sqrt{\rho}} \right) = 0 \qquad . \tag{3.38}$$

The second term of the equation above is a linear function of $\vec{v}_1$ and can be neglected. Expanding the last term one arrives at:

$$\partial_t \vec{v}_1 + \frac{c^2 n_2}{n_0^3} \nabla_\perp \rho_1 - \frac{c^2}{2k_0^2 n_0^2} \nabla_\perp \left(\frac{\nabla_\perp \rho_1}{4\rho_0^2} + \frac{\nabla_\perp^2 \rho_1}{2\rho_0} \right) = 0 \qquad . \tag{3.39}$$

In this equation the first term in the bracket can be neglected since it contains a higher power ρ_0^2 of the background fluid density at the denominator.

Inserting the time derivative of Eq. 3.37 in 3.39 one finally obtains:

$$\partial_t^2 \rho_1 - \frac{c^2 n_2}{n_0^3} \nabla_\perp^2 \rho_1 + \frac{c^2}{4k_0^2 n_0^2} \nabla_\perp^4 \rho_1 = 0 \qquad . \tag{3.40}$$

From the Bogoliubov theory, the weak perturbations can be treated as the sum of two counter-propagating plane-wave solutions, moving in the transverse plane with a frequency $\Omega = \frac{1}{\tau} = \frac{1}{z} \leftrightarrow \frac{n_0}{ct}$, that dimensionally is the inverse of a length, and a transverse momentum $k_\perp$.

Such plane-wave solutions can be expressed as:

$$\rho_1 = u e^{i(\bar{k}_\perp \bar{r} - \Omega t)} + v^* e^{-i(\bar{k}_\perp \bar{r} - \Omega t)} \qquad . \tag{3.41}$$

The complex amplitudes u,v of the two waves satisfy the optical analogue of the Bogoliubov dispersion relation:

$$\Omega(k_\perp) = \sqrt{\frac{k_\perp^2}{2k_0}\left(\frac{k_\perp^2}{2k_0} + 2g|A_0|^2\right)} \quad . \tag{3.42}$$

Sometimes the expression of the optical dispersion relation contain also a factor c/n_0 (speed of light in the medium) as in [10] and eq. 3.58 and in such a case it is measured in s^{-1}. This is done in analogy with the Bogoliubov frequencies that, dividing the eigen-energies 2.51 for a factor $\hbar$ are :

$$\omega(k)_{BOG} = \sqrt{\frac{k^2}{2m}\left(\frac{k^2}{2m} + 2g|\Psi_0|^2\right)} \quad . \tag{3.43}$$

In the linear optics limit of weak light intensities, that in the hydrodynamic context it means a small density of the fluid and a vanishing chemical potential, one has a vanishing speed of sound $c_s \to 0$, a diverging healing length $\xi \to \infty$ and all excitations have a single-particle nature i.e $\Omega \propto k_\perp^2$.

We will work fixing an intensity strong enough to achieve a collective photon behaviour and varying the in plane momentum $k_\perp$. Then the dispersion exhibits a linear relationship between frequency and transverse wave-vector for small $k_\perp$ i.e for small angles $\Omega \propto k_\perp$ that means a phonon-like dispersion.

Meanwhile for large in plane wave-vectors (large angles) the system will show a quadratic relationship $\Omega \propto k_\perp^2$ that characterizes a single particle dispersion.

In particular in the linear dispersion we observe a collective behaviour of the photon fluid and it represents one of the main superfluid features, since it defines a critical Landau velocity.

The crossover between the collective and single particle regime happen for $k_\perp = \frac{2\pi}{\xi}$. Therefore we can define again the healing length in the optical context equating the two terms in the dispersion relation 3.42:

$$\xi = 2\pi\sqrt{-\frac{1}{2k_0 g|A_0|^2}} = \frac{2\pi}{k_0}\sqrt{\frac{\epsilon_0}{\frac{3}{4}\chi^{(3)}|A_0|^2}} = \lambda\sqrt{\frac{-n_0}{2n_2|A_0|^2}} \quad . \tag{3.44}$$

The dispersion relation 3.42 could be derived also without passing through the Madelung rappresentation, but this is often used since it provides a more clear hydrodynamical analogy.

As said before the velocities in the transverse plane are dimension-less in the context of the space time mapping because physically they represent an angle. Also the speed of sound can be transformed in a dimension-less quantity. In fact, since $\frac{zn_0}{c} \longrightarrow t$, we can rewrite c_s of eq. 3.35 multiplying for $\frac{n_0}{c}$ we find:

$$c_s = \sqrt{\frac{g|A|^2}{k_0}} = \sqrt{\frac{-n_2|A_0|^2}{n_0}} \quad , \tag{3.45}$$

And also the healing length can be re-expressed in terms of the speed of sound:

$$\xi = \frac{2\pi}{k_0 c_s\sqrt{2}} \quad . \tag{3.46}$$

3.5 Simulations

3.6 Calculation of the shift

The nonlinear wave equation 3.17 can be rewritten in terms of $n_2 = -\frac{3}{8}\frac{\chi^{(3)}}{\epsilon_0}n_0$ with $\Delta n = n_2|A|^2$

$$\frac{\partial A}{\partial z} = i\frac{\nabla_\perp^2 A(\bar{r}_\perp, z)}{2k_0} - i\frac{k_0 n_2}{n_0}|A|^2 A(\bar{r}_\perp, z) \qquad . \tag{3.47}$$

Remarking that due to the $t \to z$ mapping, the phase velocity is dimensionless, we can calculate the phase velocity from the dispersion relation found in Eq. 2.39:

$$v_{ph} = \frac{\Omega(k_\perp)}{k_\perp} \qquad . \tag{3.48}$$

Transposing the Bogoliubov theory of weak perturbations on top of a weakly interacting BEC in the optical framework the dispersion of the elementary excitations on top of spatially uniform fluid of density $\rho \to |E_0|^2$ at rest can be written as:

$$\Omega(k_\perp) = \sqrt{\frac{\Delta n}{n_0}k_\perp^2 + \frac{k_\perp^4}{4k_0^2}} \qquad . \tag{3.49}$$

with $\Delta n = n_2|A|^2$.

The difference between the nonlinear and the linear regime can be measured by looking at the difference in the pump phase shift in our interference pattern.

The Bogoliubov dispersion relation has a linear and a nonlinear regime, respectively for low ($\Delta n \ll 1$) and high intensities.

In fact the shift is a consequence of the difference in the transverse phase velocity of the Bogoliubov waves for different pump intensities.

The dispersion relation and the phase velocity in the two regimes, that we denote as HI and LI are:

$$\begin{cases} \text{Low intensty :} & \Omega_\perp^{LI} = \frac{k_\perp^2}{2k_0} \longrightarrow v_{ph}^{LI} = \frac{k_\perp}{2k_0} \\ \text{High intensity :} & \Omega_\perp^{HI} = \sqrt{\frac{\Delta n}{n_0}k_\perp^2 + \frac{k_\perp^4}{4k_0^2}} \longrightarrow v_{ph}^{HI} = \frac{k_\perp}{2k_0}\sqrt{1 + \frac{\Delta n}{n_0}\left(\frac{2k_0}{k_\perp}\right)^2} \end{cases} \qquad . \tag{3.50}$$

The shift can now be understood as the difference in distance covered by the low-amplitude excitations due to the difference in phase velocities of the background fluid.

Such a shift can be calculated by computing the difference in distances covered by the HI an LI beams in the same amount of time.

For our case, the time is in fact z, i.e. the distance along the propagation axis.

Hence, the shift can be calculated as:

$$\Delta S = (v_{ph}^{LI} - v_{ph}^{HI})z \qquad . \tag{3.51}$$

Substituting the two expressions of the phase velocity in 3.50 we obtain the shift of the fringes between HP and LP regime.

$$\Delta S = \frac{k_\perp z}{2k_0}\left[\sqrt{1+\frac{\Delta n}{n_0}\left(\frac{2k_0}{k_\perp}\right)^2}-1\right] \quad . \tag{3.52}$$

This expression can be re-expressed in term of the in plane wavelength $\Lambda = \frac{2\pi}{k_\perp}$, and the laser wavelength $\lambda = \frac{2\pi}{k_0}$.

$$\Delta S = \frac{\lambda}{2\Lambda}z\left[\sqrt{1+\frac{\Delta n}{n_0}\left(\frac{2\Lambda}{\lambda}\right)^2}-1\right] \quad . \tag{3.53}$$

This expression is comfortable because experimentally we measure directly Λ.

As it will be shown later, the superfluid behaviour is suppressed for in plane wavelenght Λ smaller than the healing length ξ or the non local length σ_{nl}. Therefore with the expression of the shift 3.53 we could be able to extrapolate such characteristic lengths.

Moreover in another medium could be possible to perform this experiment varying the wavelength of the laser. In our platform the nonlinearity is strongly dependent by the detuning from the atomic resonance and therefore we choose to work at fixed wavelength and to modify the angle α to reconstruct $\Delta S(\Lambda)$ as schematized in figure **??** .

Another option could be to measure the shift for different pump intensities but, as can be understood looking at Eq. 3.52, the dependence from the in plane momentum $\Delta S \propto k_\perp$ is stronger than the one from the intensity: $\Delta S \propto \sqrt{I}$.

We choose therefore to measure the dispersion in function of the angle of the small amplitude perturbation with transverse plane momentum $k_\perp$.

Thus large values of Λ (i.e. small angles) or small values (i.e. large angles) correspond respectively to the phononic and the single particle dispersion regime.

Expressing the dispersion relation in function of the measured shift ΔS it is possible to reconstruct the Bogoliubov dispersion relation.

In fact, since the low power regime is only dependent on the in-plane momentum, the dispersion relation can be expressed inverting the expression of the shift in function of $\Omega_\perp^{HP}$:

$$\Delta S = \frac{1}{k_\perp}(\Omega_\perp^{HP}-\Omega_\perp^{LP})z \longrightarrow \Omega_\perp^{HP} = \frac{k_\perp \Delta S}{z}+\Omega_\perp^{LP} \quad . \tag{3.54}$$

3.7 Non-locality

The physical effect leading to the nonlinear optical response is the transfer of population from the ground to the excited state and the creation of coherence between these states. Although motional effects are taken in account, as for instance Doppler broadening, atomic motion also results in transport of excited atoms which leads to a nonlocal response.

In particular non-local effects are due to the fact that in a dilute gas the particles are free to move almost without collisions. Therefore a photon, after being absorbed, is re-emitted with a spatial displacement respect to the position where it was absorbed.

The degree of non-locality depends on the characteristic length scales associated with the transport of excited atoms. The first length scale is the mean free path atoms travel before a Rb-Rb collision occurs. The mean free path is given by:

$$l_c = \frac{1}{n_a \sigma_{i-f} \sqrt{2}} \quad , \tag{3.55}$$

where n_a is the atomic density and σ is the collisional cross section between atoms in two equal or different states i,f.

The cross section for collisions between excited and ground state atoms σ_{g-e} is much larger than σ_{g-g} because in the first case the collisions occur with a long range dipole-dipole interaction[47],[48]. The second length scale that is important to consider is the distance $l_d = \tilde{v}\tau$ traveled by an atom moving at the most probable speed (the velocities follow a Maxwell-Boltzmann distribution) $< v >= \sqrt{\frac{2k_B T}{m}}$.

We are looking for the in plane projection of the velocity that from the energy equipartition theorem is:

$$\tilde{v} = \sqrt{\frac{2}{3} < v^2 >} \quad . \tag{3.56}$$

For what concernes the life-time of the excited atoms τ it is still an open problem if we can use or not the value of the decay time $\tau \simeq 26ns$. In fact there is also the possibility that the photon emitted by the atoms after their decay is re-absorbed by other atoms. As it will be shown in chapter **??** we tried to measure the non-local lenght σ_{nl} and it results to be $\simeq 7$ times bigger than the one expected using $\tau \simeq 26ns$.

In a dilute gas $l_c \gg l_d$, therefore we expect a nonlinear response of the medium with a characteristic non-local length σ_{nl} of the order of l_d.

In the description of the medium response it is necessary to include a response function R that take in account non-local effects:

$$\Delta n(r,z) = \gamma \int R(r-r')I(r')dr'dz' \quad , \tag{3.57}$$

where γ is just a normalization factor.

An extension of the Bogoliubov theory for non-local medium [46], [10] leads to the following expression for the dispersion relation, that here is measured in s^{-1} and it is to equivalent to the expression **??** multiplied by a factor $\frac{c}{n_0}$:

$$(\Omega - \bar{v}\bar{k}_\perp)^2 = \frac{c^2 n_2 |E_{bg}|^2}{n_0^3} \hat{R}(k_\perp, n_0\Omega/c) k_\perp^2 + \frac{c^2 k_\perp^4}{4k_0^2 n_0^2} \quad , \tag{3.58}$$

where $\hat{R}$ is the 3-D Fourier transform of the response function $R(r_\perp, z)$.

Within the paraxial approximation $\frac{k_\perp}{k_0}, \frac{v}{c} \ll 1$, and the rescaled Bogoliubov frequency $\frac{n_0\Omega}{c} \ll k_\perp$, so the main contribution to the non-locality comes from the $k_\perp$ dependence of $\hat{R}$ that can be simplified as $\hat{R}(k_\perp, n_0\Omega/c) \simeq \hat{R}(k_\perp, 0)$.

In the figure **??** is shown how non-local effects affect the Bogoliubov dispersion relation. The effect of the non-locality is to suppress the collective excitations of the fluid and therefore the dispersion converges to the single particle behaviour for angles way smaller than the ones expected in the case of a local nonlinearity.

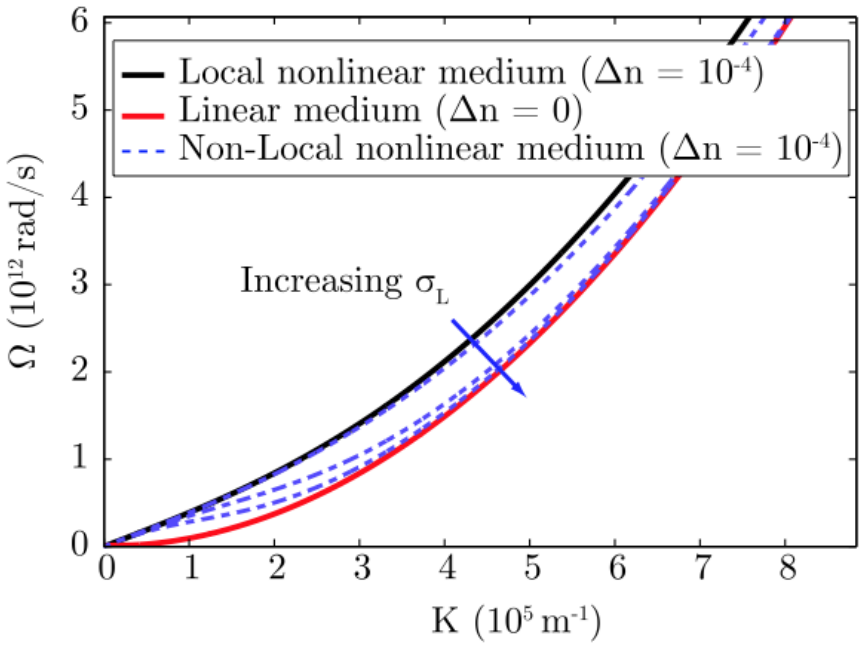

Figura 3.2. Bogoliubov dispersion relation in presence of non-locality. The black line represent the dispersion without non-local effects. For the blue dashed curves non-local effects are taken in account and increasing σ_{nl} they converge first to the single particle behaviour (red line). Taken from [10].

Moreover the non-local effects modify the shape of the dispersion relation and then also the Landau critical velocity will have a minimum at $v_c < c_s$, as shown in the plot in Fig. 3.3.

As expected in the local regime i.e. $\sigma_L < \xi/2$ we have $v_c = c_s$.

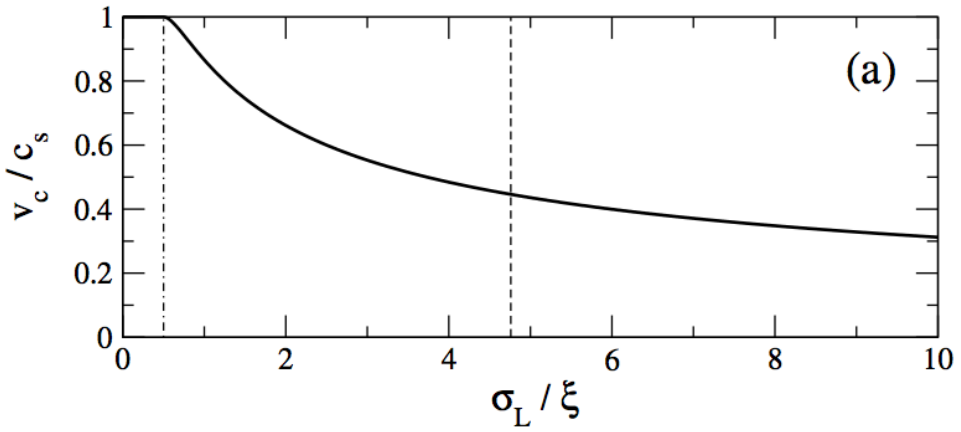

Figura 3.3. Plot of the critical velocity v_c vs the non-local length σ_L, with the units renormalized with the speed of sound and the healing length. The vertical dot-dashed line on the left identify the crossover between the two regimes $\sigma_L < \xi/2$ and $\sigma_L < \xi/2$. Taken from **??**

3.7.1 Proposal for a model to describe the non-local response

Here is followed an article [47] that studies exactly a warm Rb vapour, where the motion of the atoms is described by a ballistic model, and it obtains an expression for the non-local response function.

The goal of the following calculation is to find an expression of the non-local response that is dependent from τ and $\tilde{v}$.

The response function is the Green function who solves the collision-less Boltzmann equation 3.59 for the density of excited atoms n_e. In the two-dimensional case, and working within the paraxial approximation, we consider the propagation in the transverse plane $\mathbf{r}_\perp = x\hat{x} + y\hat{y}$ and $\mathbf{v}_\perp = v_x\hat{x} + v_y\hat{y}$:

$$\frac{dn_e}{dt} = \frac{\partial n_e}{\partial t} + \mathbf{v}_\perp \nabla_\perp n_e = \delta(t) n_0(\mathbf{r}_\perp, \mathbf{v}_\perp) \tag{3.59}$$

Considering the solution for $n_0 = \delta(\mathbf{r}_0) f(\mathbf{v}_\perp)$, where

$$f(\mathbf{v}_\perp) = \frac{m}{2\pi k_B T} e^{-\frac{\mathbf{v}_\perp^2}{\tilde{v}^2}} \tag{3.60}$$

is the two-dimensional thermal velocity distribution, it is found that the function that solves eq. 3.59 is :

$$R(\mathbf{r}_\perp, t, \mathbf{r}_0, t_0) = \delta(\mathbf{r}_\perp - \mathbf{r}_0 - \mathbf{v}_\perp(t - t_0)) f(\mathbf{v}_\perp) \quad , \tag{3.61}$$

and to obtain the Green function that describes the spatial response of the medium it is necessary to integrate the response function over the velocities :

$$R_r(\mathbf{r}_\perp, t; \mathbf{r}_0, t_0) = \int d\mathbf{v}_\perp \delta(\mathbf{r}_\perp - \mathbf{r}_0 - \mathbf{v}_\perp(t-t_0)) f(\mathbf{v}_\perp) = \frac{1}{\pi \tilde{v}^2 (t-t_0)^2} e^{-\frac{|\mathbf{r}_\perp - \mathbf{r}_0|^2}{\tilde{v}^2 (t-t_0)^2}} \quad . \tag{3.62}$$

At this point it is possible to take in account the exponential decay $e^{-\gamma t}$ and to re-express the Green response function in term of the decay rate $\gamma = \frac{1}{\tau}$:

$$R_r(\mathbf{r}_\perp, t; \mathbf{r}_0, t_0; \gamma) = \frac{1}{\pi \gamma^2 l_d^2} \frac{e^{-\gamma(t-t_0)}}{(t-t_0)^2} e^{-\frac{|\mathbf{r}_\perp - \mathbf{r}_0|^2}{\cdot \tilde{v}(t-t_0)^2}} \quad . \tag{3.63}$$

In order to calculate the spatial distribution of the density of excited states n_e is necessary to know the rate of local excitations. The total atomic density can be written as $n_a = n_g + n_e$ and the rate equations for the two atomic densities are the following:

$$\begin{cases} \frac{\partial n_g}{\partial t} = -\frac{I\alpha(I)}{\hbar\omega} + \gamma n_e - \mathcal{L}_e[n_e] & , \\ \frac{\partial n_e}{\partial t} = \frac{I\alpha(I)}{\hbar\omega} - \gamma n_e + \mathcal{L}_e[n_e] & , \end{cases} \tag{3.64}$$

where the first term is the rate of local excitations that depends on the absorption coefficient that contains also a non linear absorption term that saturate with the intensity

$$\alpha(I) = \alpha_0 + \alpha_2(I) \quad . \tag{3.65}$$

In the equations 3.64 it is also assumed that the total atomic density is unchanged by the presence of the laser field. This can be a good assumption for hot vapours but not for cold atoms.

The term $\mathcal{L}_e[n_e]$ is a linear operator that depend on the nature of the excited states transport processes.

The first terms on the right of equations 3.64 is the rate of local excitation $\frac{\alpha I}{\hbar\omega}$ and the spatial distribution of the excited state density n_e is therefore given by :

$$n_e(\mathbf{r}_\perp, t) = \int_{-\infty}^{t} dt_0 \int d\mathbf{r}_0 R_r(\mathbf{r}_\perp, t, \mathbf{r}_0, t_0, \gamma) \frac{\alpha I(\mathbf{r}_0, t_0)}{\hbar\omega} \quad . \tag{3.66}$$

At this point it is possible to insert in this formula a spatially dependent intensity profile and to compute $n_e(\mathbf{r}_\perp)$.

The article **??** also suggests that is possible to stabilize a vortex thanks to the combination of non-locality and nonlinear saturation.

3.8 Scattering on an optically induced defect

In this section it will be discussed how an optical analogue of superfluidity can be observed in the present context of fluids of light in a propagating geometry.

One of the main feature of a superfluid behaviour is the suppression of the scattering of a flow around an obstacle.

In a normal fluid, the kinetic energy of the fluid is dissipated in the form of waves that are scattered from the obstacle. Instead in a superfluid exists a critical

flow speed (as explained in 2.2) below such waves are not allowed to be excited, and consequently the fluid passes the obstacle undisturbed. At the breakdown of superfluidity, i.e. at flows speeds close to the critical flow velocity, the turbulences manifests in the form of quantized vortex nucleation and this is commonly considered to be a hallmark signature of such superfluids [20].

The suppression of the friction felt by a physical defect has been observed with exciton-polariton [12].

In this experiment an external potential is added to the NLSE using another laser beam with a radius way smaller than the other one.

$$i\frac{|\partial A(\bar{r}_\perp,z)|}{\partial z} = (-\frac{1}{2k_0}\nabla_\perp^2 + V_0 + g|A(\bar{r}_\perp,z)|^2)A(\bar{r}_\perp,z) \qquad . \tag{3.67}$$

The situation studied here is that of a fluid of light propagating at a finite speed and hitting a gaussian defect.

Using a Gaussian lasers profile such a defect can be described as a gaussian modulation of the linear dielectric constant:

$$\delta\epsilon(r_\perp,z) = \delta\epsilon_{max}e^{-\frac{r_\perp^2}{2\sigma^2}} \qquad , \tag{3.68}$$

that is centered at $r_\perp = 0$ and with FWHM σ.

That define the external potential $V(r_\perp,z) = -k_0\frac{\delta\epsilon(r_\perp,z)}{2\epsilon}$.

The superfluidity condition is achieved when the dimensionless speed of light in the medium v is smaller than the critical velocity, that correspond to the analogue speed of sound for a local nonlinearity while it is smaller in presence of non-locality. We recall the expression of the two speeds, where the speed of the fluid is considered as an angle in the transverse plane :

$$\begin{cases} v = \frac{\sin\phi}{n_0} \simeq \frac{\phi}{n_0} \\ c_s = \sqrt{\frac{g|A_0|^2}{k_0}} \end{cases} \qquad . \tag{3.69}$$

Therefore the superfluidity condition for a local nonlinearity is:

$$\phi < n_0 c_s = \sqrt{-\frac{n_0^2 g|A_0|^2}{k_0}} \qquad . \tag{3.70}$$

In such a case, since no states are any longer available for scattering at the frequency of the driving photon field, the photon scattering from the defect is inhibited and the photon fluid is able to flow without friction.

The idea for this experiment (and the simulations) come from an article of I.Carusotto [5]. Here the simulations of the expected behaviour of the fluid in presence of a defect will be presented.

The figure 3.4 presents three different propagation regimes for the fluid at a fixed in-plane velocity $v = 0.034$, in presence of a constant gaussian defect while the incident background intensities is increased from left to right (the speed of sound increases).

Also here varying the incidence angle at a fixed light intensity the physics is the same, i.e it is possible to modify the speed of light in the medium instead of the speed of sound

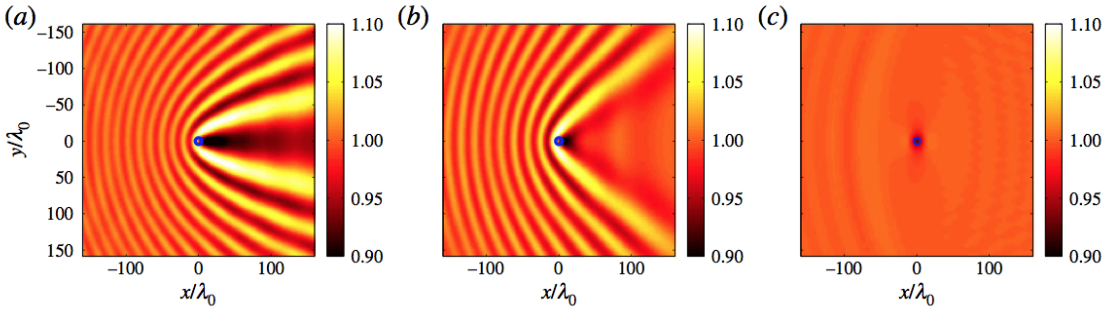

Figura 3.4. Long-distance asymptotic transverse profiles of the laser beam intensity hitting a cylindrical defect located at $r_\perp = 0$. The flow velocity is the same $v = 0.034$ along the positive x-direction (the right-ward direction in the figure). The colour scale is normalized to the incident intensity. The Mach numbers for the three panels are: a) Linear regime $v/c_s = \infty$; b) Supersonic regime $v/c_s = 1.88$; c) Superfluid regime $v/c_s = 0.86$.

Figure 3.4 a) shows the linear regime with $v \gg c_s$ that occurs in the linear optics regime at very low incident intensities (or big angle): in this case, the linear interference of the incident and scattered light is responsable of the parabolic shape of the fringes.

As it will be shown later in a nonlinear medium interference fringes could be observed also because of self-phase modulation, but in this case they have a bigger visibility and are not parabolic for $k \neq 0$.

It is worth to notice, looking at the colour scale, that the visibility of the fringes is around 10%.

Figure 3.4 b) shows a supersonic flow regime where $v > c_s$ and superflow is broken: a Mach–Cerenkov cone appears after the defect, with an aperture angle $\theta = \arcsin \frac{c_s}{v}$.

In the panel c) the fluid of light moves at a subsonic speed, and therefore it flows without friction, that means that there is no scattered light that interfere with the incident one. as is explained better in Fig. 3.5.

From an optical point of view a suppressed scattering is associated to a suppressed radiation pressure acting on the defect **??**.

The healing length ξ is the typical length scale above which the fluid can feel the radiation pressure. Below this length scale the photon fluid can be considered as incompressible and it auto-repair itself. Therefore the defect have to bigger than the healing length in fact below ξ, also if the fluid can experience scattering, we would never be able to observe it.

Looking in the reciprocal space (3.5, below) it is possible to observe all the range of k-vector acquired by the scattered light, i.e. a scattering ring around the range of $k_\perp^{inc}$ proper of the beam.

In the linear case $c_s \ll v$ shown in panel (a), scattering on the defect is responsible for a ring- shaped feature passing through the incident wave-vector k_{inc}.

When c_0 grows towards v, the ring is is deformed developing a corner at $k_\perp^{inc}$ and a weaker copy of it appears at symmetric position with respect to $k_\perp^{inc}$. In the

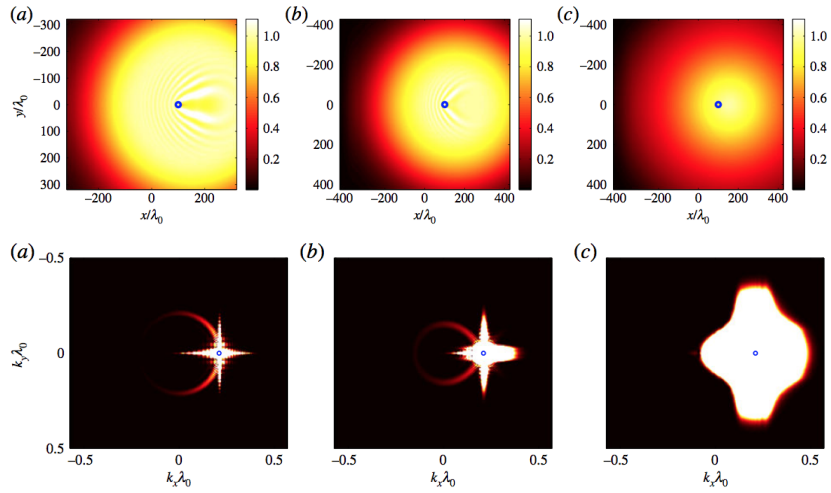

Figura 3.5. Above are shown the transverse profiles of the laser beam intensity after a propagation distance $L/\lambda_0 = 4500$ in the nonlinear medium. The parameters for a),b),c) are the same of figure 3.4. Below are shown the far-field emission patterns for the same configurations as in the figure above in a logarithmic scale.The blue circle indicates the incident wavevector $k_\perp^{inc}$.

superfluid regime ($c_s > v$) shown in panel (c), the ring disappears and only a single peak at $k_\perp^{inc}$ remains visible: the strong broadening of this peak, that is evident in the figure, is due to the overall rapid expansion of the spot under the effect of the Kerr defocusing.

We tried to observe a scattering ring analogue to the one in Fig. 3.5 a),b) because it is a clear and immediate demonstration of the presence of scattering and it is widely used for instance in exciton-polaritons experiments [59].

The scattering ring is expected to be really intense close to the defect, while on the opposite side it has really low intensity. This is because the probability to scatter with a $k_\perp$ close to the incident one is higher than the probability to scatter to a $k_\perp$ far from the initial one, and in particular this probability is minimized for a $k_\perp$ opposite to the initial one.

The intense part of the ring is superposed to the spot but also subtracting the background (i.e. the image without the defect) we were not able to observe it.

Then we tried to observe the low intensity part of the ring. The scattering ring has a radius that is equal to the distance of the two spots in the k space and choosing a big relative angle between them this distance is such that the bright part and the opposite side of the ring are far one each other and the bright part is outside of the view-range of the camera (we image the far-field with a 10x objective). In this way we are free to increase the exposure time of the CCD up to 5-10 seconds without saturating (and potentially breaking) the camera. In this way we are able to reveal also the smallest amount of scattered light but unfortunately we anticipate here that experimentally no scattering has been observed.

Probably it was because the non-locality doesn't enable us to see the scattering around the defect, since the effect of the defect appear further from the spot, but the scattering is expected to be close to the defect.

That is like to say that the healing length ξ is smaller than the non-local length σ_{nl}. In particular from the shift experiment, using the same theory used in the Edinburgh's experiment we can estimate $\sigma_{nl} \simeq 400\mu m$, instead from a simple calculus $\sigma_{nl} = v_{gauss}\tau \simeq 10\mu m$.

The value of the nonlinearity depends on which theory we use to fit the shift datas.

We use the simple theory explained in the section about the calculation of the shift to extrapolate the nonlinearity as a parameter that we find fitting the shift vs $k_\perp$. With this procedure we find $\Delta n = 1.5 \times 10^{-4}$.

Considering $n_0 = 1$ we find :

$$\xi = \lambda\sqrt{\frac{-n_0}{2\Delta n}} = 45\mu m \qquad . \tag{3.71}$$

With theory of [54] instead we found $\Delta n = 10^{-5}$, that means $\xi \simeq 12\mu m$.

3.9 Edinburgh's experiment

Recently some experiments strictly related to ours have been realized in Edinburgh [10], [**?**]. The platform they are using to demonstrate a superfluid behaviour of the photon fluid is a thermal non liner medium composed by graphene flakes in a methanol solution.

They tried the same two experiments that we want to realize, i.e. the measurement of the Bogoliubov dispersion from the phase shift in an interference pattern and the suppression of the friction of the photon fluid when it hits a defect.

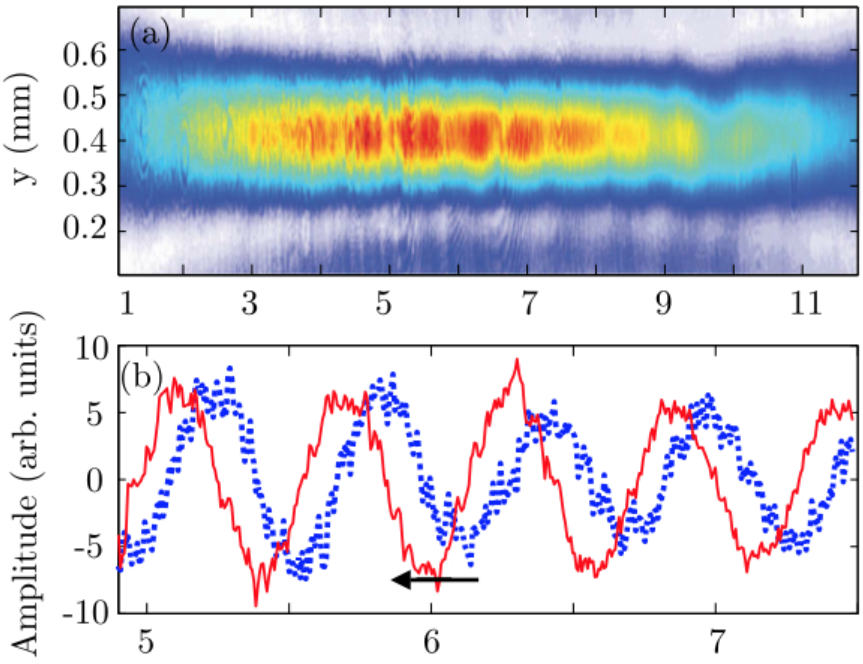

Figura 3.6. Taken from [11].

Here the two experiments will be described briefly, looking in particular at how they describes the non-local response of a thermal medium.

Differently from fluorescent dyes or Rb vapour, the fluorescence mechanism of graphene has a low efficiency and most of the absorbed laser energy is converted into heat. The methanol instead is responsable of the nonlinear response and it have a negative thermo-optic coefficient and a low absorption coeffiecient.

Here the heat diffusion influence the non-locality on long time-scales and a Lorentzian response function in the 2-d k-space ($k_\perp = k_x, k_y$) can be expressed as $\hat{R}(k_\perp, 0) = 1/(1 + \sigma_{nl}^2 k_\perp^2)$, where σ_{nl} is the range of the non-local interaction, i.e. the non-local length.

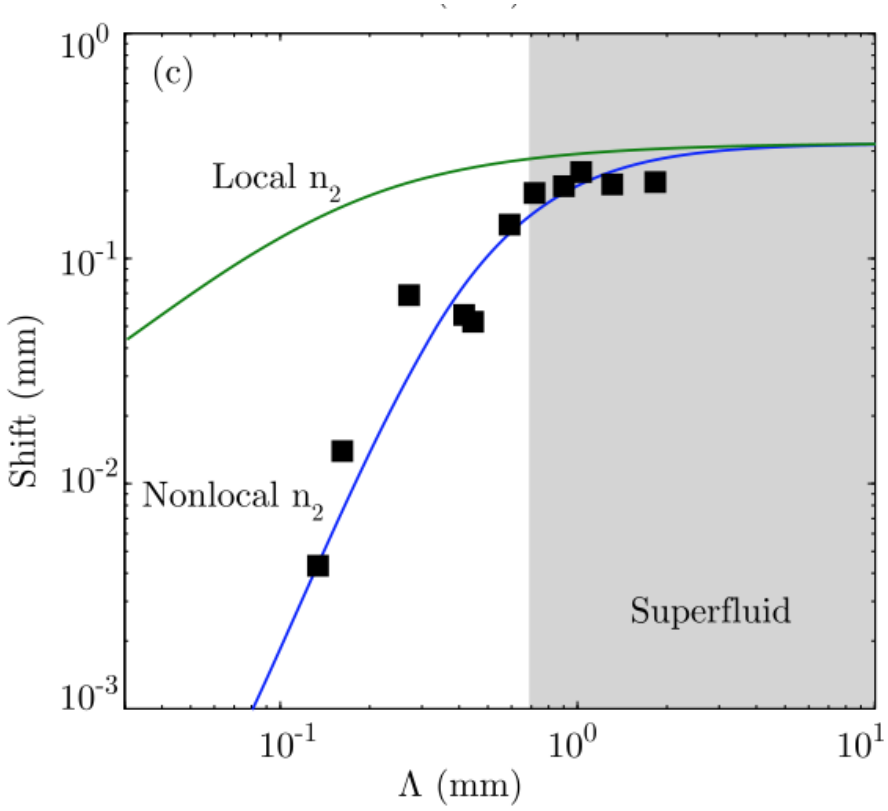

Figura 3.7. Taken from [11].

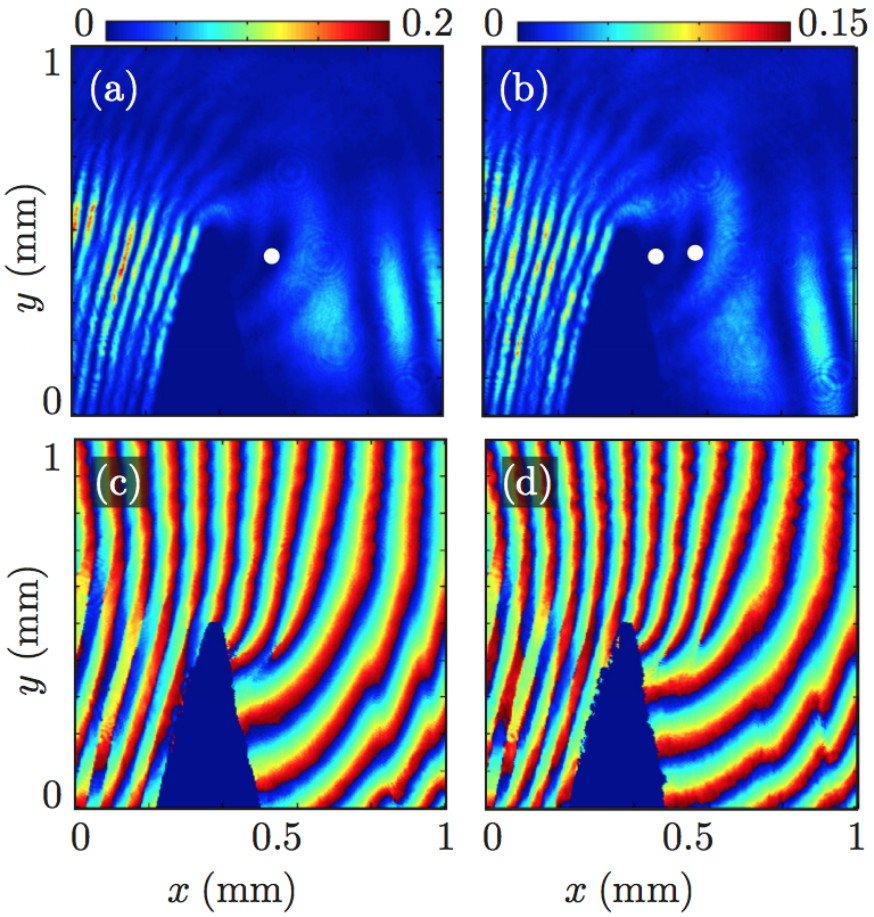

Figura 3.8. Taken from [10].

Capitolo 4

Characterization of the Rb cells

Rb is a metallic element of the alkali metal group, with an atomic mass of 85.4678 u.

Rb is present in nature as a mixture of with two isotopes of ^{85}Rb (72,2%) and ^{87}Rb (27,8%). Rubidium 85 has 37 electrons, only one of which is in the outermost shell. 85Rb is the only stable isotope of rubidium (although 87Rb is only very weakly unstable, and is thus effectively stable).

The Rb cell is heated at 120-140 $C°$ in order to have it in the vapour state and to achieve a good negative nonlinearity.

In fact, as it will be shown in section 4.2.1, the nonlinear susceptibility is a function atomic density, that is related to the temperature by a law that, since we are not dealing with a perfect gas is not $PV = nRT$.

At the first stage of my internship we were working with Rb in the natural proportion.

Soon we have decided to buy a new cell with a pure isotope of ^{85}Rb, to have a better trade-off between nonlinearity and absorption.

We also tried to use a mixture of Rb with Ne as buffer gas, to suppress non-local effect, but surprisingly we found that the value of the non-local length extrapolated from the shift measurement was the same of the preceding system and this lead us to reconsider the non-local effects only in terms of the dynamic of the excited atoms.

4.1 A two level system

This section describes a semiclassical model for a two-level system [38]. After calculating the probability of having an atom in the excited state and then solving the optical Bloch equations some important parameters as the $\chi^{(3)}$ will be calculated theoretically.

The hyperfine structure of the energy levels of ^{85} Rb is shown in Fig. 4.1 . The hyperfine structure occurs due to the energy of the nuclear magnetic dipole moment in the magnetic field generated by the electrons, and the energy of the nuclear electric quadrupole moment in the electric field gradient due to the distribution of charge within the atom.

The transition we mainly use for our purpose is $5^2S_{\frac{1}{2}}, (F = 3) \longrightarrow 5^2P_{\frac{3}{2}}$, that is know as the D_2 transitions and it is centered at a frequency $f_0 = 384.2304$ THz.

Anyway it is possible to achieve a good negative Kerr nonlinearity, under a proper detuning, also using the D_1 line centered at $f_0 = 377.1073$ THz.

We can modelize the D_2 transition with a two-level system [38] and describe it with a semiclassical model where the field is classical and the energy levels are quantized.

Such a system can be described by a time-dependent Schrödinger (TDSE) equation:

$$i\hbar\frac{\partial\Psi}{\partial t} = (\hat{\mathcal{H}}_0 + \hat{\mathcal{H}}_1(t))\Psi \quad , \tag{4.1}$$

where $\hat{\mathcal{H}}_0$ is the unperturbed Hamiltonian and $\hat{\mathcal{H}}_1$ describes the interaction with the oscillating electric field that perturbs the system.

In absence of the electromagnetic radiation the system admit the following stationary solutions (omitting the vectorial notation):

$$\Psi_n(r,t) = \Psi_n(r)e^{-iE_nt/\hbar} \quad , \tag{4.2}$$

where E_n are the solutions for the unperturbed system. Therefore the wave function for the level $|1\rangle, |2\rangle$ are Ψ_1, Ψ_2 that obeys to the following eigen-values equations:

$$\begin{cases} \hat{\mathcal{H}}_0\Psi_1(r) = E_1\Psi_1(r) & , \\ \hat{\mathcal{H}}_0\Psi_2(r) = E_2\Psi_2(r) & . \end{cases} \tag{4.3}$$

With the addiction of the interaction term is not possible to have stationary solutions anymore.

Anyway, since $\Psi_1(r)$,$\Psi_2(r)$ constitute a base in the vectorial space (are orthogonal state) the total wave function can be expressed as a linear combination of two states:

$$\Psi(r,t) = c_1(t)\Psi_1(r) + c_2(t)\Psi_2(r) \quad . \tag{4.4}$$

The normalization condition is such as:

$$\int |\psi(r,t)|^2 dV = |c_1(t)|^2 + |c_2(t)|^2 = 1 \quad . \tag{4.5}$$

Substituting $\Psi(r,t)$ in the TDSE we obtain:

$$\hat{\mathcal{H}}_I(c_1(t)\Psi_1(r) + c_2(t)\Psi_2(r)) = i\hbar(\dot{c}_1(t)\Psi_1(r) + \dot{c}_2(t)\Psi_2(r)) \quad . \tag{4.6}$$

That can be multiplied for the bra $\langle 1|$ (in the first equation) or Ψ_2^* (in the second one), and then integrated obtaining the two coupled equations[1]:

$$\begin{cases} c_1\int \Psi_1^*\hat{\mathcal{H}}_I\Psi_1 dV + c_2e^{-i\omega_0t}\int \Psi_1^*\hat{\mathcal{H}}_I\Psi_2 dV = i\hbar\dot{c}_1 & , \\ c_1e^{i\omega_0t}\int \Psi_2^*\hat{\mathcal{H}}_I\Psi_1 dV + c_2\int \Psi_2^*\hat{\mathcal{H}}_I\Psi_2 dV = i\hbar\dot{c}_2 & . \end{cases} \tag{4.7}$$

Considering the interaction of the electric field of a beam propagating in the z-direction $\bar{E} = \bar{E}_0\cos(kz - \omega t\ )$. It is possible to neglect the transversal part of the field assuming that the Bhor length is really small compared to the wavelength

[1] $\omega_0 = (E_2 - E_1)/\hbar$

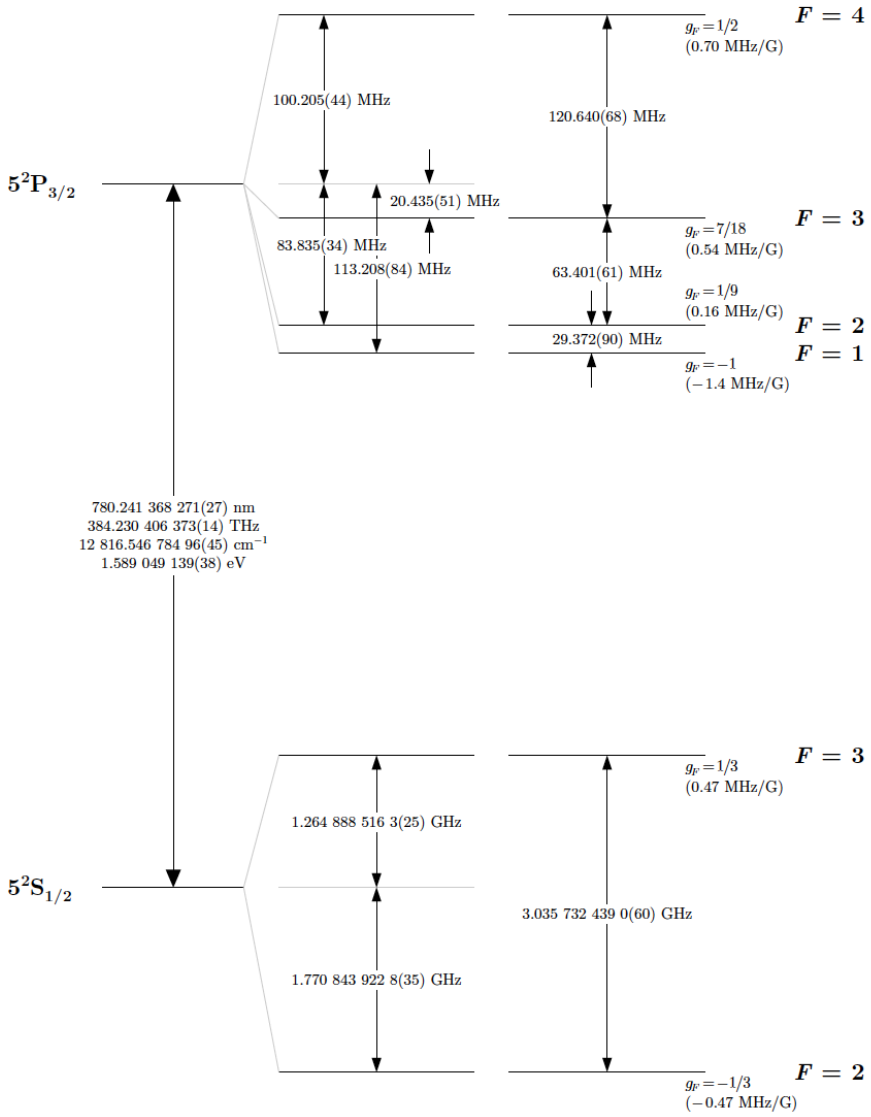

Figura 4.1. Hyperfine structure for the ^{85}Rb D_2 transition. Here also the approximate Landè g_F factors are given for each level, with the corresponding Zeeman splittings between adjacent magnetic sublevels. The ground state energy values are taken from [33] while the excited states energy values are taken from [34]. Image taken from 4.1.

of the field. Therefore the field that arrives on the atoms is substantially a plane wave-front.

The electric field interact with the dipole $-e\bar{\mu}$ generated by the field itself giving:

$$\hat{\mathcal{H}}_I = e\bar{\mu}\bar{E}_0 \cos(\omega t) \quad . \tag{4.8}$$

Inserting this in 4.7 we notice that the diagonal terms of the system i.e the terms $\int \Psi_i^* H_I \Psi_i$ or, in Dirac notation $\langle i| H_I |i\rangle$ are nullified.

Defining the frequency $\nu = \frac{\langle 1|e\bar{\mu}\bar{E}_0|2\rangle}{\hbar}$ we can rewrite the equations 4.7 as:

$$\begin{cases} i\dot{c}_1 = \nu \cos(\omega t) e^{-i\omega_0 t} c_2 & , \\ i\dot{c}_2 = \nu^* \cos(\omega t) e^{i\omega_0 t} c_1 & . \end{cases} \tag{4.9}$$

Since we work slightly detuned from resonance :

$$\omega_0 + \omega \gg \omega_0 - \omega \quad . \tag{4.10}$$

Expanding the cosine and performing the so-called rotating-wave approximation (RWA)[2] it is possible to rewrite the Eq. **??** as:

$$\begin{cases} i\dot{c}_1 = \nu \cos(\omega t) e^{i(\omega-\omega_0)t} c_2 & , \\ i\dot{c}_2 = \nu^* \cos(\omega t) e^{-i(\omega-\omega_0)t} c_1 & . \end{cases} \tag{4.11}$$

Supposing that initially all the atoms of the system are in the lower energy level:

$$c_1(0) = 1, \qquad c_2(0) = 0 \quad . \tag{4.12}$$

Supposing $c_1(t) = 1$ (zero order, unperturbed system, weak electric field) we obtain:

$$c_2(t) = \frac{\nu^*}{2} \frac{1 - e^{-i(\omega-\omega_0)t}}{\omega_0 - \omega} \quad , \tag{4.13}$$

and the time dependent probability of the transition for a weak electric field is:

$$|c_2(t)|^2 = \left| \frac{\nu \sin[(\omega_0 - \omega)t/2]}{\omega_0 - \omega} \right|^2 \quad . \tag{4.14}$$

If we don't want to assume the hypothesis of a weak electric field we have to solve the system of equation 4.11 that gives:

$$\ddot{c}_2 + i(\omega - \omega_0)\dot{c}_2 + \frac{\nu^2}{4} c_2 = 0 \quad . \tag{4.15}$$

From the initial condition 4.12 we have:

$$\begin{cases} c_1(t) = e^{i(\omega_0-\omega)t/2} \left[\cos(\Omega_R t/2) - i \frac{(\omega_0-\omega)}{\Omega_R} \sin(\Omega_R t/2) \right] & , \\ c_2(t) = i \frac{\nu}{\Omega_R^2} \sin(\Omega_R t/2) & . \end{cases} \tag{4.16}$$

where the Rabi-frequency Ω_R is:

$$\Omega_R = \sqrt{(\omega_0 - \omega)^2 + \nu^2} \quad . \tag{4.17}$$

The probability tho find an atom in the excited state $|2\rangle$ therefore is

$$|c_2(t)|^2 = \frac{\nu^2}{\Omega_R^2} \sin^2(\Omega_R t/2) \quad . \tag{4.18}$$

[2]The physical meaning of this approximation is that, since we have two counter-propagating waves, during the integration in the rotating frame one of them is neglectable.

4.2 Optical Bloch equations

To calculate the polarization response i.e the susceptibility can be useful to write the optical Bloch equations (OBE)with the formalism of the density matrix that can be deifned as:

$$\hat{\rho} = \langle\Psi|\,|\Psi\rangle = \begin{pmatrix} |c_1|^2 & c_1 c_2^* \\ c_2 c_1^* & |c_2|^2 \end{pmatrix} = \begin{pmatrix} \rho_{11} & \rho_{12} \\ \rho_{21} & \rho_{22} \end{pmatrix} \quad . \tag{4.19}$$

Where the diagonal elements represent the occupation probabilities of $|1\rangle$ and $|2\rangle$, while the off-diagonal ones are called coherences and represent the response of the system at driving frequency.

In this model we can add the decay term Γ to the coherence terms (diagonal state).

The evolution of the density matrix is given by the Heisenberg equation:

$$-i\hbar\frac{\partial\Psi}{\partial t} = [\hat{\rho}, \hat{\mathcal{H}}] \tag{4.20}$$

Where $\hat{\mathcal{H}}$ can be expressed in a matricial form:

$$\hat{\mathcal{H}} = \begin{pmatrix} \hbar\omega_1 & V_{12} \\ V_{21} & \hbar\omega_1 \end{pmatrix} \quad . \tag{4.21}$$

Where, under the RWA $V_{ij} = -\mu_{ij}Ee^{-i\omega t}$.

All the calculation to solve Eq. 4.20, reported in [38], is omitted here. In the steady-state condition $\rho_{11} + \rho_{22} = 0$, and including the dephasing the OBE gives:

$$\rho_{22} - \rho_{11} = -\frac{1 + [(\omega - \omega_{21})\Gamma_{21}^2/4}{1 + (\omega - \omega_{21})^2\frac{\Gamma_{21}^2}{4} + \frac{2}{\hbar^2}|\mu_{21}|^2|E|^2\Gamma_{21}^2} \quad , \tag{4.22}$$

$$\rho_{21} = \rho_{12}^* = \frac{\mu_{21}Ee^{(i\omega t)}(\rho_{22} - \rho_{11})}{\hbar(\omega - \omega_{21} + i\Gamma_{21}/2} \quad . \tag{4.23}$$

4.2.1 Calculation of the susceptibility

This calculation of the susceptibility is taken from [31], adapting the notation in order to be coherent with the definitions of **??**.

The polarization is defined as the density of dipole moment per unit of volume:

$$\hat{P}(t) = N < \mu >= N(\mu_{12}\rho_{21} + \mu_{21}\rho_{12}) \quad . \tag{4.24}$$

Being $\bar{P} = \epsilon_0\chi\bar{E}$, the susceptibility can be expressed as:

$$\chi = \frac{N|\mu_{21}|^2(\rho_{22} - \rho_{11})}{\epsilon_0\hbar(\omega - \omega_{21} + i\Gamma_{21}/2))} \quad . \tag{4.25}$$

Using the solution 4.22 and defining the detuning $\delta = \omega - \omega_{21}$, the decay rate $\Gamma = \Gamma_{21}$, and using the frequency defined previously $\nu = \frac{e\mu|E|}{\hbar}$:

$$\chi = \left(-4N|\mu_{21}|\frac{\nu}{E\epsilon_0\Gamma^2}\right)\frac{\delta - i\Gamma/2}{1+4\delta^2/\Gamma^2+8\nu^2/\Gamma^2} \quad . \tag{4.26}$$

Defining

$$\begin{aligned} C &= \left(-4N|\mu_{21}|\tfrac{\nu}{E\epsilon_0\Gamma^2}\right) \quad , \\ |E_{sat}|^2 &= \tfrac{\Gamma\hbar^2}{8|\mu_{21}|^2} \quad , \end{aligned} \tag{4.27}$$

it is possible to rewrite the susceptibility as:

$$\chi = C\frac{\delta - i\Gamma/2}{1+4(\delta/\Gamma)^2+(\frac{|E|^2}{|E_{sat}|^2})^2} \quad . \tag{4.28}$$

It is also possible to perform a Taylor expansion in the parameter $\frac{|E|^2}{|E_{sat}|^2}$obtaining:

$$\chi = C\frac{\delta - i\Gamma/2}{1+4(\delta/\Gamma)^2}\left(1-\frac{|E|^2}{|E_{sat}|^2}\frac{1}{1+4(\delta/\Gamma)^2}\right) = \chi^{(1)}+\epsilon_0\chi^{(3)}|E|^2 \quad , \tag{4.29}$$

and finally we have an analytical expression for the first and third order susceptibility:

$$\chi^{(1)} = C\frac{\delta - i\Gamma/2}{1+4(\delta/\Gamma)^2} \quad . \tag{4.30}$$

Where the constant C is measured in s^-1 and therefore $\chi^{(1)}$ is dimension-less as expected.

To be coherent with the notation used in section **??** the term ϵ_0 in equation 4.29 is included in the non linear susceptibility $\chi^{(3)}$, that in this way is measured again in Cm/V^3.

$$\chi^{(3)} = \frac{C}{3}\frac{(\delta - i\Gamma/2)}{(1+4(\delta/\Gamma)^2)^2}\frac{\epsilon_0}{|E_{sat}|^2} \quad . \tag{4.31}$$

That can be re-expressed isolating his real part (the imaginary part is responsable of the non linear absorption) and substituting $|E_{sat}|^2$:

$$\chi^{(3)} = \frac{32}{3}\frac{N\mu_{21}^4}{\hbar^3}\frac{\delta/\Gamma^4}{(1+4\delta^2/\Gamma^2)^2} \quad . \tag{4.32}$$

From this expression we can see that the nonlinearity has a dependence from the detuning that goes as $\frac{1}{\delta^3}$.

Using the definitions of n_2^* (3.28) or n_2 (3.29) it is possible to find the value of n_2 in function of the susceptibility[3].

Here I use the definition 3.29 with $n_2 = -\frac{3}{8}\frac{\chi^{(3)}n_0}{\epsilon_0}$ can be expressed as:

$$n_2 = \frac{4N|\mu_{21}|^4 n_0}{\hbar^3\epsilon_0}\frac{\delta/\Gamma^4}{(1+4\delta^2/\Gamma^2)^2} \quad . \tag{4.33}$$

From the equation 4.31 it seems that is possible to achieve a negative nonlinearity just achieving a red-detuning, i.e. $\delta < 0$. Tendentially this is true far from the

[3]In the reference [31] the value of n_2 for $\Delta n = n_2|A|^2$ is $n_2 = \frac{3}{8}\frac{\chi^{(3)}}{n_0}$, this is because we included the permeability of the vacuum ϵ_0 directly in the definition of $\chi^{(3)}$.

resonance but when one goes closer the fact that our Rb is not exactly a two level system becomes relevant. As shown in 4.1 in fact Rubidium has a more complex structure than the two level one and could be necessary an experimental characterization to know exactly how the nonlinearity changes with the detuning.

Moreover here the Doppler broadening has not been taken in account yet. To calculate properly the non linear response in fact is necessary to integrate over the thermal velocity distribution of the atoms, given by:

$$W(v) = \sqrt{\frac{m}{2\pi k_B T}} e^{-\frac{v^2}{2\sigma^2}} \quad , \tag{4.34}$$

and the detuning is a function of the velocity of an atom:

$$\delta(v) = \delta_0 - kv \quad . \tag{4.35}$$

Now we have all the ingredients to calculate the local non linear response:

$$n_2(T) = \int n_2(v,T) W(v) dv \quad . \tag{4.36}$$

Eventually the non-local response function have to be included in this integral, as in eq.3.62.

4.3 Heating system

We've performed the experiments using several different Rb cells.

The first trial was done with a mixture (in the natural proportion) of Rb87 and Rb85.

For the measurement of the Bogoliubov dispersion relation we used a cell with pure 85Rb with a length of 7.5 cm and a diameter of 1 inch.

For the measurement of the non-locality we used a cell with the Rb in the natural proportion with a length of 1 mm and a diameter of 1 inch.

Few considerations are necessary to understand how to design properly the heating system of the cell and how to choose the proper detuning and temperature:

- All the cells we used have a small protuberance that is maintained colder than the rest to favorite the condensation inside of it. Heating this protuberance it is possible to increase the density of particles inside the cell.
- Longer is the cell and more the nonlinear effects are accumulated along it, but at the same time also the absorption is bigger.
- We want to work in a condition where the losses are negligible to mantain a good mapping between the NLSE and the GPE.[4] At the same time we increase the average temperature of the cell to increase the atomic density and then the nonlinearity, but this generates a Doppler broadening in the absorption spectrum and a radiation too close to resonance is absorbed too much.
- The nonlinearity strongly depends also by the detuning from the D_2 line.

[4] There is also a model that take in account losses but it goes beyond the scope of this thesis [54].

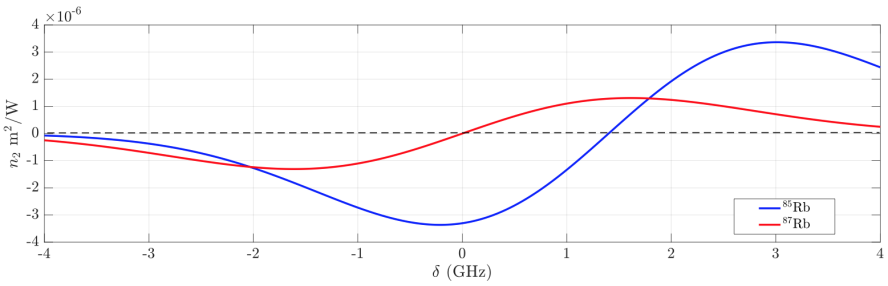

Figura 4.2. Non linear coefficient n_2 vs detuning for both the isotopes of Rb. The 0 is at 384,2291 THz, i.e the transition at lower frequency of Rb 85 in 4.1.

After considering carefully all the conditions above is necessary to find a good trade-off between cell's length, temperature and detuning.

In figure 4.2 is reported the dependence of the nonlinearity from the detuning for the two natural isotopes of Rb. Due to the different masses of the two isotopes, the lines of ^{85}Rb and ^{87}Rb are slightly shifted and therefore also the non-linear response is different.

For the experiments is necessary to make the laser pass through the 85Rb in the vapour state, in fact the light-matter quasi-particles have to be weakly interacting and we have to mantain the diluteness condition.

We inserted the Rb cell in a copper cilinder, to heat it uniformly, since the copper has a good thermal conductivity ($401\frac{W}{m\times K}$). The copper cylinder is covered with resistive heating elements elements, alimented by a DC voltage generator.

The resistive heating elements are mainly on the sides of the copper to try to mantain the windows warmer than the protuberance in the center.

We use alluminium paper, a thermical insulating wool and an alluminium box to isolate the cell and to mantain its internal temperature as stable as possible.

Also if the temperature of the liquid-solid phase transition for the Rb is around 39.3 °C, inside the cell there are both liquid and solid phase, in a dynamical equilibrium (at fixed voltage) such as the metal continuously melt and condensate inside the cell and it can happen that drops of Rb condense on the windows.

Also if the condensation at that temperature is not very likely to happen, once one drop condenses there are avalanche nucleation phenomenas that lead a lot of particle to condense together.

Is really important to avoid condensation of the Rb on the windows of the cell because it generates an unwanted phenomena such as scattering. By the way the condensed spot is too big to perform an experiment on the suppression of the scattering.

Sometimes the condensation on the windows can be removed just by using an heat gun, taking care to stop to heat when there is still a small halo of Rubidium on the window and let it slowly (around 1 min) evaporate alone. Otherwise, if we heat one window too much we induced a significant gradient of temperature between the two windows of the cell and the particles tends to move to the other colder window, where they condense again.

If the heat gun is not sufficient it means that the protuberance of the cell is to warm, in fact all the copper cylinders are provided with a small hole to keep the protuberance in contact with the external environment and keep it colder. In this case is necessary to design the heating system in order to mantain the protuberance cold and let condense most of the Rb of the cell inside of it.

If cooling the protuberance is not sufficient it means that one of the windows is heated, or isolated differently from the other one and there is a gradient of temperature that leads the particles to condense together (in this case tendentially on the same window).

Once we've heated the Rb cell we still don't know the average effective temperature inside the cell because we measure it just in one point, that usually is the coldest one (the protuberance) .

We need the effective temperature to estimate the numerical density that is useful for estimate theoretically the nonlinearity, another way to evaulate it is the z-scan.

It is possible to extrapolate the effective temperature of the Rb cell using an application that run on the local server that is able to to perform a manual fit, that is way better than a standard polynomial fit because we know with a very good precision the center of the Rb D_2 transitions.

4.3.1 Absorption measurements

We have to find a trade-of between the nonlinearity and the transmitted signal to choose properly our working frequency.

Is important to remember in fact that for the shift experiment is required to be in conservative conditions, that we will assume to be at 70% transmission. This is because we want to neglect the losses terms in Eq. 3.22.

To characterize the absorption we measure the output signal of the Rb cell while we scan in frequency.We evaluate the linear absorption profile, so we sent a low power beam ($I < I_{sat}$) through the cell and we record the signal with a photodiode connected to an oscilloscope.

We are connected with the oscilloscope via USB through a Raspberry-Pi 2, (i.e. a support hardware), with an operative system Raspbian Jessie 2.0, that is a Linux version made specifically for it and that can be installed and supported also via mathlab. I install the new operative system (the preceding wasn't updated), and a modification of the kernel was necessary to be able to communicate with other instrument through an USB connection.

One powerful feature of the Raspberry Pi is the row of GPIO (general purpose input/output) pins along the edge of the board, on the right of Fig. 4.3. These GPIO can be controlled via Matlab, but only if the operative system is installed via Matlab itself.

It that can be controlled also from our PC via LAN through a program called Bitwise. We launch a python program from the Raspberry to extract datas from the oscilloscope.

We run an application on the LKB local server to fit this absorption profile manually and, since we know from the literature [32] the frequencies of the Rb transitions, it works better than a standard polynomial fit procedure.

Figura 4.3. Raspberry Pi 2.

In fact we measure directly the temperature in the protuberance of the cell that, as explained in the preceding section, is not the same in the whole cell in order to avoid the condensation on the windows.

In figure 4.4 is shown the graphic interface of this application where the free parameter of the fit is the effective temperature of the cell.

The case shown is for a quasi-pure 85Rb The measured temperature here was 132.0°C while the effective temperature is 137 C°.

In a calibration we have seen that in the range between 110 and 140 °C, for the cell under exam, there is a fixed offset of 5 °C between the recorded and the effective temperature.

The calibration we have done is not general and cannot be extended to other cells. The difference between the two temperatures depends on the geometry of the heating system and on the point of the cell we choose to measure the temperature .

The Rb effective temperature can be useful to calculate parameters as the numerical density.

In order to calculate is necessary to calculate first the vapour pressure p for a given temperature (in Kelvin).

For pure 85Rb we use the formula calculated in [39] [45] :

$$\log p = \alpha + \beta - 4040/T \qquad , \tag{4.37}$$

where $\alpha = 5.006$, $\beta = 4.312$ to express the pressure in Pascal.

This equation reproduces the observed vapor pressures to an accuracy of $\pm 5\%$ or better.

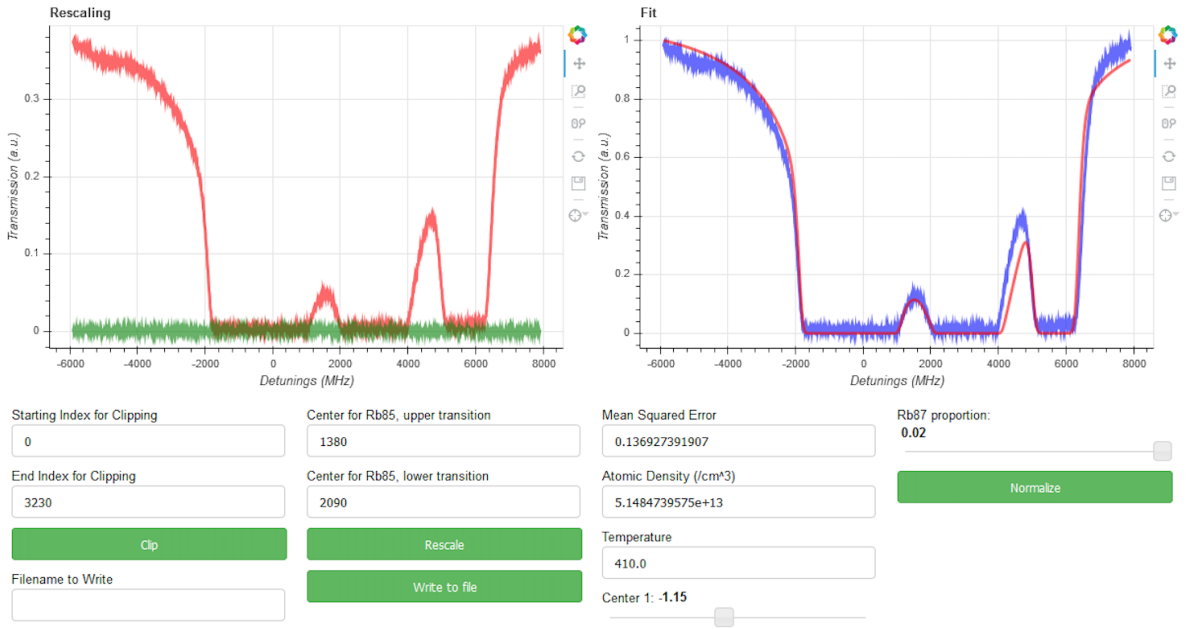

Figura 4.4. Interface of the application to fit the absorption profile of an almost pure Rb85. From this fit we extrapolate an effective temperature of 137 °C that is 5 °C bigger than the one measured with a thermocouple (132 °C).

4.4 Choosing the working frequency

In our hydrodynamical analogy we want to consider our system in a situation where the optical losses are negleigible and at the same time we can achieve an appreciable negative nonlinearity. The nonlinear effects are maximized on resonance, where the absorption is maximized. Therefore we have to choose a detuning such as we have a good trade-off between the two effects.

4.4.1 Z-scan

4.5 Self-phase modulation: a simple way to measure the sign of the optical nonlinearity

Field-curvature effect on the diffraction ring pattern of a laser beam dressed by spatial self-phase modulation in a nematic film E. Santamato* and Y. R. Shen (1984, optic letters)

Fine structure in spatial self-phase modulation patterns: at a glance determination of the sign of optical nonlinearity in highly nonlinear films L Lucchetti, S Suchand and F Simoni J. Opt. A: Pure Appl. Opt. 11 (2009) 034002.

Far field intensity distributions due to spatial self phase modulation of a Gaussian beam by a thin nonlocal nonlinear media E. V. Garcia Ramirez,1,* M. L. Arroyo Carrasco,1 M. M. Mendez Otero,1 S. Chavez Cerda,2 M. D. Iturbe Castillo2, OSA(2010).

Formation and evolution of far-field diffraction patterns of divergent and convergent Gaussian beams passing through self-focusing and self-defocusing media Luogen Deng1, Kunna He, Tiezhong Zhou and Chengde Li. J. Opt. A: Pure Appl. Opt. 7 (2005) 409–415

Capitolo 5

Measurement of the optical analogue of the Bogoliubov dispersion relation

5.1 Setup

In this experiment the wave-matter interaction is described by the following NLSE, without an external potential.

$$\frac{\partial A}{\partial z} = i\frac{\nabla_\perp^2 A(\bar{r}_\perp, z)}{2k_0} - i\frac{k_0 n_2}{n_0}|A(\bar{r}_\perp, z)|^2 A(\bar{r}_\perp, z) \qquad . \tag{5.1}$$

We want to perform experimentally a weak perturbation on top of the fluid that, from an optical point of view, can be realized adding a sinusoidal perturbation on top of our pump beam.

This small sinusoidal perturbation is introduced through a Mach-Zender interferometer, superposing a low intensity probe beam to the pump, with a different in plane $k_\perp = k_0 \sin(\alpha)$.

From the measurement of this shift we want to reconstruct the Bogoliubov dispersion relation and than to prove a superfluid behaviour of our system.

Recalling the expression of the shift:

$$\Delta S = \frac{k_\perp z}{2k_0}\left[\sqrt{1 + \Delta n\left(\frac{2k_0}{k_\perp}\right)^2} - 1\right] \qquad . \tag{5.2}$$

Is necessary to perform the experiment for a broad range of angle and for each angle we have to compare the fringes between the high power (HP) and low power (LP) regime.

Initially we started to work on an an already mounted setup where we were measuring the shift switching between the LP and the HP configurations. We tried to do this as fast as possible automatizing all the shutter (less than 0.5 s to switch between the HP and LP configuration) but still the fluctuations of the signal were to fast to obtain a reliable result.

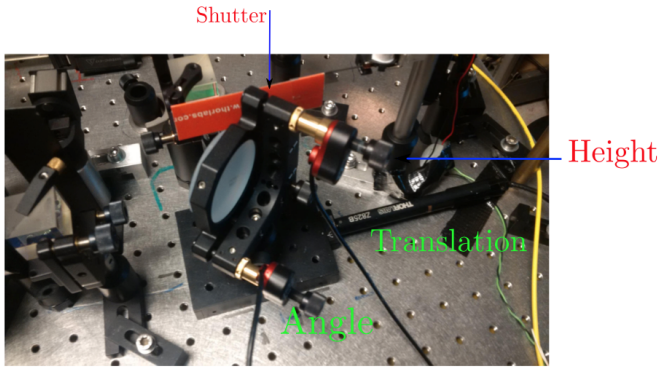

Figura 5.1

Our new setup is shown in Fig. 5.2. The main goal is to have two stables interference patterns that we can compare in the same time, in order to improve the precision of the measurement.

Moreover we tried to extend the measurement in the biggest possible range of angle.

The beam is manipulated as described in the following:

1. The beam is cutted in the k-space with a $75\mu m$ diameter pin-hole. We lose only around 1% of the signal doing this. This allow us to access to smaller angles. In fact the main factor that doesn't allow us to investigate smaller angles is the ability we have to to cut the conjugate that indeed for smaller angle goes closer to the pump and we cannot cut it anymore. So smaller the pump is in the $k-$-space and better is it. Still a problem that we cannot avoid is the side-band of the pump due to FWM processes.

2. Using two cylindrical lenses, respectively with $f_1 = 500mm$ and $f_2 = 100mm$, we have a magnification $M = 1/5$ along the y direction only.

3. The Mach-Zender interferometer is under a plastic box to prevent unwanted fluctuations of the signal. The mirror (Fig. 5.1 that control the angle of the probe (green path) can be piloted electonically. In this way we can change the angle with high precision and fixed step. Changing the angle also the relative spatial position between the two beam is slightly modified, therefore the mirror have to be translated (ever electronically) to recover the spatial superposition.

4. The beam is splitted in two path with a PBS. The relative power between the two beams can be regulated with the $\lambda/2$ before of this PBS. We choose to put the high power beam upper. The low power beam will be used as a reference and it can be furtherly attenuated modifying its polarization. The two beams are then recombined at different height on a PBS. This is done using a D-shaped mirror that let pass the HP beam and reflects the LP.

[htbp]

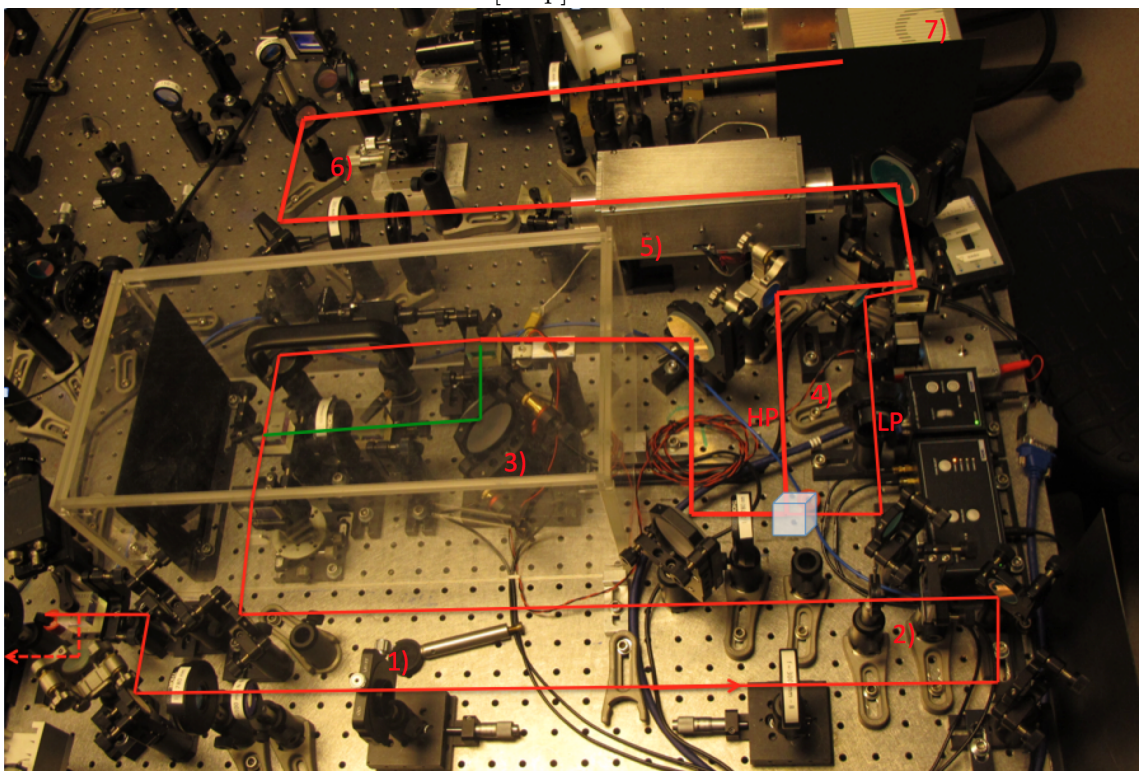

Figura 5.2

5. The two interference patterns pass through the 85Rb cell that is putted inside an oven, as explained in the preceding chapter (at 4.3), where the pump beam of the HP interference pattern experiences nonlinear effects.

6. To image the output plane of the cell we used two $f = 300mm$ lenses .

   A razor blade is putted in the focus of the first lens to cut the conjugate in the k-space. The reciprocal space can be observed putting an objective with a $10x$ magnification at his focal length $f \simeq 1cm$ from the blade.

7. The output plane of the cell is reprojected on a CCD camera Hamamatsu OrcaFlash C11440 with a magnification equal to 1.

In Fig. 5.3 are shown the shifted HP (above) and the reference LP (below) interference patterns

Imaging the two beams at the same time we also avoid problems due to the noise, since the two patterns are affected in the same way.

Moving the relative angle the position of the probe in the real space change, while the position of the pump is fixed. We can realligne the two patterns just by translating the probe beam, that in fact can be controlled by a mirror on an automatized translation stage 5.1.

A more accurate way to check if the position of the reference is good, instead of trust our eyes and put the center of the elliptics probe spots in the same x pixel, is

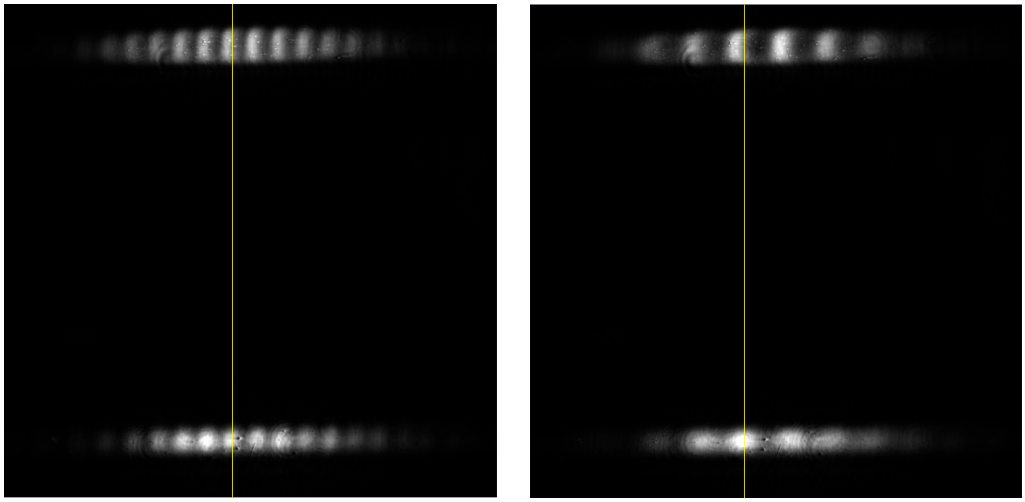

Figura 5.3. Images of the shift for big(on the left) and small (on the right) relative angles between pump and probe. Above the HP beam, whose experiences the nonlinear effects, on the bottom the LP beam. The yellow line put in evidence the shift between the two beams, that increases with the angle.

to check in the k-space where, if the x-coordinate of the two beam is the same, we observe a vertical interference as shown in figure 5.4.

Using a strong probe beam this platform may be also used in the future also to test the interaction between two superfluids.

5.2 Four wave mixing processes

Third order processes involve interaction between four photon, but is possible to give a classical description of this phenomena. From a quantum-mechanical point of view, FWM occurs when photons from one or more waves are annihilated and new photons are created at a frequency such that the energy and momentum are conserved during the parametric interaction.

Classically the first input field causes an oscillating polarization in the dielectric which re-radiates with a phase shift determined by the damping of the individual dipoles: this is just traditional Rayleigh scattering described by linear optics.

The application of a second field will also drive the polarization of the dielectric, and the interference of the two waves will cause harmonics in the polarization at the sum and difference frequencies.

Now, application of a third field will also drive the polarization, and this will beat with both the other input fields as well as the sum and difference frequencies. This beating with the sum and difference frequencies is what gives rise to the fourth field in four-wave mixing. Since each of the beat frequencies produced can also act as new source fields, a lot of interactions and fields may be produced from this basic process.

In general, the third order nonlinear susceptibility $\chi^{(3)}$ is a fourth rank tensor with $3^4 = 81$ elements and each of these elements consists of a sum of 48 terms.

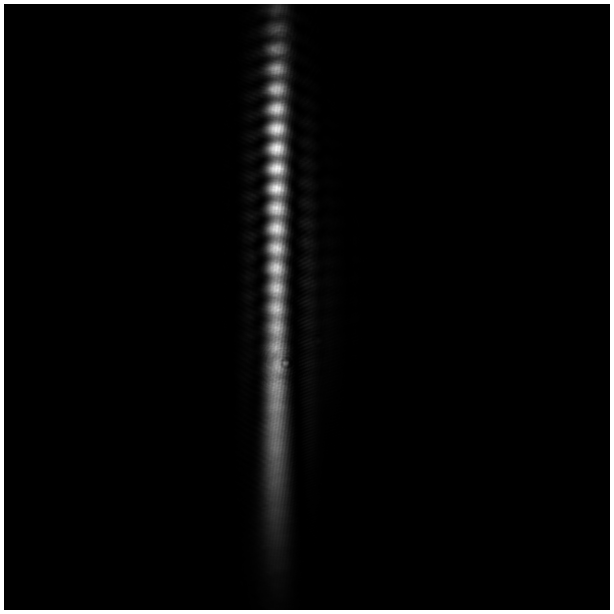

Figura 5.4. Interference in the k-space between the 2 pump-only beams

Fortunately this huge number of terms is drastically reduced through material symmetries and resonance, but unlike $\chi^{(2)}$, the suceptibility $\chi^{(3)}$ may have nonzero elements for any symmetry.

Each term has a typical form with three resonant factors in the denominator.

$$\chi^{(3)} = \frac{NL}{6\hbar^3} \sum_{g,k,n,j} \frac{\mu_{gk}\mu_{kn}\mu_{nj}\mu_{jg}\rho_{gg}}{[\omega_k g - \omega_1 - i\Gamma_{kg}][\omega_n g - i\Gamma_n g - (\omega_1 - \omega_2)][\omega_j g - i\Gamma_j g - (\omega_1 - \omega_2 + \omega_3)]} + 47 terms \quad . \tag{5.3}$$

Here N is the oscillator density, μ_{gk} is the electric dipole matrix element between states g and k of a two level system, ω_{kg} is the frequency of the transition from g to k, Γ_{kg} is the damping of the off-diagonal element of the density matrix that connects g to k, and $\omega_{1,2,3}$ are the frequencies of the fields.

The main difference between the 48 terms is the ordering of the frequencies involved in the summation.

The susceptibility can be simplified further by considering terms which have small factors in the denominators due to resonance with oscillator frequencies. For example, Raman processes are described by the terms which contain $\omega_1 - \omega_2$ and $\omega_3 - \omega_2$, while two-photon absorption is described by terms that contain $\omega_1 + \omega_3$.

The main features of FWM can be understood from the third order polarization term:

$$\vec{P}_{NL} = \epsilon_0 \chi^{(3)} \vec{E}\vec{E}\vec{E} \quad . \tag{5.4}$$

In general FWM is polarization dependent and one must develop a full vector theory for it.

We will consider the scalar case, in which all the four field are linearly polarized along the $\hat{x}$ axis. Assuming the quasi-CW condition it is possible to neglect the time dependence of the field component A_j ($\frac{\partial A_j}{\partial t} = 0$).

The total electric field can be written as:

$$\vec{E}_{tot} = \frac{1}{2}\sum_{j=1}^{4} \underbrace{\hat{x}A_j e^{i(k_j z-\omega_j t)}}_{\vec{E}_j} + c.c \tag{5.5}$$

Substituting E_{tot} in the expression of the nonlinear polarization 5.4 :

$$\vec{P}_{NL} = \hat{x}\frac{1}{2}\sum_{j=1}^{4} P_j e^{i(k_j z-\omega_j t)} + c.c. \tag{5.6}$$

We need to write the Helmholtz equation 3.8 for each frequency ω_j:

$$\vec{\nabla}^2\vec{E}_j + \frac{\omega_j^2}{c^2}\epsilon(\omega_j)\vec{E}_j = \frac{4\pi}{c^2}\frac{\partial^2 P_j}{\partial t^2} \qquad . \tag{5.7}$$

We consider a beam propagation along the z axis, so we can avoid the vectorial notation.

We have two field ω_1, ω_2 entering in our nonlinear medium (with length L) and two (in general) new frequency ω_3,ω_4 generated at the output.

Where one generic component, for instance P_4 can be expressed as:

$$\begin{aligned} P_j = \frac{3}{4}\epsilon_0\chi^{(3)}_{xxxx}[|A_4|^2 A_4 e^{-i(k_4 z-\omega_4 t)} + 2(|A_1|^2 + A_2|^2 + A_3|^2)A_4 e^{i(k_4 z-\omega_4 t)} \\ +2A_1A_2A_3 e^{i(k_1+k_2+k_3-k_4)z-i(\omega_1+\omega_2+\omega_3-\omega_4)t} \\ +2A_1A_2A_3^* e^{i(k_1+k_2-k_3-k_4)z-i(\omega_1+\omega_2-\omega_3-\omega_4)t} \\ +2A_1A_2^*A_3 e^{i(k_1-k_2+k_3-k_4)z-i(\omega_1-\omega_2+\omega_3-\omega_4)t} + ...] \end{aligned} \tag{5.8}$$

The first four terms containing A_4 are responsible for phenomena such as self phase modulation or cross phase modulation.

In the expression of the fourth component of the polarization there are included several kind of FWM processes and the effectiveness of every situation depends strongly on the phase mismatch between E_4 and P_4.

Let's define:

$$\theta_+ = (k_1 + k_2 + k_3 - k_4)z - (\omega_1 + \omega_2 + \omega_3 - \omega_4)t \qquad , \tag{5.9}$$

that correspond to the case where three photons transfer their energy to a single photon (third armonic generation):

$$\omega_4 = \omega_1 + \omega_2 + \omega_3 \qquad . \tag{5.10}$$

Instead the term

$$\theta_- = (k_1 + k_2 - k_3 - k_4)z - (\omega_1 + \omega_2 - \omega_3 - \omega_4)t \qquad , \tag{5.11}$$

correspond to the case where 2 photons (ω_1 and ω_2) are annihilated, while two photons ω_3 and ω_4) are generated simultaneously satisfying the condition:

$$\omega_3 + \omega_4 = \omega_1 + \omega_2 \qquad . \tag{5.12}$$

In the case $\omega_1 = \omega_2$, under the condition above, the FWM can be initiated also with a single pump beam [30].

In our experiment we have FWM coming from the pump itself and also from the interference between pump and probe. This explain why the pump is broader on resonance and 2 sidebands are clearly visible as shown in figure 5.5.

In our situation, i.e. two photon of the pump are absorbed while the probe is re-emitted, we can identify our pump and probe, respectively with the index 1, 2.

The energy and momentum conservation condition give:

$$\omega_p - \omega_{pr} + \omega_3 - \omega_4 = 0 \qquad . \tag{5.13}$$

$$\bar{k}_p - \bar{k}_{pr} + \bar{k}_3 - \bar{k}_4 = 0 \qquad . \tag{5.14}$$

The second condition can be more clear with a graphical representation as shown in Fig. 5.6, where $k_3 = k_p$.

Neglecting all the situations with a different energy conservation condition we can write a simpler expression for the four nonlinear polarization. Here we express every ω_j or k_j respectively in function of the other three frequencies or momentum. The amplitude of the field are choosen in order to match the right phase factor.

$$\begin{cases} P_1 = \frac{3\epsilon_0\chi^{(3)}}{8} A_{pr} A_3^* A_4 e^{i[(k_{pr}-k_3+k_4)z-(\omega_{pr}-\omega_3+\omega_4)t]} + c.c \\ P_2 = \frac{3\epsilon_0\chi^{(3)}}{8} A_p A_3 A_4^* e^{i[(k_p+k_3-k_4)z-(\omega_p+\omega_3-\omega_4)t]} + c.c \\ P_3 = \frac{3\epsilon_0\chi^{(3)}}{8} A_p^* A_{pr} A_4 e^{i[(-k_p+k_{pr}-k_4)z-(-\omega_p+\omega_{pr}-\omega_4)t]} + c.c \\ P_4 = \frac{3\epsilon_0\chi^{(3)}}{8} A_p A_{pr}^* A_3 e^{i[(k_p-k_{pr}+k_3)z-(\omega_p-\omega_{pr}+\omega_3)t-]} + c.c \end{cases} \tag{5.15}$$

We have to substitute the nonlinear polarization into the Helmholtz equation for each frequency. For instance we consider the field $A_{j=4}$, and expanding the double derivatives in time and space :

$$\partial_t^2 [A_4 e^{i(k_4 z - \omega_4 t)}] = -\omega_4^2 A_4 e^{i(k_4 z - \omega_4 t)} \qquad . \tag{5.16}$$

$$\partial_z^2 [A_4 e^{i(k_4 z - \omega_4 t)}] = (\partial_z^2 A_4 + 2ik_4 \partial_z A_4 + k_4^2 A_4) e^{i(k_4 z - \omega_4 t)} \qquad . \tag{5.17}$$

Substituting this into Eq. 5.7, and recalling that $k_j^2 = \frac{\omega_j^2}{c^2}\epsilon(\omega_j)$ we find:

$$-\partial_z^2 A_4 - 2ik_4 \partial_z A_4 = \frac{16 d\pi\omega_4^2}{c^2} A_1 A_2^* A_3 e^{i(k_p - k_{pr} + k_3 - k_4)z} \qquad . \tag{5.18}$$

Where $d = \frac{3}{4}\chi^{(3)}$ and we can define:

$$\Delta k = k_p - k_{pr} + k_3 - k_4 \qquad . \tag{5.19}$$

That finally with the SVEA become:

$$\partial_z A_4 = C_4 A_1 A_2^* A_3 e^{i(\Delta k)} \qquad . \tag{5.20}$$

$$\begin{cases} \frac{\partial A_p}{\partial z} = iC_p A_{pr} A_3^* A_4 e^{-i\Delta k z} \\ \frac{\partial A_{pr}}{\partial z} = iC_{pr} A_p A_3 A_4^* e^{i\Delta k z} \\ \frac{\partial A_3}{\partial z} = iC_3 A_p^* A_{pr} A_4 e^{-i\Delta k z} \\ \frac{\partial A_4}{\partial z} = iC_4 A_p A_{pr}^* A_3 e^{i\Delta k z} \qquad . \end{cases} \tag{5.21}$$

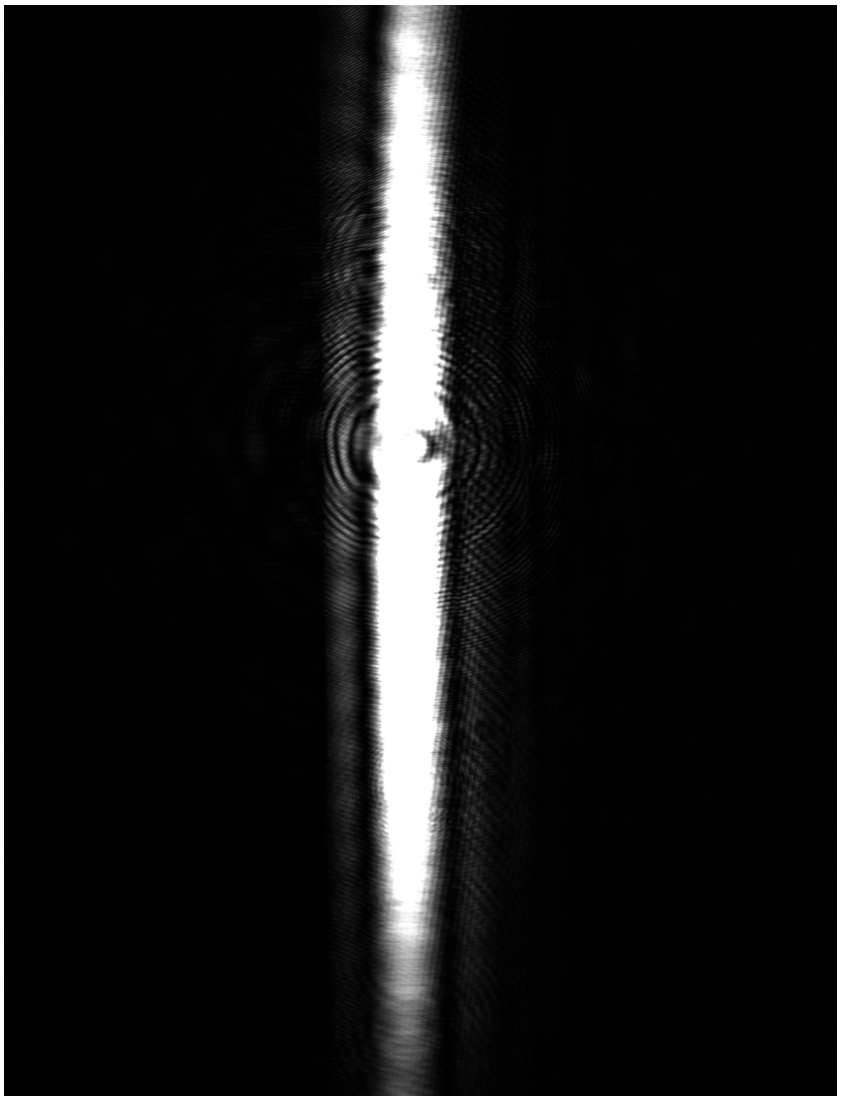

Figura 5.5. Side-bands of the pump due to FWM processes. The interference on the line is due to the experimental conditions, not to FWM processes.

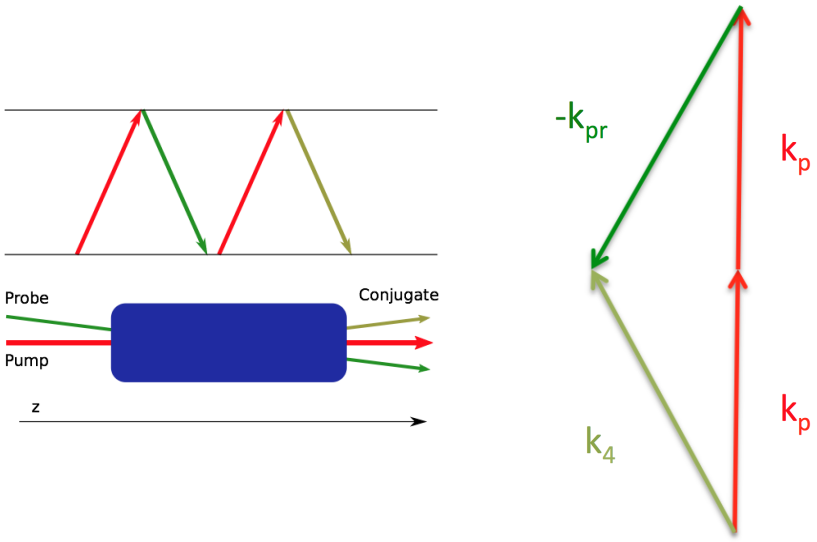

Figura 5.6

With this set of equations it is possible to calculate the intensity of each signal. For example:

$$A_4(L) = C_4 \int_0^L e^{i\Delta kz} = \frac{C_4}{i\Delta k}(e^{i\Delta kL} - 1) \quad . \tag{5.22}$$

Another important assumption is to have no pump depletion, that here means $A_3 \simeq A_p$. In fact in the process are involved two photons from the pump. Therefore we can write the intensity of the field:

$$I_4 = |A_4|^2 \frac{n_4 c}{2\pi} = C_4^2 |A_p|^2 |A_{pr}|^2 |A_p|^2 \frac{n_4 c}{2\pi} \left| \frac{e^{i\Delta kL} - 1}{i\Delta k} \right|^2 \quad . \tag{5.23}$$

So the intensity of the conjugate beam in the shift will have a *sinc*-like profile as in Fig. 5.7:

$$I_4 = I_p^2 I_{pr} C_4^* sinc(\Delta kL/2) \quad . \tag{5.24}$$

5.2.1 The problem of clearing the conjugate

Since in our experiment we need a strong $\chi^{(3)}$ nonlinearity we cannot avoid four-wave-mixing processes.

As seen in the preceeding section such phenomenas can be induced with one or more beam.

For a single intense pump the FWM gives two side-band, visible in the k-space as shown in Fig. 5.5.

Adding the probe the phase matching and energy conservation conditions between these two waves (are taken two photons from the pump and one from the probe) are such as is generated a third beam with opposite k and same frequency of the others beam.

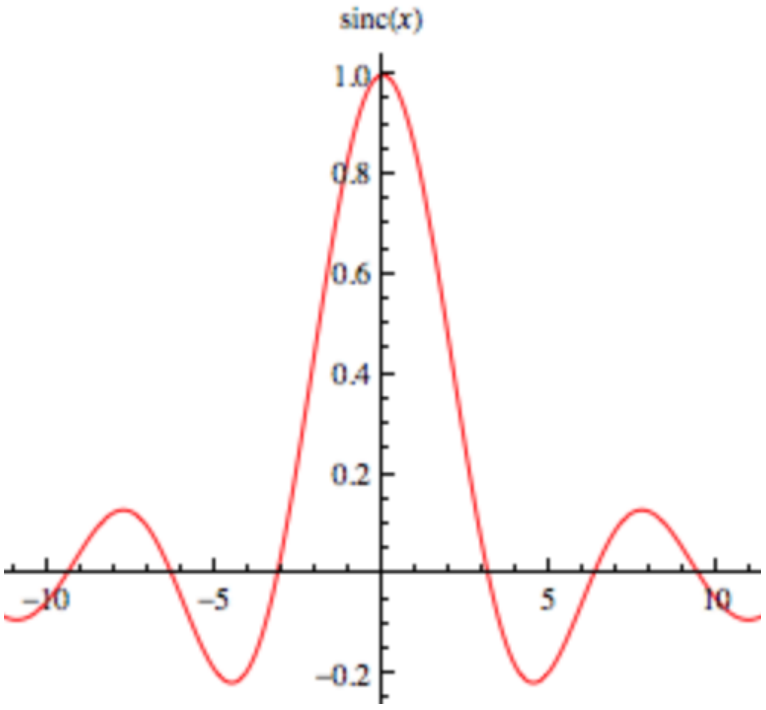

[htbp]

Figura 5.7

In this way the conjugate generate a shift in the interference pattern that is equal and opposite the one generated by the probe. In the Bogoliubov framework this can be understood as the fact that the conjugate generates a sound wave with opposite direction.

In figure 5.8 is shown the image of the pump, probe and conjugate beam in the reciprocal space.

Since we have to avoid the unwanted effects coming from the conjugate we put a razor blade on a translation stage in the focus of the imaging lens, where we are able to cut it with a good precision. The translation stage is necessary because, since the beam experiences also a self-defocusing effect, the focal point changes for different nonlinearities.

We stop the measurement when we are not able anymore to cut the conjugate without cutting the pump. If we go further with the measurement without properly cutting the conjugate we can clearly observe a decreasement in the shift due to the partial contribute of the conjugate.

In figure 5.9 is shown the k-space relative to the measurement for small angles. Here the razor blade is cutting from the left, as can be seen by the sharpness of the black line.

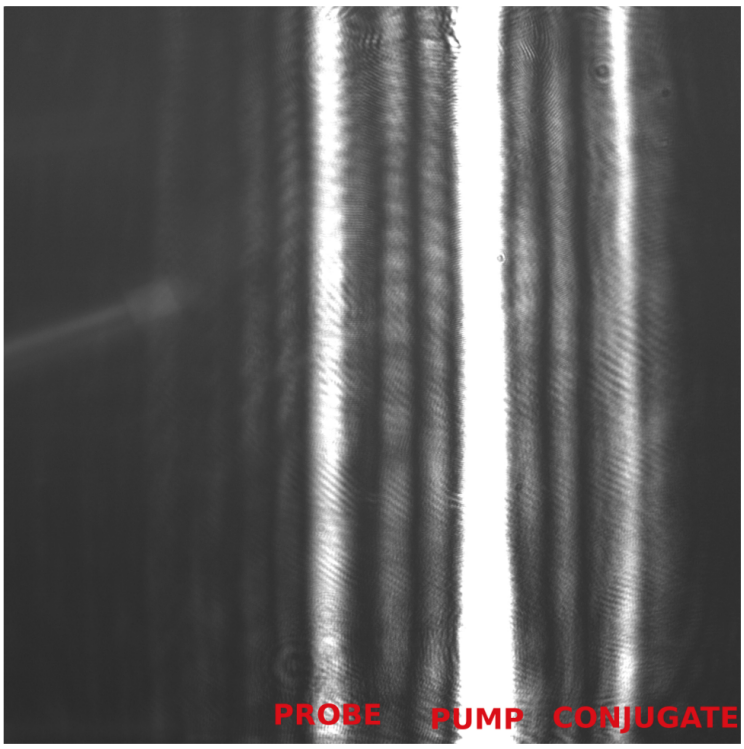

Figura 5.8

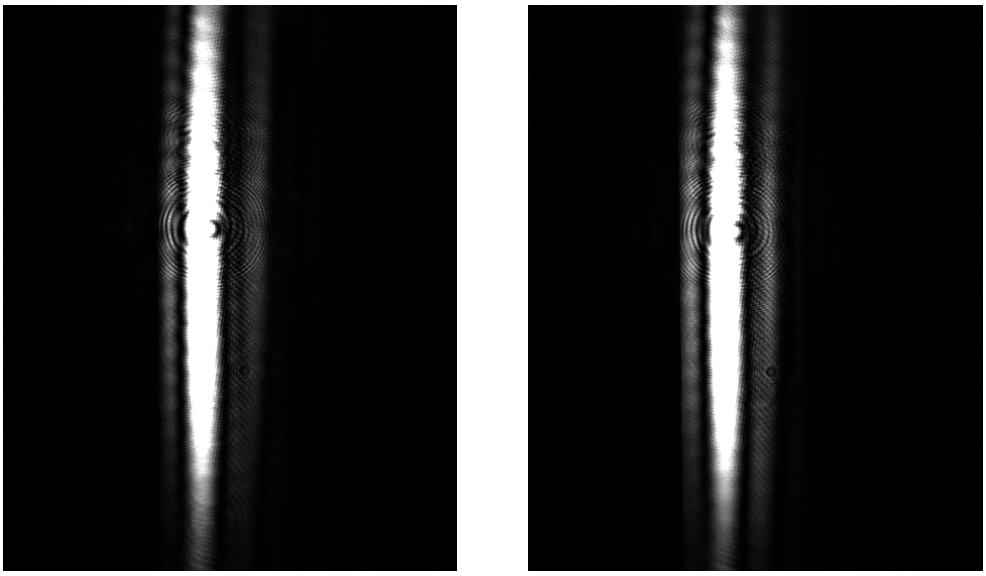

Figura 5.9. On the left is shown a limit condition where we are still able to fully cut the conjugate. On the right probe and conjugate start to superpose with the side-bands of the pump and is not possible to cut the conjugate without cutting the pump.

5.3 Results

We tried this experiment several times using different Rb cells with different temperatures and different detuning. The results shown here are obtained for a quasi-pure ^{85}Rb (99.9% concentration) cell with $L = 7.5cm$, a diameter of 1" at an effective temperature of $T_{eff} = 131$ °C.

We use a continuous Ti-Sa laser that we bring on our optical table using a single-mode fiber. Here we lock the laser frequency at $f = 384,2269$THz, using a SolsTiS locking system, bought from the M squared company. In such a situation we are 2.2 GHz detuned from resonance where we have a nonlinearitystrong enough and relatively low absorption. In this condition we achieve a 70% transmission and we can assume to be in a conservative regime.

We substract in post-processing the pump-only background to reconstruct the shift with better accuracy. To improve the precisions of each measurement we acquire 10 consecutive images in less than 0.5s and we average over them. The error on each shift measurement in this way can be extimated (1px =6.5 μm) as $\sigma(\Delta S) = \pm 0.5px = \pm 3.2\mu m$.

As shown in figures **??**, 3.2 the dispersion relation is linear with a local nonlinearity, instead in presence of non-locality it tends to converge to the single particle behaviour for large $k_\perp$. That is like to say that the non-locality tends to suppress the collective behaviour of our particles.

First are reported the experimental datas of the shift vs probe angle **??**. The k of the pump is fixed perpendicularly to the cell and we move the angle of the probe in each measurement.

In Fig. **??** is shown the reconstructed dispersion relation.

For a local nonlinearity we expect a behaviour like the linear one fitted for really small k.

The non-locality is such as the effectiveness of the nonlinearity is suppressed for $\Lambda < \sigma_{nl}$.

5.4 Buffer gas

We tried to measure the Bogoliubov dispersion relation also using another cell ($L = 7.5cm, D = 2.54cm$) with 85Rb and neon as a buffer gas, i.e. a noble gas that adds pressure in the system, that in our case is 30 Tor. In chemical systems buffer gas such as helium, neon, or argon are used to control the speed of combustion with any oxygen present.

We choose to try this cell to prevent non-local effect, that we were believing to be due to the atomic motion that in a dilute gas is almost collision-free.

Despite this with such a pressure the absorption spectrum suffers a Lorentzian broadening the same value of the non-local length and this bring us to arrange an experiment to understand better the nature of the non-local phenomenas.

We perform few measurements of the shift at T= 140 C° for three different frequencies $f_1 = 384,2168THz, f_2 = 384,2198THz, f_2 = 384,2168THz f_3 = 384,2212THz$, that corresponds respectively to 0.5%,2% and 10% transmission.

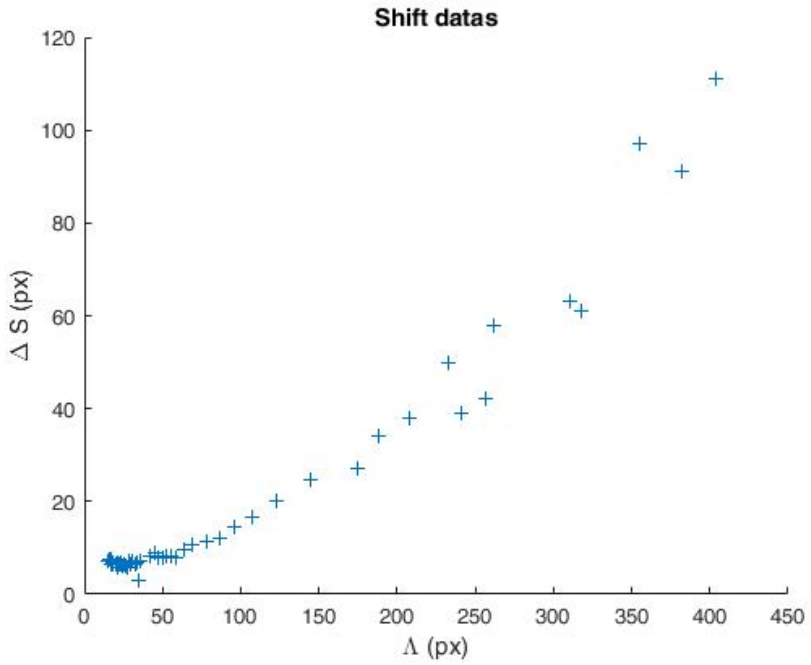

Figura 5.10. The observed shift in function of the wavelength of the modulation ($\Lambda = 2\pi/k_\perp$), both in pixels. The detuning was 2.2 GHz, the power of the probe 2mW and the power of the pump 150mW.

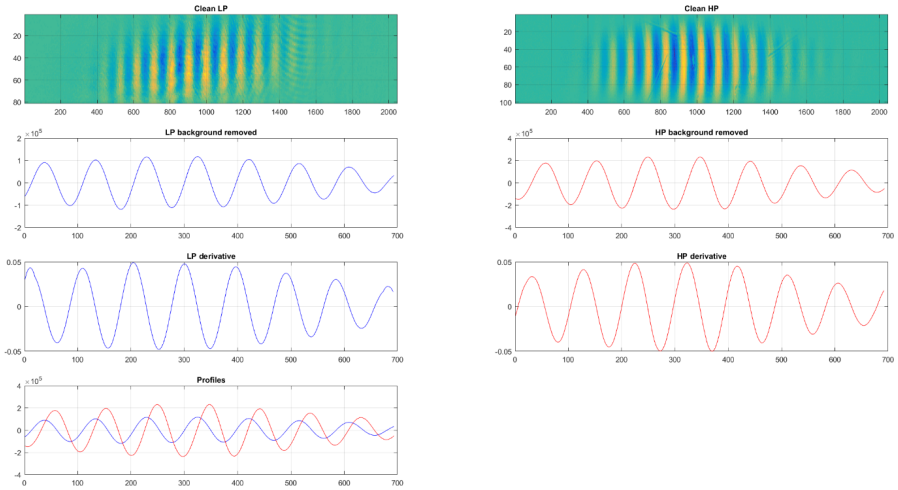

Figura 5.11

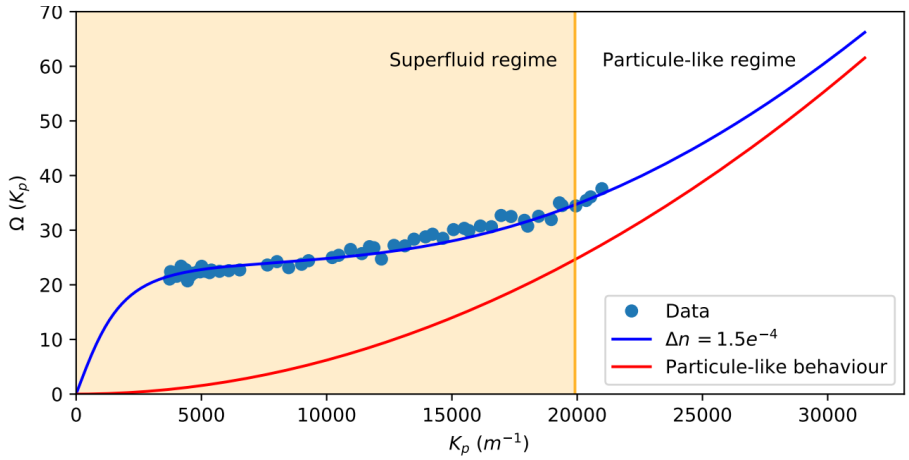

Figura 5.12

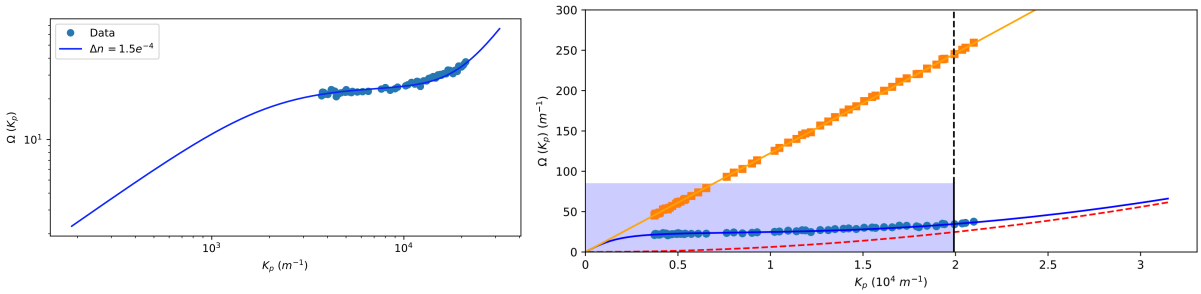

Figura 5.13. On the left the same plot of Fig. 5.12 in log-log scale. On the right in orange is shown the expected dispersion with a local nonlinearity. The dashed red line represents the the single-particle behaviour, i.e. the expected one without nonlinearity.

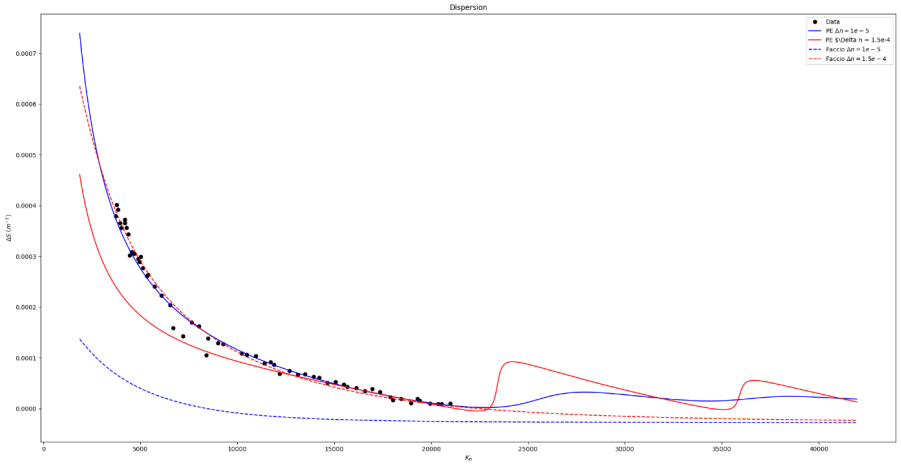

Figura 5.14. Fit of the shift using the two different theories and two values of the nonlinearity.

In this way we are out of conservative conditions, but we try the experiment anyway to gain more information about the new system.

Surprisingly we find again $\sigma_{nl} = 400\mu m$ for every detuning and this lead us to investigate better the problem of non-locality.

Capitolo 6

Non-locality experiment

Once we analyzed carefully the results of the preceding experiment was clear the necessity to understand better and be able to quantify precisely the size of the non-local effect on our system.

We want to isolate the pure non-local effect from the nonlinear effects that are accumulated along the cell. To do that we used a 1 mm thick cell with a diameter of 1 inch.

Here we want to observe how the local phase is modified by a Gaussian defect, and in particular how big is the size of the nonlinear modulation of the refractive index compared to the size of the spot who excites the atoms.

We recall here that the main parameter that determines the non-local length are the most probable speed of the particles and the life-time of the excited states.

With a rough extimation the non-local length, for $T \simeq 200$ °C, $\tau = 26,23459ns$, $m_{Rb} = 84,9 \times 1,41 \times 10^{-25} Kg$ [32] can be evaluated as:

$$\sigma_{nl} = \sqrt{\frac{2k_B T}{m}}\tau \simeq 10\mu m \qquad . \tag{6.1}$$

Compared with the preceding experiment we switch the role of the two beams, since we don't care about the sign of the nonlinearity anymore, but only about the dimension of the zone where the background fluid feel the nonlinearity. For the same reason we can increase the temperature, in fact

Therefore we decided to use the AOM's zero order beam as the defect and the first order beam as background-fluid.

The defect is focused in the middle of the cell with a size of the spot of $w_0 \simeq 13\mu m$.

The procedure we use to put the cell exactly in the focal point is to put on focus the defects on the two windows of the cell (that could be little scratches or really small cluster of condensed particles) and we adjust the position of the cell in the middle.

In the counter-propagating configuration in fact the lens who focus the defect beam is also one of the two lenses of the 10x telescope that image the other beam in camera.

The main part of the setup is shown in figure 6.1.

The diffraction in the AOM slightly change the shape of the two beams. Both the zero and the first order beam became slightly oval, with the bigger axis along

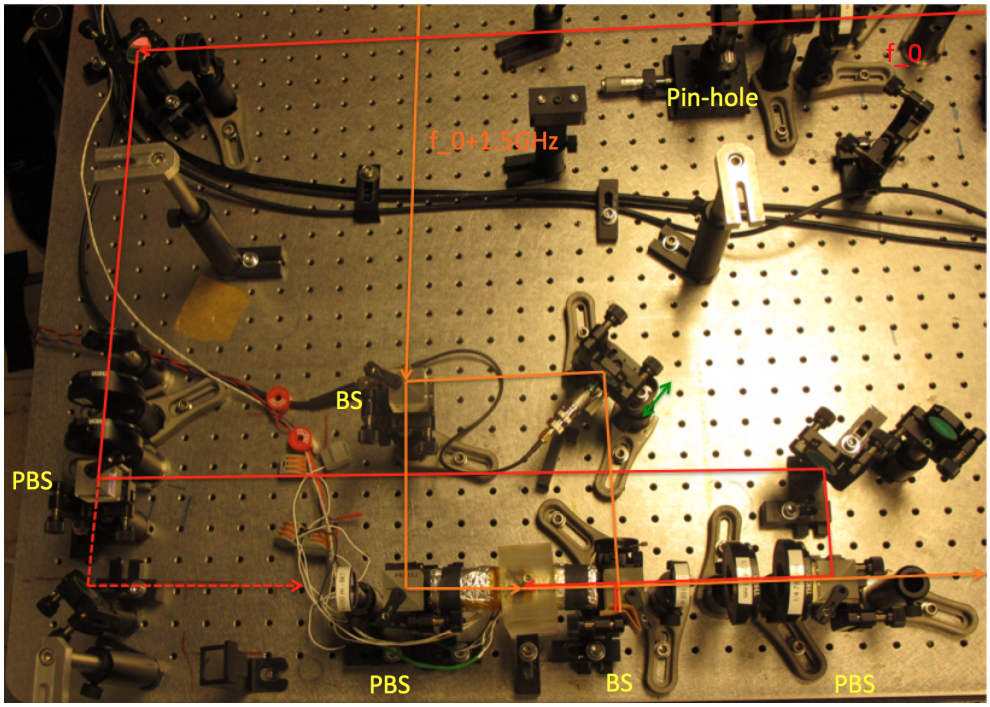

Figura 6.1

the y direction. We spatially filter the defect beam (red) in the reciprocal-space with a $75\mu m$ pin-hole in the focus of two lenses to recover a good gaussian profile. Then the beam is re-collimated with a 8x magnification, this is because bigger is the size of the beam and smaller will be the size of the focus:

$$w_0 = \frac{2f\lambda}{\pi D} \quad , \tag{6.2}$$

where f is the focal length and D is the diameter of the beam on the lens. For the space available the shortest focal lens we can use is $f = 10cm$.

The setup was tested first in a co-propagating regime (dashed line) but we decided immediately to switch in counter-propagating regime because we weren't able to fully cut the defect after the cell and it was disturbing the imaging.

What we want to image in fact is only the effect of the nonlinearity on the phase of the probe.

To evaluate the phase of the probe beam passing through the nonlinear medium we make it interfere with a reference beam in a simple Mach-Zender interferometer.

The mirror on the arm of the reference beam can be translated precisely by a piezo-electric transducer. This allow us to scan over a precise range of phase.

As in the shift experiments the interferometer is under a box to prevent noise.

Moreover using a double generator of signal we can precisely synchronize the ramp signal that pilots the piezo with another square signal that we use to trigger the camera and acquire frame at regular intervals during the phase scan.

In this configuration we observed also a weak spontaneous emission signal, coming from the particles excited by the defects, that is isotropically polarized and we cannot

fully cut it also in this case. Anyway it is not a big issue because we can make a background subtraction live or in post-processing. We will find that this spontaneous emission spot has the same size of the modulation of the index.

6.1 Spatial phase measurement

We can extrapolate the phase profile also just by one image.

A more precise algorythm that relies on the phase scan and is based on the orthogonality of the trigonometric function is described here.

With such a small focus the power necessary to saturate the transition is about 1mW, and we can roughly estimate $I_{sat} \simeq 10^3 W cm^{-2}$.

We can clearly see that the saturation of the atomic transition create a flat-profile in the fringes, because also the nonlinear refractive index reach his maximum value at I_{sat}.

We observed a phase profile that can be fitted with a gaussian, due to the velocity distribution of the particles, convolved to the probability of decay that fall is exponentially in time $e^{-t/\tau}$.

6.2 Phase scan technique

Capitolo 7

Optically induced defect experiment

In this chapter is described the experimental realization of a trial to suppress the scattering, as proposed by [5], using an optically induced defect.

Despite the results obtained are not matching with the expectations and are not fully understood I report it here, hoping that it will be useful for the future researchers who are going to investigate on this topic.

In this experiment we used the same Ti-Sa laser of the first (the experiments are mounted simultaneously on the same optical table).

Here we need two different laser frequencies for the background fluid and the defect. We use the first order diffraction of an AOM to create the defect beam that is blue-detuned of +1.5GHz from the other beam .

The small "defect" beam will be resonant with the lower energy transition of the 85Rb D2 line $5^2S_{\frac{1}{2}}, (F = 3) \longrightarrow 5^2P_{\frac{3}{2}}$ in order to create the strongest possible modulation of the refractive index.

Meanwhile a second "fluid" laser, red-detuned from to the atomic resonances (i.e. in Kerr self-defocusing), will scatter on the optical defect until, tuning the angle or the relative intensities between the two lasers, the scattering will be suppressed.

This could be a clear proof of the possibility to simulate a superfluid using light.

Depending on the relative geometry and intensities between the 2 beams it is possible to achieve different propagating regimes.

7.1 First trial: co-propagating beams

In a first trial I sent two co-propagating beams, shifted of 1.5 GHz by an AOM, in a 85Rb cell with a temperature T=130 C°, in order to have the defect resonant and the "superfluid" beam in negative nonlinearity regime.

The cell used was the same of the preceding experiment with a length $L = 7.5cm$ and a diameter of one inch (2.54 cm). Anyway the system cell+oven was $\simeq 20cm$ long.

In a simple imaging scheme I image the output plane of the cell.

Is important to have the defect collimated along the whole cell, otherwise we would have a system where the both the FWHM and the intensity of the Gaussian

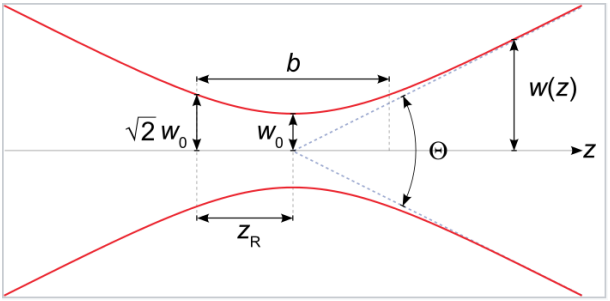

Figura 7.1

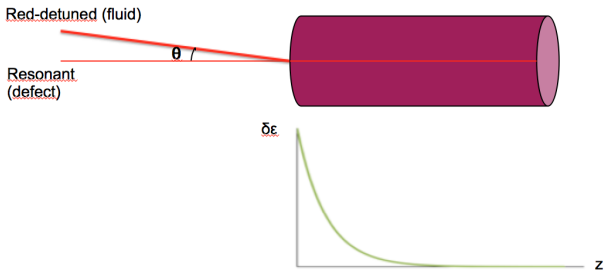

[!htbp]

Figura 7.2

modulation changes along the cell, making too hard to give a reliable interpretation of the result.

In this configuration there were several problem to face with:

- The Rayleight length $z_R = \frac{\pi w_0}{\lambda}$ impose a constraint on the size of the collimated defect, and so on the length of the cell. In fact smaller is the collimated beam and first it will diverge.
- The resonant defect is absorbed, therefore the modulation of the refractive index $\delta\epsilon$ is exponentially decaying along the cell as shown in Fig. **??**.
- As the superfluidity effect relies on the spatial modulation of the nonlinear refractive index shift, it is however important to choose a medium where the characteristic non-locality length is shorter than the healing length:

$$\sigma_{nl} < \xi = \frac{\lambda}{2}\sqrt{\frac{-n_0}{\Delta n}} \simeq 15 - 30\mu m \quad . \tag{7.1}$$

- The size of the defect w_0 should be bigger than the healing length.

  From the shift experiment we extract a value of the nonlinearity for $f = 384,2269\text{THz}$.

  Assuming that for a frequency of $f = 384,2280$ the value of the nonlinearity is $\Delta n \in (2:5) * 10^{-4}$ for our background fluid.

$$w_0 > \xi \simeq 15 - 30\mu m \quad . \tag{7.2}$$

The last condition can be understood from the fact that below the healing length the fluid behave as an incompressible fluid (because of the radiation pressure) and the scattering is ever suppressed.

I created a defect as small as possible in order to be collimated along $z_R = 20cm$ that for our wavelength means a FWHM of the spot of $w_0 = 220\mu m$. Then the maximum intensity of the defect is $I = \frac{20mW}{\pi w_0^2} \simeq 10^5 \frac{W}{cm^2}$.

Here are shown the preliminar results I obtained in this configuration.

Switching off the background, with the defect on, no signal was observed, in fact the defect is fully absorbed before of the end of the cell. We can observe a residual defect spot if we increase the defect intensity to way more than I_{sat} or if we go out of resonance.

The procedure we use to alligne the two beams at $k = 0$ is in fact to alligne the center of the modulation with the center of this residual spot. In Fig. **??** where the $k \neq 0$ is evident that the residual spot doesn't correspond to the center of the modulation of the index (black spot).

The position of the defect beam is fixed, while we move the background fluid. So the observed effect is the effect of the modulation of the refractive index created on the background fluid, that enter with an angle inside the cell, accumulating the effects of all the propagation planes.

In Fig. **??** is shown the result obtained with the beams superposed along all the cell i.e. for $\Delta k = 0$.

To have a better contrast in the image shown the fluid is at 384,2280 THz, and the defect is blue detuned of 400 MHz from the atomic resonance (it is still in Kerr defocusing).

Decreasing the intensity of the defect the fringes become less visible and the size of the black spot decrease because of the decreasing modulation of the refractive index .

Is remarkable that, with the background subtraction, is highlightened how the transmission is increased in presence of the defect.

This can be understood in terms of tunneling through a potential barrier[35]. For $k \neq 0$ a parabolic-like shape of the fringes was observed as shown in the figure **??**.

Moreover the inter-fringes space decrease with the intensity. That means that they propagate faster along their "temporal" path.

In the image with high power defect the atomic transition is strongly saturated as can be observed from the residual spot. This residual spot can be used to precisely alligne the two beams at k=0.

The aim of this experiment anyway was to suppress the scattering of the defect by increasing the fluid intensity and decrease the angle until the achievement of the superfluidity condition:

$$\phi < \sqrt{\epsilon} c_s = \sqrt{-\frac{\chi^{(3)}\rho}{2}} \qquad . \tag{7.3}$$

Unfortunately I didn't observe a suppression of the scattering. As will be shown later it is because there is no scattering at all and the initial interpretation of this result was wrong.

[!htbp]

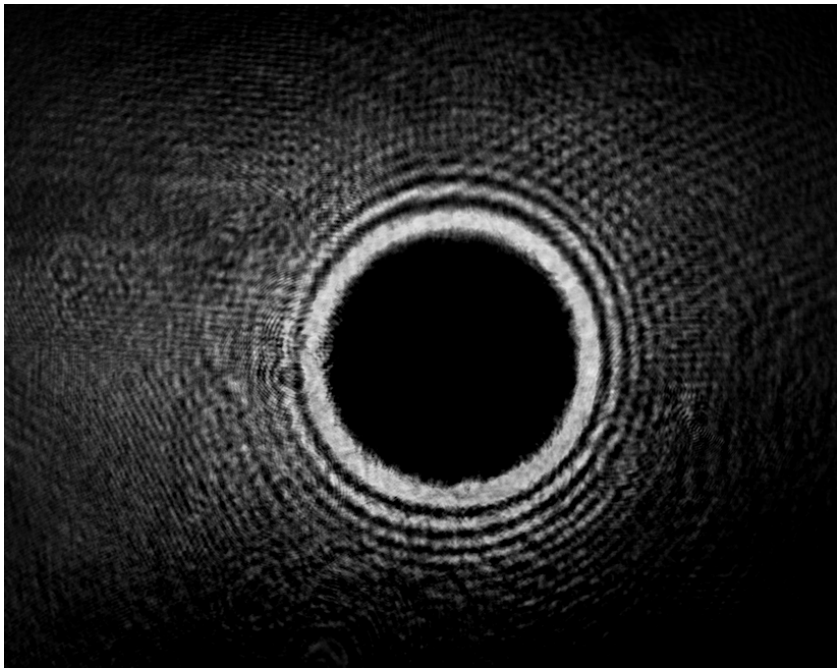

Figura 7.3. In this image the background without the defect is subtracted. In this way the variation of intensity due to the defect are put in evidence. Here $I \simeq 10^5 \frac{W}{cm^2}$.

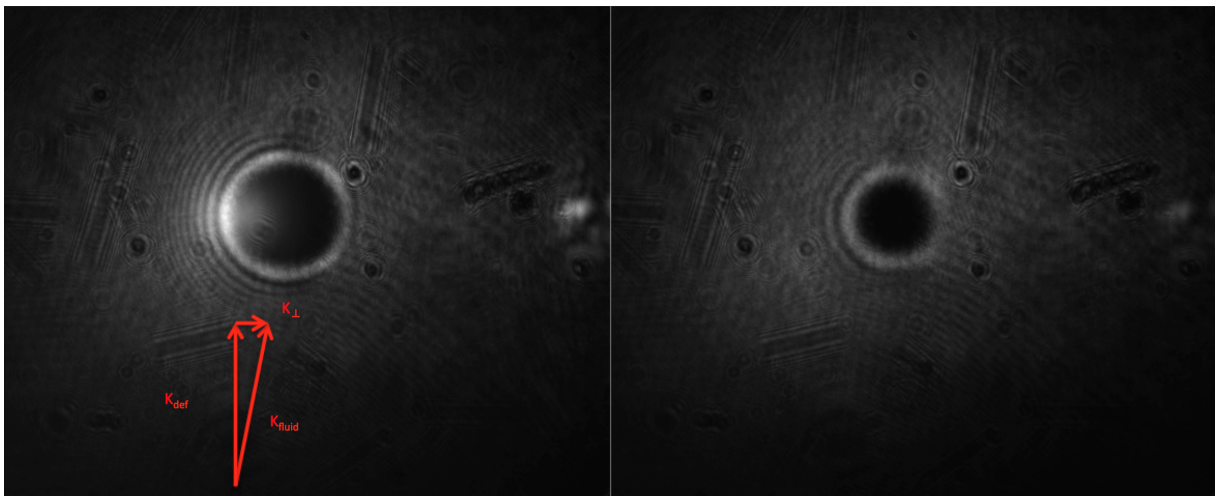

Figura 7.4. Here there is a small angle between the two beams that introduce an in plane component $k_\perp$. On the left $I_{def} = 10^5 W/cm^2$, on the right $I_{def} = 3 \times 10^4 W/cm^2$.

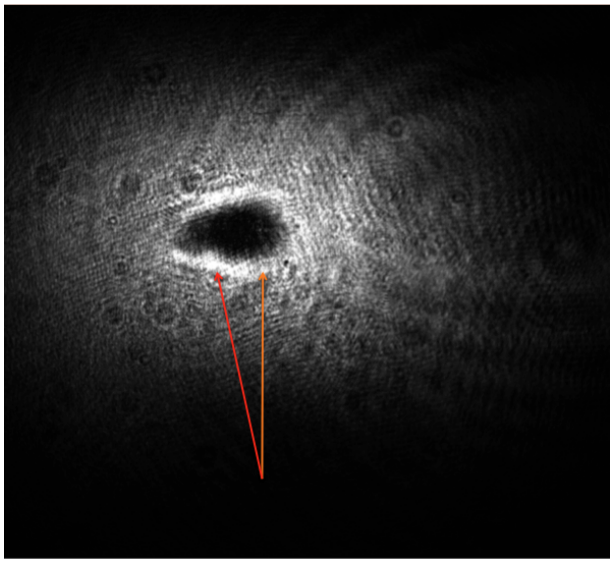

Figura 7.5

Anyway the parabolic-like shape of the fringes was suggesting a fluid-like behaviour. Despite this the visibility of the fringes, due to the interference between the incident and the scattered light, is way bigger than the one predicted in the simulations 3.4 that is around 10% .

For a big relative k the parabolic-like shape of the fringes is more evident as shown in Fig. 7.5.

In this configuration a big problem was also that I wasn't able to discriminate if the parabolic shape of the fringes for $k_\perp \neq 0$ was a real effect or it was a "shadow" built by the effects accumulated along all the planes of the cell.

In particular I believe to this second hypothesis, for which the Fig. 7.5 can be explained with the fact that the spatial superposition between the background fluid and the defect is different in different plane. Moreover the defect is absorbed along the cell, therefore the beam will feel the nonlinear effects mainly in the initial part of the cell. The bigger part of the spot on the right can be reconducted to nonlinear effects in the start of the cell, where the size of the modulation is maximized. The smaller black part instead is originated in the end of the cell, where the defect has already been almost totally absorbed.

An option to verify this could have been to switch the imaging system, that at that moment was made by just two lenses to image the output plane, into a confocal scheme, in order to isolate the plane on focus.

We decide instead, to try first another configuration with a focused counter-propagating defect. In this way, focusing the defect on the image plane (i.e. the output plane of the cell) we could have a better understanding of the in plane effect.

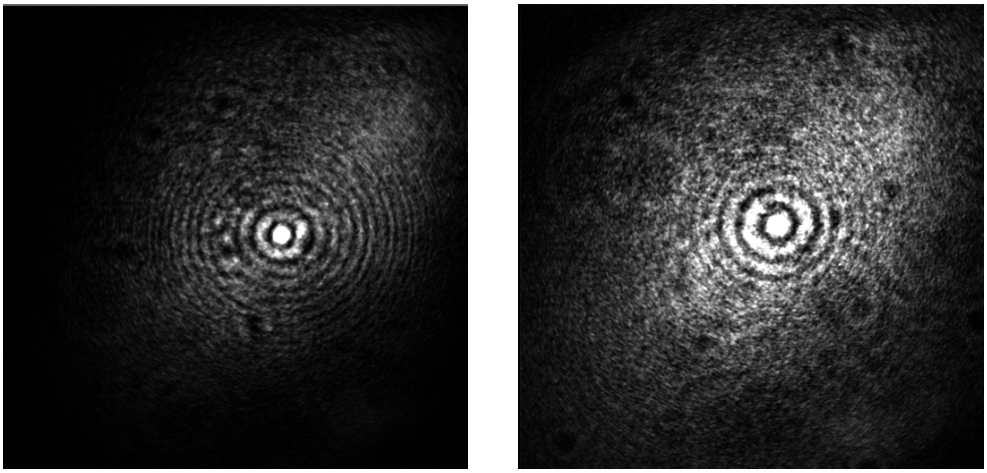

Figura 7.6. On the left high power defect P=8 mW. On the right low power P= 3.3 mW

7.2 Counter-propagating beams

I perform the experiment also in a counter-propagating regime, whil in the other case I was using a collimated defect, this time I focus the defect on the output plane of the cell, that correspond to the image plane. In this way it is possible to avoid "shadow"effect and to maximize the in plane effects.

The results were totally different from the expectations and this bring us to reconsider the interpretation of this images. In fact under a negative nonlinearity the defect is expected to act as a potential barrier where the fluid scatter. In this interpretation we expected a black spot on the fluid beam.

Instead we observe a central bright spot in the pattern as shown in figure **??**.

In the counter propagating beam configuration the defect is not projected into the camera, as shown in the setup. Therefore the observed effects are due only to the modulation of the index induced by the defect and felt by the background fluid.

Differently from the preceding configuration moving the relative k the pattern just translate and the fringes mantain the same shape.

The setup allow to switch between the two configurations just by flipping a mirror. In this configuration the size of the focus is around $10 - 20\mu m$, that probably is below the healing length.

This observed effect match partially with self-phase modulation patterns. But if it was the case I should be able to observe it also for a single intense beam.

We observed the same pattern also with a single intense focused beam but in conditions R<0,dphi>0 and I wasn't able to reproduce it, maybe was a sort of mistake, maybe not.

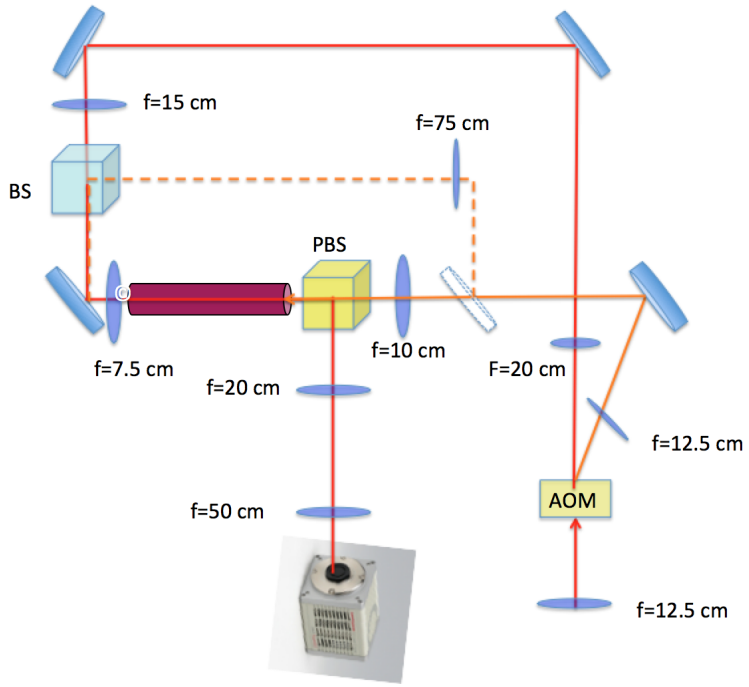

Figura 7.7

With a positive nonlinearity there are effect of instability phase modulation that leads to the effect observed in **??**. In this situation the effect depends on the relative angle between the two beams.

Here the observed effect is presented 384,2315 THz, where the defect is in focusing regime and the other beam has a frequency lower than the transitions. This effect happen exactly when the defect beams overcome the resonance of the upper energy D_2 transition (384,2324 THz) i.e. when the sign of the nonlinearity change. This can be used to see when the nonlinearity change sign without needing for the Z-scan.

7.3 Comparison with self-phase modulation patterns

In several articles [51][52][53][50] the formation and evolution of the far field patterns of a Gaussian beam passing through a focusing-defocusing nonlinear medium are widely studied.

Here the far field is intended in the context of the Fresnel-Kirchoff diffraction theory.

[**?**]

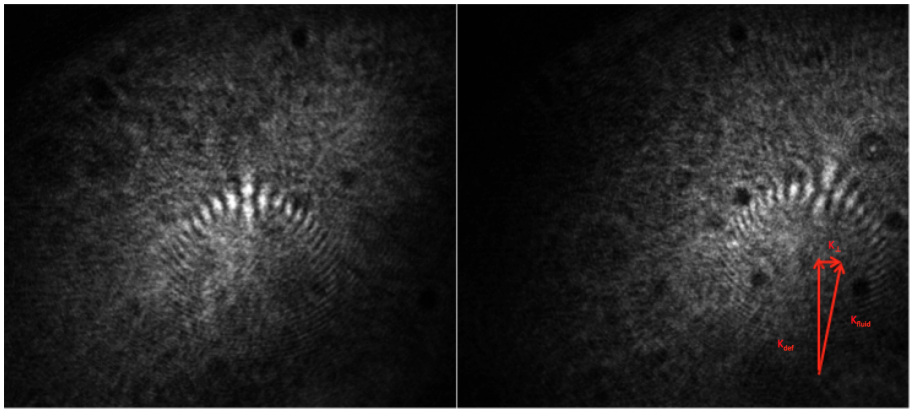

Figura 7.8

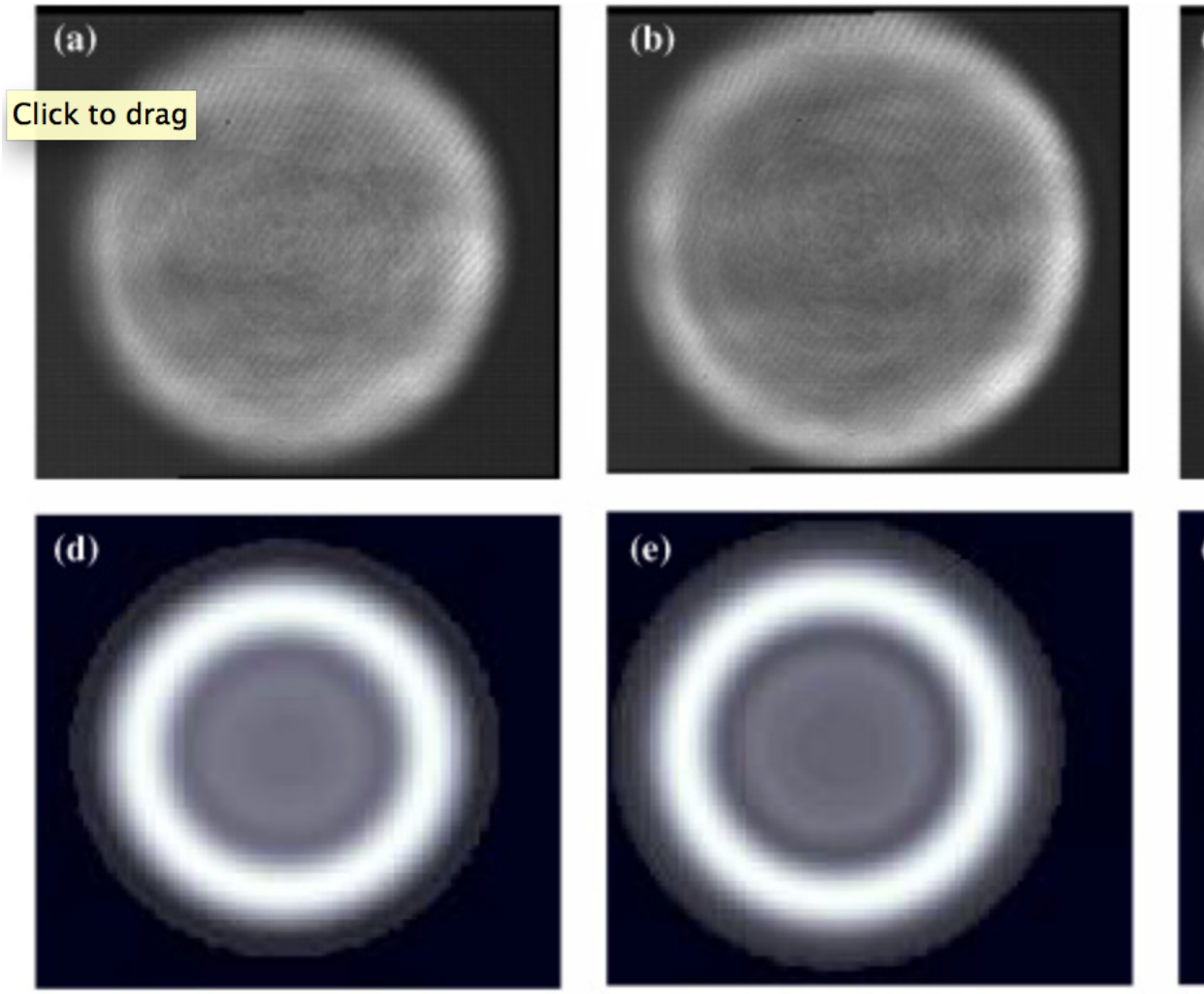

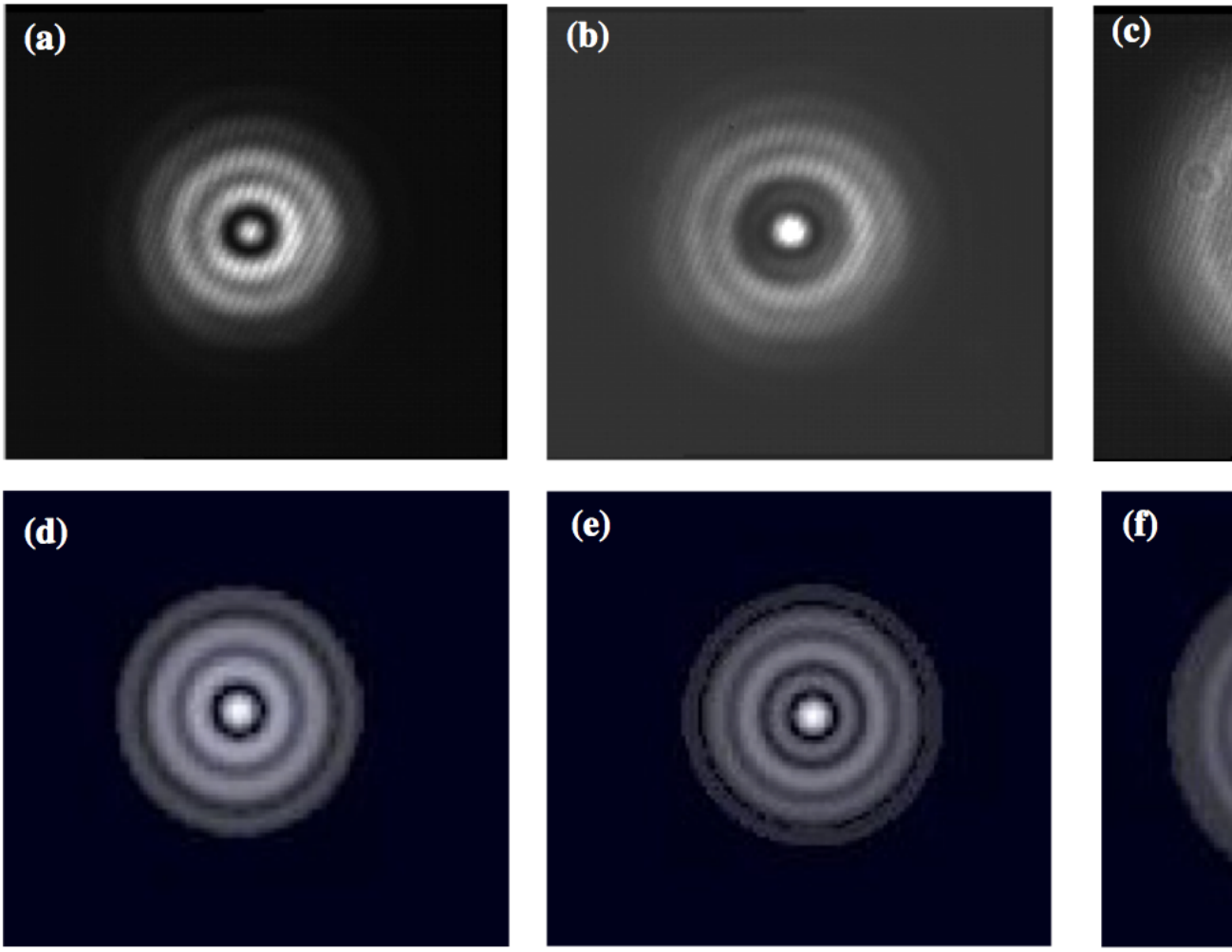
(a)
(b)
(c)
(d)
(e)
(f)

This experiment can be interpretated also in terms of wave-tunneling through a potential barrier [35]. Fresnel's equations become independent of polarization and yield the transmission and reflection coefficients

This fourth-order equation for transmission can support bistability and hysteresis, with threshold values determined by the strength of the nonlinearity.

There is a clear crossover behavior when the barrier height equals the incident kinetic energy.

Moreover, since the tunneling is nonlinear, there is a bi-stability in the transmission.

Capitolo 8

Conclusions and future perspective

All the theory about the shift take in account a uniform fluid and this is not exactly our case, since we are using a Gaussian beam.

The intensity of the gaussian is not uniform, and this can affect the shift measurement, expecially for small angle, where the spatial displacement between the central and the side fringe is around the FWHM of the gaussian pump beam.

For big angle instead we can consider that the intensity of the pump is the same for the two central fringes.

To verify this the plan is to perform the experiment with a really broad gaussian beam to verify this. In this way we lose intensity and therefore the shift will be less accentuated. Another option is to take in account different pump intensity in the analysis.

Try the non-locality experiment with an elliptical beam, in analogy with the Edinburgh experiment. To measure the polarization response could be useful to use a pulsed laser and to have a camera that is able to access time scale of the order of μs, or even ns. minchiate su Hawking radiation

Superfluid vacuum theory (SVT) is an approach in theoretical physics and quantum mechanics where the physical vacuum is viewed as superfluid.

The ultimate goal of the approach is to develop scientific models that unify quantum mechanics (describing three of the four known fundamental interactions) with gravity. This makes SVT a candidate for the theory of quantum gravity and an extension of the Standard Model.

It is hoped that development of such theory would unify into a single consistent model of all fundamental interactions, and to describe all known interactions and elementary particles as different manifestations of the same entity, superfluid vacuum.

In the measurement of the dispersion relation we limits to observing the output plane of the cell. Using a cell with bevelled window, as the one shown in Fig.8.1 is possible to access different time frame of the propagation.

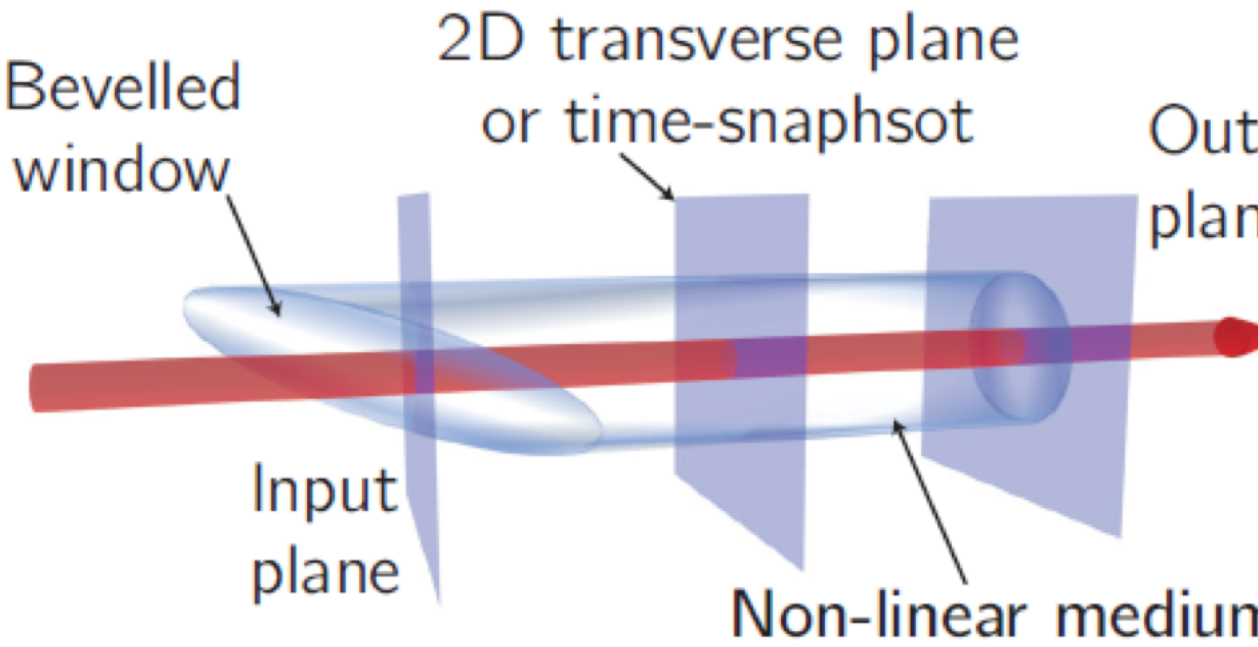

Figura 8.1

8.1 Implementing an EIT scheme to enhance the nonlinearity

Bibliografia

[1] P. Kapitza. “Viscosity of Liquid Helium below the λ-Point”. In: Nature 141.3558 (1938), pp. 74– 74. doi: 10.1038/141074a0.

[2] J. F. Allen and A. D. Misener. “Flow Phenomena in Liquid Helium II”. In: Nature 142.3597 (1938), pp. 643–644. doi: 10.1038/142643a0.

[3] F. London. “The λ-Phenomenon of Liquid Helium and the Bose-Einstein Degeneracy”. In: Nature 141.3571 (1938), pp. 643–644. doi: 10.1038/141643a0.

[4] N. N. Bogoliubov. On the theory of superluidity. J. Phys. (USSR), 11:23, 1947.

[5] I.Carusotto, Superfluid light in bulk nonlinear media (2014).

[6] L. Landau,Theory of the Superfluidity of Helium II,Phys. Rev. 60, 356, 1941.

[7] R. P. Feynman, "Simulating Physics with Computers", Int. J. Theor. Physics, vol. 21, no. 6/7, p 467-488, 1982.

[8] L. Pitaevskii and S. Stringari. Bose-Einstein Condensation. Clarendon Press, Oxford, 2003.

[9] Quantum fluids of light. I.Carusotto. Phys. Rev. A 85, 2013.

[10] D.Vocke et al.The role of geometry in superfluid flow of non-local photon fluids(2016).

[11] D. Vocke, T. Roger, F. Marino, E. M. Wright, I. Carusotto, M. Clerici, and D. Faccio. ”Experimental characterization of nonlocal photon fluids”. Optica, 2(5):484, 2015.

[12] A.Amo *et.al*. Superfluidity of polaritons in semiconductor microcavities.*Nat. Phys 5, 805-810*.

[13] G.Lerario *et.al*, Room-temperature superfluidity in a polariton condensate, Nature Physics (2017) doi:10.1038/nphys4147.

[14] J. Klaers, J. Schmitt, F. Vewinger, and M. Weitz, “Bose-Einstein condensation of photons in an optical microcavity.,” Nature, vol. 468, pp. 545–548, nov 2010.

[15] J. Kasprzak, M. Richard, S. Kundermann, A. Baas, P. Jeambrun, J. M. J. Keeling, F. M. Marchetti, M. H. Szyman, R. Andre, J. L. Staehli, V. Savona, P. B. Littlewood, B. Deveaud, and L. S. Dang, “BoseEinstein condensation of exciton polaritons,” Nature, vol. 443, pp. 409–414, sep 2006.

[16] http://www.nii.ac.jp/qis/first-quantum/e/forStudents/lecture/pdf/qis385/QIS385_chap5.pdf .

[17] Boris V. Svistunov, Egor S. Babaev, Nikolay V. Superfluid States of Matter.

[18] Quantum Analogues: From Phase Transitions to Black Holes and Cosmology edited by William Unruh, Ralf Schützhold. doi 10.1007/3-540-70859-6 .

[19] Pierre-Élie Larré and Iacopo Carusotto Phys. Rev. A 91, 053809,2015.

[20] Nardin G, Grosso G, Leger Y, Pietka B, Morier-Genoud F, Deveaud-Pledran B. 2011 Hydrodynamic nucleation of quantized vortex pairs in a polariton quantum fluid. Nat. Phys. 7, 635–641. (doi:10.1038/nphys1959).

[21] A.Amo et al. 2011 Polariton superfluids reveal quantum hydrodynamic solitons. Science 332,1167–1170.

[22] T.Boulier *et al.* Injection of orbital angular momentum and storage of quantized vortices in polariton superfluids.*Physical review letters*,116(11):116402,2016.

[23] Nardin G, Grosso G, Leger Y, Pietka B, Morier-Genoud F, Deveaud-Pledran B. 2011 Hydrodynamic nucleation of quantized vortex pairs in a polariton quantum fluid. Nat. Phys. 7, 635–641.

[24] J.Goldstone*et al*, Broken symmetries Phys. Rev. 127, 965 – Published 1 August 1962.

[25] Sanvitto D et al. 2011 All-optical control of the quantum flow of a polariton condensate. Nat. Phot. 5, 610–614.

[26] Bohm, David (1952). "A Suggested Interpretation of the Quantum Theory in Terms of "Hidden Variables", II". Physical Review. 85: 180–193.

[27] J. Michael Kosterlitz - Nobel Lecture: Topological Defects and Phase Transitions, 2016.

[28] R.Y. Chiao, J. Boyce:Bogoliubov dispersion relation and the possibility of superfluidity for weakly interacting photons in a two-dimensional photon fluid. Phys. Rev. A 60 (1999).

[29] P.E.Larrè,I.Carusotto. Propagation of a quantum fluid of light in a cavityless nonlinear optical medium: General theory and response to quantum quenches.Phys. Rev. A 92, 043802 (2015).

[30] G. P. Agrawal, Nonlinear Fiber Optics (Academic, San Diego, 1995).

[31] R. W. Boyd, Nonlinear Optics (Academic, Orlando, 2008).

[32] Daniel A. Steck, "Rubidium 85 D Line Data," available online at http://steck.us/alkalidata (revision 2.1.6, 20 September 2013).

[33] E. Arimondo, M. Inguscio, and P. Violino, "Experimental determinations of the hyperfine structure in the alkali atoms," Reviews of Modern Physics 49, 31 (1977).

[34] A. Banerjee, D. Das, and V. Natarajan, "Absolute frequency measurements of the D1 lines in 39K, ^{85}Rb, and ^{87}Rb with $\simeq$ 0.1 ppb uncertainty," Europhysics Letters 65, 172 (2004).

[35] Wan W, Muenzel S, Fleischer JW. 2010. Wave tunneling and hysteresis in nonlinear junctions. Phys. Rev. Lett. 104, 073903.

[36] M.Andrews et al., Phys.Rev.Lett. 79,553(1997).

[37] W Heisenberg and H Euler. "Folgerungen aus der diracschen theorie des positrons". In: Zeitschrift fur Physik 98.11-12 (1936), pp. 714–732.

[38] C.Gerry and P.Knights, Introductory Quantum Optics.

[39] Paul Siddons et al. "Absolute absorption on the rubidium D lines: comparison between theory and experiment". In: Journal of Physics B: Atomic, Molecular and Optical Physics 41.15 (2008), p. 155004. doi: 10.1088/0953-4075/41/15/155004.

[40] E. Madelung, "Quantentheorie in hydrodynamischer Form," Z. Phys. 40, 322–326 (1927).

[41] F. Marino, "Acoustic black holes in a two-dimensional photon fluid," Physical Review A, vol. 78, p. 063804, dec 2008.

[42] F. Dalfovo, S. Giorgini, L. Pitaevskii, S. Stringari, Rev. Mod. Phys. 71, 463, (1999).

[43] W. Wan, S. Jia, and J. W. Fleischer, "Dispersive, superfluid-like shock waves in nonlinear optics," Nature Physics, 2007.

[44] C. Sun, S. Jia, C. Barsi, S. Rica, A. Picozzi, and J. W. Fleischer, "Observation of the kinetic condensation of classical waves," Nature Physics, vol. 8, pp. 471–475, apr 2012.

[45] Alcock, C. B., Itkin, V. P., and Horrigan, M. K., Canadian Metallurgical Quarterly, 23, 309, 1984.

[46] S. Bar-Ad, R. Schilling, and V. Fleurov, "Nonlocality and fluctuations near the optical analog of a sonic horizon," Phys. Rev. A 87, 013802 (2013).

[47] S.Skupin, "Nonlocal stabilization of nonlinear beams in a self-focusing atomic vapor". https://arxiv.org/pdf/physics/0612200.pdf .

[48] V.M Lashkin *et.al* , Phys. Rev. E 73, 066605 (2006).

[49] D. J. Thouless, Mahito Kohmoto, MP Nightingale, and M Den Nijs. Quantized hall conductance in a two-dimensional periodic potential. Physical Review Letters, 49(6):405, 1982.

[50] L.Deng et al., " Formation and evolution of far-field diffraction patterns of divergent and convergent Gaussian beams passing through self-focusing and self-defocusing media", J. Opt. A: Pure Appl. Opt. 7 (2005) 409–415.

[51] E. Santamato,Y. R. Shen. "Field-curvature effect on the diffraction ring pattern of a laser beam dressed by spatial self-phase modulation in a nematic film".1984, Optic Letters.

[52] L Lucchetti et al. "Fine structure in spatial self-phase modulation patterns: at a glance determination of the sign of optical nonlinearity in highly nonlinear films",J. Opt. A: Pure Appl. Opt. 11 (2009) 034002.

[53] E. V. Garcia Ramirez et al. ,"Far field intensity distributions due to spatial self phase modulation of a Gaussian beam by a thin nonlocal nonlinear media", OSA(2010).

[54] P.-E.Larrè et al. Pump-and-probe optical transmission phase shift as a quantitative probe of the Bogoliubov dispersion relation in a nonlinear channel waveguide. arXiv:1612.07485 (submitted to Phys. Rev. A).

[55] Immanuel Bloch, Jean Dalibard, and Sylvain Nascimbene. Quantum simulations with ultracold quantum gases. Nature Physics, 8(4):267–276, 2012

[56] Zoran Hadzibabic, Peter Kruger, Marc Cheneau, Baptiste Battelier, and Jean Dalibard. Berezinskii–Kosterlitz–Thouless crossover in a trapped atomic gas. Nature, 441(7097):1118–1121, 2006.

[57] W. Unruh, “Experimental Black-Hole Evaporation?,” Physical Review Letters,vol. 46, pp. 1351–1353, may 1981.

[58] J. Steinhauer, “Observation of quantum Hawking radiation and its entanglement in an analogue black hole,” Nature Physics, aug 2016.

[59] P. G. Savvidis et al. Ring emission and exciton-pair scattering in semiconductor microcavities, PHYSICAL REVIEW B, VOLUME 65, 073309 .